Haptotropic Rearrangements in Metal Complexes of

4H-Cyclopenta[def]phenanthrene

By

Andreas Decken, Diplom

A Thesis

Submitted to the School of Graduate Studies

In Partial Fulfillment of the Requirements

for the Degree

Doctor of Philosophy

McMaster University

August 1993

Metal Complexes of 4H-Cyclopenta[def]phenanthrene

To my parents

who always believed in me

DOCTOR OF PHILOSOPHY (1993) McMaster University

(Chemistry) Hamilton, Ontario

Title: Haptotropic Rearrangements in Metal Complexes of

4H-Cyclopenta[def]phenanthrene

Author: Andreas Decken

SUPERVISOR: Dr. M.J. McGlinchey

NUMBER OF PAGES: xxi

176

Abstract

Transition-metal complexes of the tetracyclic system 4H-cyclopenta[def]phenanthrene (cppH) have been prepared for a series of metals, *i.e.* (η^6-cppH)$Cr(CO)_3$, (η^6-cppH)$Mn(CO)_3^+$ and (η^6-cppH)$Fe(C_5H_5)^+$; in all cases the metal is bonded to a terminal six-membered ring. Upon deprotonation, the corresponding (η^6-cpp) species can be trapped at low temperatures. Raising the temperature results in a η^6- to η^5- haptotropic shift, in the case of the $Cr(CO)_3$ complex at temperatures above -30 °C and +20 °C for the $Mn(CO)_3$ complex. However, heating of a sample of (η^6-cpp)$Fe(C_5H_5)$ did not result in a haptotropic rearrangement.

The corresponding 8,9-dihydro-cpp derivatives (η^6-H_2-cppH)$Cr(CO)_3$ and [(η^6-H_2cppH)$Mn(CO)_3$] PF_6 have also been prepared. Deprotonation of the $Mn(CO)_3$ complex yielded the thermally stable compound (η^6-H_2cpp)$Mn(CO)_3$ which only undergoes an η^6- to η^5- haptotropic shift upon heating to 60 °C for one hour. The relative ease of haptotropic shifts in the cpp complexes can be rationalized in terms of a transition state in which the migrating organometallic fragment is η^3-bonded to the polycyclic ligand in which a 10π (naphthalene like) system is retained. EHMO calculations predict that the barriers to migration in case of the (cpp)FeCp system can be expected to be some 4.5 kcal mol^{-1} lower than in the corresponding fluorenide system. Furthermore, calculations for the system (cpp)$Mn(CO)_3$ reveal that the barriers to migration can be expected to be much lower than in the analogous (cpp)$Fe(C_5H_5)$ system. The barriers were calculated

to be 17.5 kcal mol^{-1} and 30.0 kcal mol^{-1} respectively. Reactions have been carried out to prove the existence of the proposed η^3- transition state. In the course of these studies, the complexes (η^1-cpp)Fe(C_5H_5) and (η^1-cpp)Mn$(CO)_3(P(C_2H_5)_3)_2$ have been synthesized, both of which were found to be unexpectedly stable.

Acknowledgements

During the course of this work, numerous people have influenced my life and I would like to take this opportunity to acknowledge them.

To my supervisor, Dr. Michael J. McGlinchey, I am sincerely grateful for his guidance and support over the past years. Without his help I would not have had the opportunity to obtain my degree from McMaster University. Even before I started graduate school he devoted much of his time to ensure financial support from OGS and also to find a place to stay. I am very thankful for the many discussions we had and the encouragement I received at times when chemistry didn't quite work; one day the triple deckens will give reproduceable results!

I would also like to thank the members of my supervisory committee, Drs. Brian E. McCarry and Alex D. Bain for their assistance and helpful suggestions they have made. They kept me on track and ensured that I would not get lost in the EHMO or 2-D NMR jungle. Furthermore, they were always available during the time of my thesis writing.

A special note of appreciation goes to all the technical staff in the department. Dr. Richard W. Smith and Fadjar A. Ramalan for all the mass spec work. Many samples of supposingly interesting organometallic compounds were submitted and many spectra of free organic ligands were obtained. Thank you for running many samples of decomposed or side products as well as starting material and always giving me a chance for another attempt to run a *real* molecule.

Without their help I would have had a hard time identifying all the column chromatography products especially in the $Fe(CO)_2Cp$ work. I appreciate all the help I received from the NMR staff: Dr. Don W. Hughes, Brian G. Sayer and George Timmins. I would have not been able to produce the nice 2-D NMR spectra without their help, but I would have managed to irreversibly destoy the wiring while setting up for an inverse technique experiment. Their enthusiasm made the acquisition of spectra a very enjoyable experience.

Dr. James F. Britten, Jim: besides teaching me everything I know about X-ray crystallography he was always willing to look at some material that I had under the microscope. In most instances it turned out that my *beautiful crystals* were nothing more than nice looking dust and *not quite good enough*. I am very thankful that I had the privilege to learn how to run the Siemens P4 diffractometer. Even though my last few uses ended in major breakdowns, he never (officially) blamed it on me. I am very glad to enjoy his friendship and the many conversations we had. The number of crystal structures we solved makes me proud and it is clear that I would not be able to present this work without his input.

I am very grateful to the members of Dr. McGlinchey's group when I first arrived at McMaster to complete my 4th year. Debbie Clark who introduced me to the projects, while the boss was away, and taught me all the little things one needs to know in order to survive in an organometallic research lab. To Michael D'Agostino, Richard Perrier (Walt), Karen Burke (Sutin), Bavani Mailvaganam and Lijuan Li; their patience and enthusiasm meant a lot to me, especially in the early

days of my synthetic attempts. I learned how to work and have fun at the same time and I always enjoy meeting them again, long after they have left McMaster.

I would like to thank Patty Anacleto (Downton) for becoming a close friend, for all the academic and non-academic discussions we had and also for teaching me how to prepare arene chromium tricarbonyl complexes.

To Luc Girard: I never knew that EHMO calculations could be so colorful. From massively painful to painful is a big step and my view on anything *theoretical* has changed since EHMO calculations do not need to be run on a VAX any more but rather on a PC, with automated input file generation, output file extraction and 3D color representation. None of this would have happened based on my limited computer literacy. Sorry for not converting to WORD!

Thanks to all the people who have worked in the lab during my reign of terror for making ABB 357 such a fun place to work.

I also enjoyed all the help I received from the department. Dr. Thomas Hemscheidt and Dr. Fred Capretta for showing me how to safely reduce cppH to H_2cppH and Dr. Alicja Mika, who helped me setting up all my UV radiation experiments.

To the many people at ABB who had a major impact on my life. The numerous soldiers who had a friendly word even at early hours, Anna who gave me a chance to wake up every morning and the secretarial staff who took care of so many important things and kept me in line.

I am thankful to Dr. Simmons and Eugene Tan for showing me how to scan printed matter into a word processing program; their help came in handy after losing some files of structure factor tables.

My best wishes go out to very special friends: Heather Halabourda and her husband Ed. Without you I would have spent my first night in Canada under a bridge. You gave us shelter and became our step parents over the years. I am glad to have known you and we will keep in touch even after you guys have retired and my work has just begun.

An meine Eltern, denen diese Arbeit gewidmet ist. Dies ist die einzige Stelle in dieser Arbeit in der ich die Sprache wechseln darf und ich möchte es nutzen um Euch für Eure Unterstützung, Liebe und Verständnis zu danken. Über all die Jahre hinweg, auch über diese weite Entfernung. Diese Arbeit ist Euch gewidmet, in Erinnerung an alle Kleinigkeiten und die großen Dinge des Lebens die Ihr mir beigebracht habt.

In Liebe, Andreas.

Table of Contents

List of Figures

List of Schemes

List of Tables

Chapter 1: Introduction

1.1 Historical perspective

Over a period of about 200 years, the domain of organometallic chemistry has developed from simple compounds such as organo-arsenicals, which were discovered in 1760 by Cadet, to coordination compounds, metal carbonyls and highly unstable catalytic intermediates. Originally, these molecules were considered as complexes since the metals showed coordination numbers higher than expected from their group number in the periodic table of the elements. The numerous experimental approaches to new molecules and complex systems were accompanied by a variety of theories which aimed to explain the physical properties of these new compounds, such as their stability, color and magnetic behaviour. Models such as Werner's complex theory, the valence bond approach, ligand field theory, EHMO theory, and other more sophisticated methods have helped chemists to understand the properties of existing complexes, and even predict the physical and chemical properties of unknown materials.

With the advent of powerful and relatively cheap personal computers, the modern organometallic chemist can complement his or her synthetic, spectroscopic and structural investigations with a theoretical analysis of the reactions studied. In this thesis, we have attempted to blend these two approaches and so we introduce the necessary background in this opening chapter.

1.1.1 $(\eta^5\text{-}C_5H_5)_2Fe$

The chemistry of organometallic complexes underwent a major upheaval in 1951 with the discovery of $(\eta^5\text{-}C_5H_5)_2Fe$ by two independent research groups. Miller et al. reported on the reaction of C_5H_6 fumes on the surface of freshly reduced iron at 300 °C,[1] whereas Kealy and Pauson obtained the same material upon reaction of C_5H_5MgBr with $FeCl_3$.[2] Pauson was attempting to prepare dihydrofulvalene, **1**, and proposed a structure in which both cyclopentadiene rings were σ-bonded to the metal, **2** (Figure 1.1).

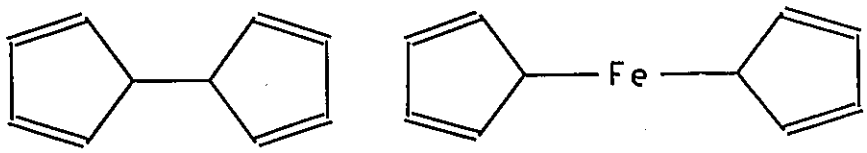

1 **2**

Figure 1.1

It appeared to be very unlikely that the proposed structure was correct since it did not explain the observed diamagnetism and the highly inert character of the new complex. Based on the X-ray diffraction pattern, Fischer suggested a double-cone structure for $(\eta^5\text{-}C_5H_5)_2Fe$ in 1952.[3] In the same year, on the basis of infrared spectroscopic data, Wilkinson and Woodward proposed the sandwich structure and coined the name ferrocene because of its perceived relationship to other aromatic systems (Figure 1.2).[4] This novel structure was confirmed in 1956 by Dunitz and co-workers who obtained the X-ray crystal structure of ferrocene.[5]

Atypical of organometallic systems known at that time, ferrocene was found to be extremely stable, thermally even up to 400°C, and towards air, moisture, and acids. However it was noted that ferrocene reacted with strong oxidizing reagents, *e.g.* HNO_3, to give the ferrocinium ion $(\eta^5\text{-}C_5H_5)_2Fe^+$.

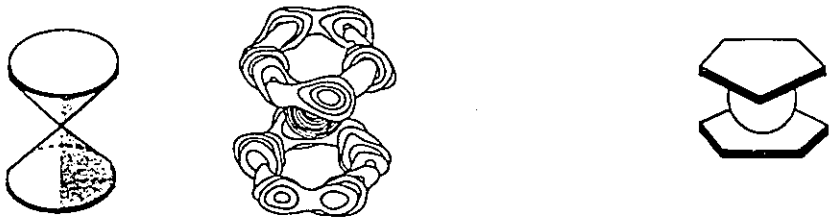

Fischer Wilkinson, Woodward

Figure 1.2 Proposed structures for ferrocene

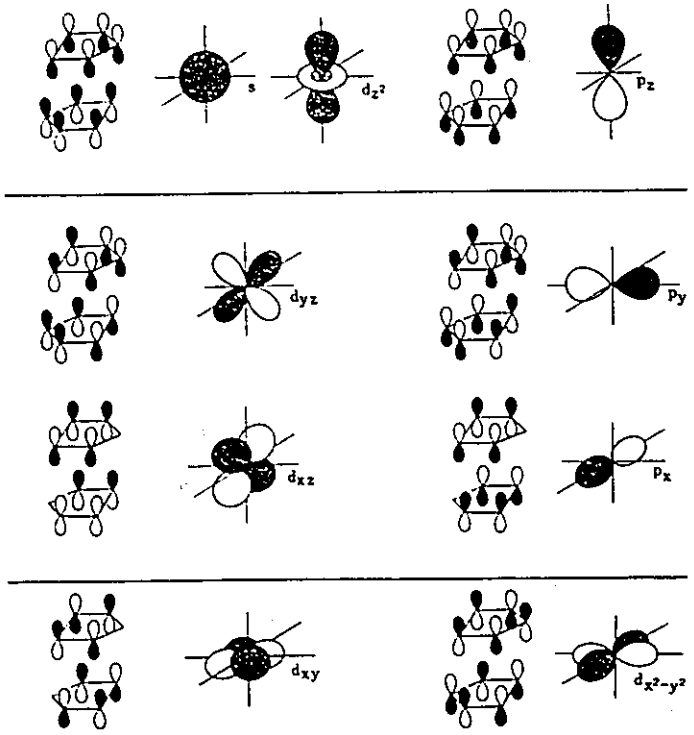

Figure 1.3 Linear combination of atomic orbitals for ferrocene

A generally accepted bonding model which accounts for the chemical stability and also the sites of reactivity of ferrocene is based on the molecular orbital approach. This involves the interaction of linear combinations of ligand orbitals with metal orbitals of the same symmetry (Figure 1.3). Even though some quantitative aspects of the energy level diagram, especially the order of orbitals of similar energy, are still under discussion, a generally accepted molecular orbital scheme for metallocenes can be presented, and is shown in Figure 1.4. One can thus account for the magnetic behaviour of the series of first row metallocenes.

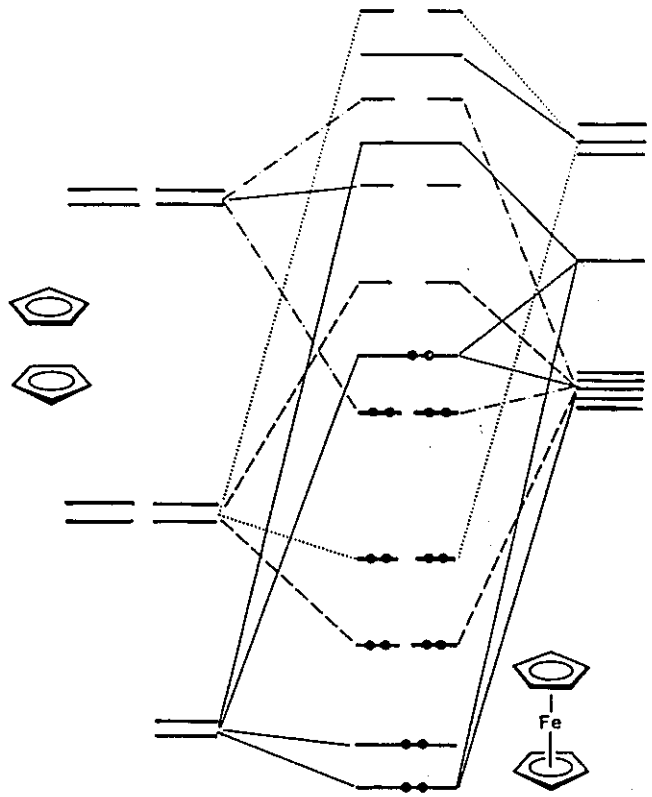

Figure 1.4 Qualitative MO diagram for ferrocene

An important reaction in ferrocene chemistry is the replacement of one of the C_5H_5 rings by an arene, first reported in 1966 by Nesmeyanov.[6] Treatment of ferrocene with $A\ell C\ell_3$, $A\ell$ and the arene, followed by anion metathesis, yields complexes of the type $(\eta^6\text{-arene})Fe(\eta^5\text{-}C_5H_5)^+$ (Scheme 1.1).[7,8]

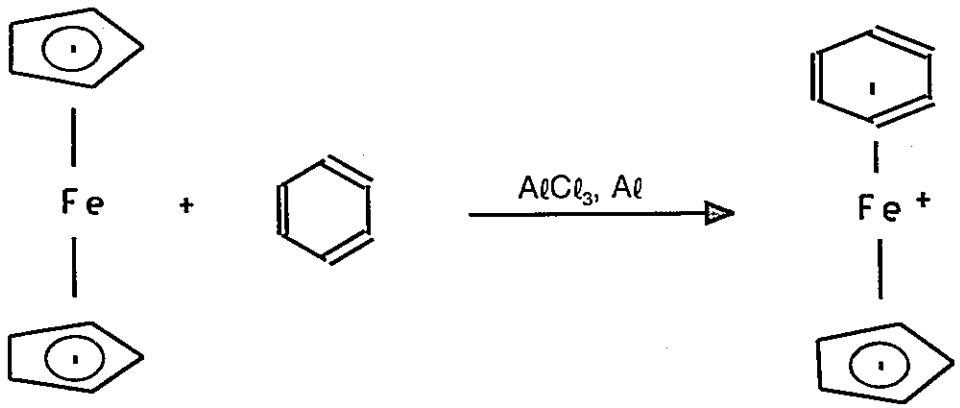

Scheme 1.1

1.1.2 $(C_6H_6)_2Cr$

The bis(benzene)chromium cation, $(C_6H_6)_2Cr^+$ was first prepared in 1919 by Hein. He reacted $CrC\ell_3$ with PhMgBr in diethylether but was unable to identify the "phenyl-chromium" complexes.[9] A rational synthesis was found by Fischer and Hafner in 1955.[10] They prepared the bis(benzene)chromium cation via reaction of $CrC\ell_3$ with benzene, $A\ell C\ell_3$ and $A\ell$; subsequent reduction with sodium dithionite gave the required neutral molecule (Scheme 1.2).

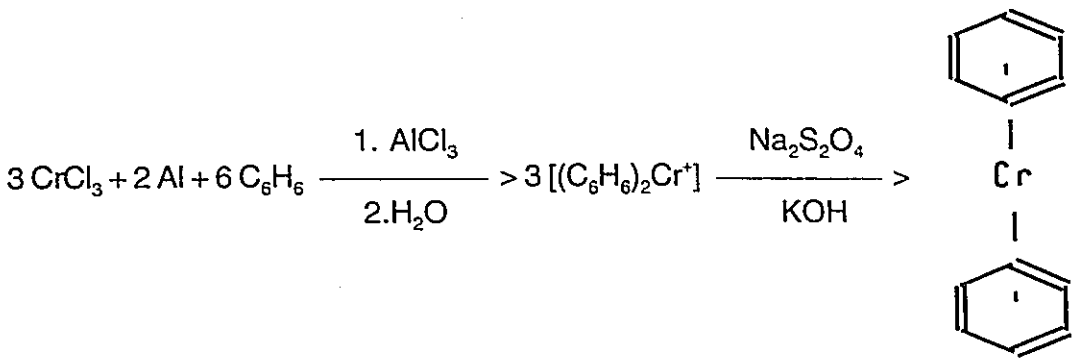

Scheme 1.2

A very important method of preparing neutral arene chromium complexes was developed by Timms in 1969.[11] This involved the vaporization of metals, such as chromium, in a high vacuum system and then cocondensing the these metal vapors with suitable ligands at -196 °C. These techniques were extended by Skell, McGlinchey, Klabunde, Green and others to provide a general route to sandwich complexes in synthetically useful quantities, and yielded such molecules as $(C_6H_5C\ell)_2Cr$, $(C_6F_6)Cr(C_6H_6)$, $(C_6H_6F)_2V$, and $(C_8H_8)_3Ti$.[12]

By analogy to the molecular orbital calculations for ferrocene, a similar approach reveals that the interaction of the π-orbital manifold of the two C_6H_6 ligands with the metal orbitals of the same symmetry gives rise to a molecular orbital diagram for $(C_6H_6)_2Cr$ qualitatively very similar to that of $(\eta^5\text{-}C_5H_5)_2Fe$; the linear combinations of atomic orbitals are shown in Figure 1.5, and the MO scheme is shown in Figure 1.6.

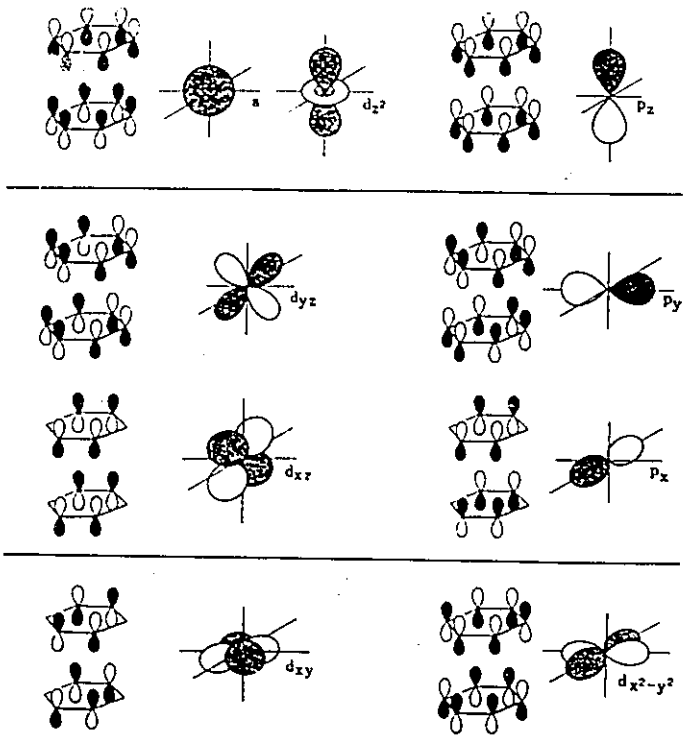

Figure 1.5 Linear combination of atomic orbitals for $(C_6H_6)_2Cr$

A somewhat heated discussion about the structure of $(C_6H_6)_2Cr$ developed shortly after Fischer's preparation of the molecule. The symmetry was believed to be either D_{3h} or D_{6h}. Infrared spectroscopy and neutron diffraction suggested localized double bonds within the C_6H_6 ligands,[13-16] whereas electron diffraction and low temperature X-ray diffraction studies revealed the aromatic character of the ligand, involving equal C-C bond lengths.[17]

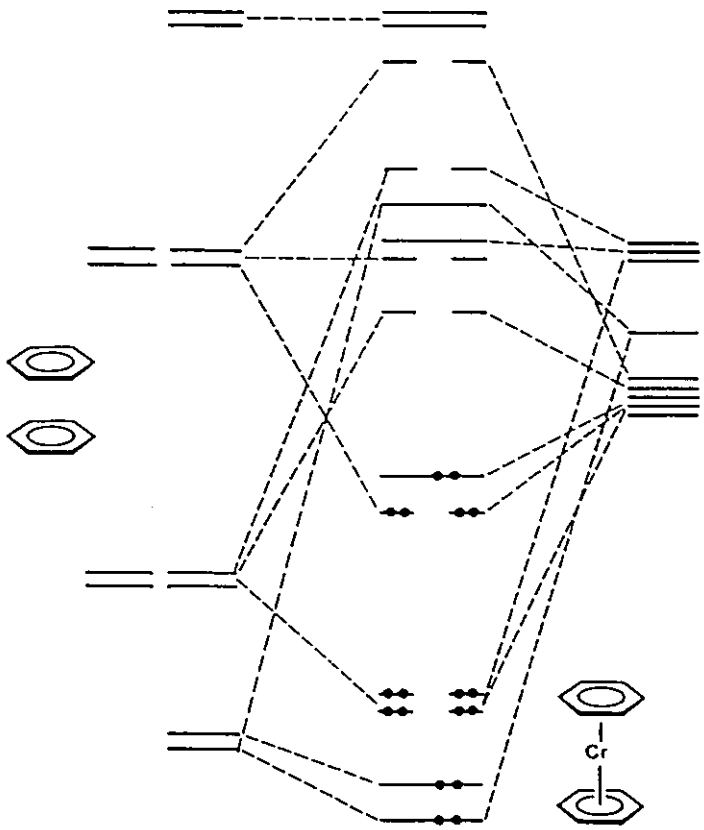

Figure 1.6 Qualitative MO diagram for $(C_6H_6)_2Cr$

1.1.3 $(\eta^6\text{-}C_6H_6)M(CO)_3$ complexes

The tricarbonyl complexes $(\eta^6\text{-}C_6H_6)Cr(CO)_3$ and $(\eta^6\text{-}C_6H_3Me_3)Mn(CO)_3^+$ were first reported in 1957. $(C_6H_6)Cr(CO)_3$ was prepared from $Cr(CO)_6$ and $(C_6H_6)_2Cr$ in a sealed tube at 220°C.[18] However, this route is very inconvenient and limited in scope, and has been replaced by a variety of more straightforward and often high-yield syntheses. The most convenient method is that of the thermal interaction of $Cr(CO)_6$ with C_6H_6, which was reported by three different groups in 1958 (Scheme 1.3).[19-21]

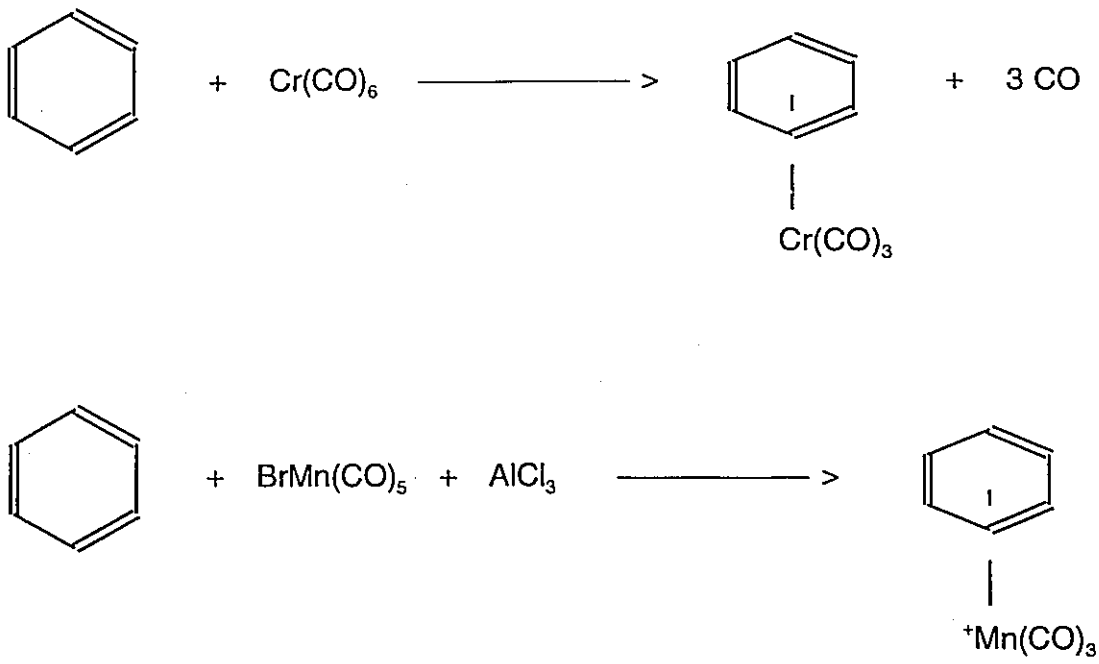

Schemes 1.3 and 1.4

The initial report on the preparation of $[(arene)Mn(CO)_3]^+$ salts is still the most commonly used procedure today.[22] It involves reaction of the arene with $BrMn(CO)_5$ and $A\ell C\ell_3$, followed by anion metathesis (Scheme 1.4).

To understand the bonding in metal carbonyl complexes, it is necessary to consider the molecular orbital picture of carbon monoxide itself. The highest occupied molecular orbital (HOMO) of CO is a σ^* orbital which can overlap with a vacant metal orbital of σ-symmetry to produce a σ-donor interaction. Back-bonding is achieved via donation of a filled metal orbital into the π^* lowest unoccupied molecular orbital (LUMO) of the carbonyl ligand (Figure 1.7). One can then consider that the resulting frontier orbitals of the metal carbonyl fragment, $M(CO)_3$, are able to interact with the π-orbitals of arene or cyclopentadienide ligands. Figure 1.8 shows the interaction of an $Mn(CO)_3^+$ fragment with the $C_5H_5^-$

ligand orbitals and figure 1.9 shows the interaction of an $Cr(CO)_3$ fragment with the C_6H_6 ligand orbitals.

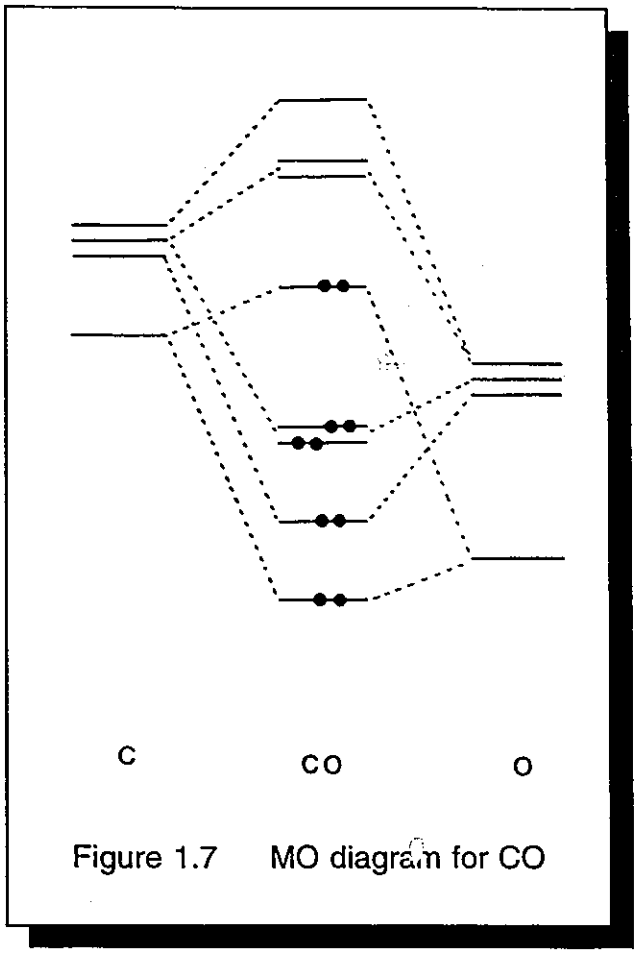

Figure 1.7 MO diagram for CO

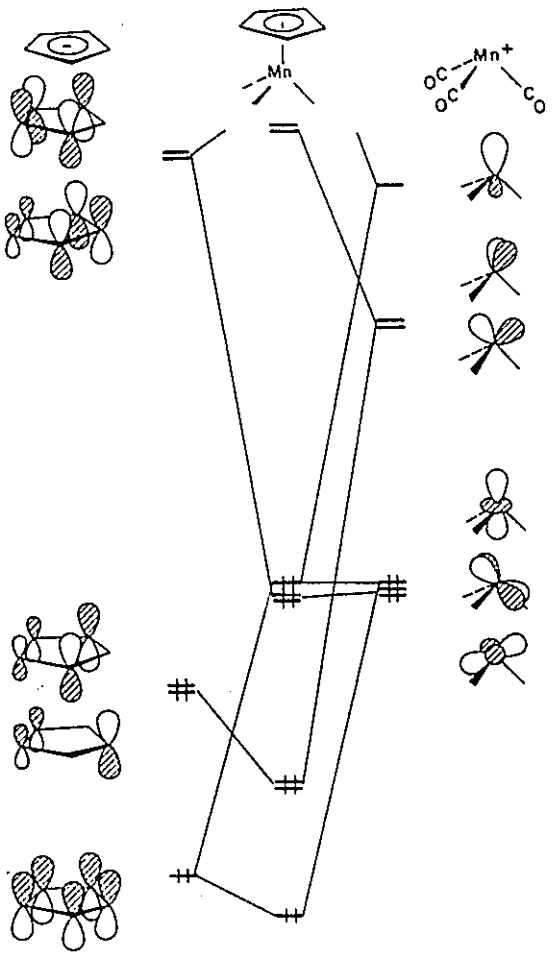

Figure 1.8 Qualitative MO diagram for $(C_5H_5)Mn(CO)_3$

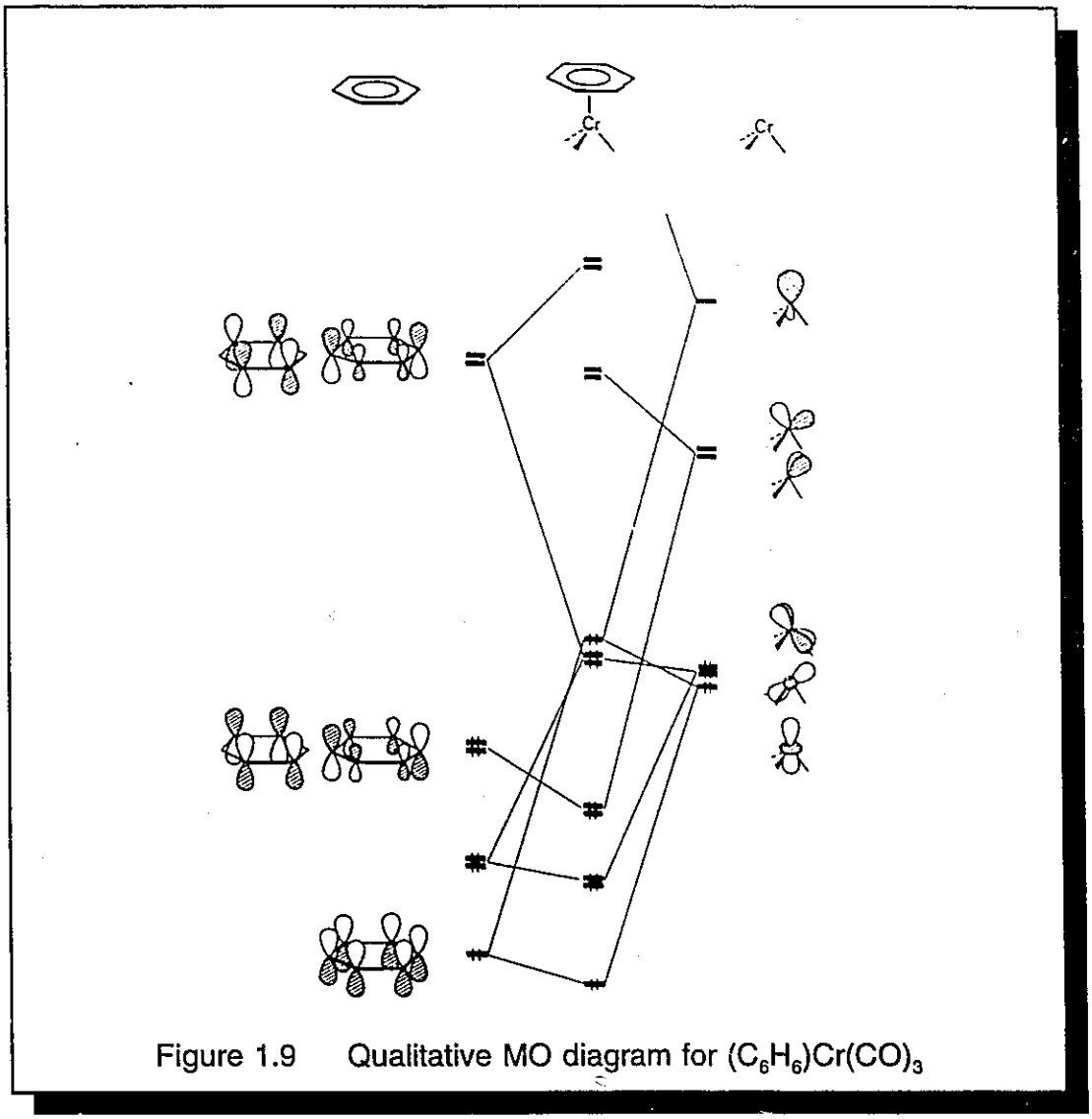

Figure 1.9 Qualitative MO diagram for $(C_6H_6)Cr(CO)_3$

1.1.4 Metal complexes of multi-fused ring systems

In a number of synthetic approaches to benzene complexes, the C_6H_6 ring can be replaced by a multi-fused ring system containing one or more six-membered rings. Polycyclic complexes of $Cr(CO)_3$, $Mn(CO)_3^+$ and $Fe(\eta^5\text{-}C_5H_5)^+$ can be prepared for a number of ligands. It was noted that in all these systems the metal binds to the terminal six-membered ring as depicted in Figure 1.10. This has been explained either by attributing greater aromatic character to a terminal

ring[23] or, alternatively, by noting that in each case the observed isomer leaves conjugated the maximum number of non-complexed rings.[24]

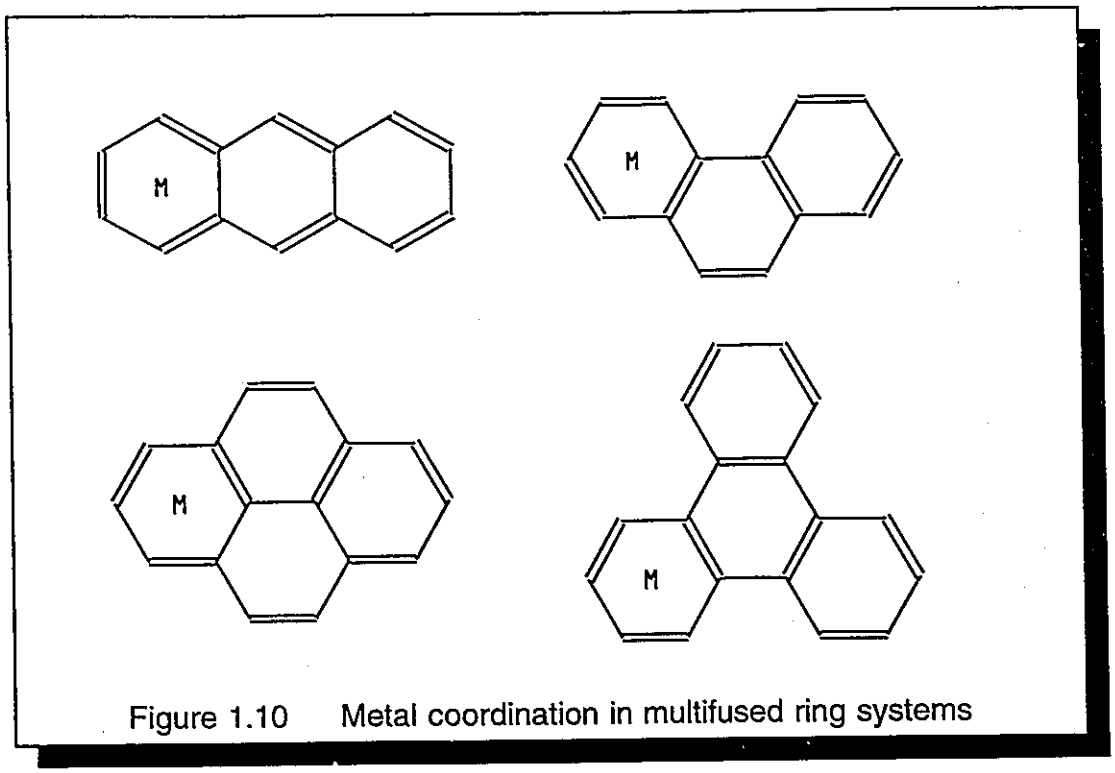

Figure 1.10 Metal coordination in multifused ring systems

1.2 Haptotropic rearrangements

The term haptotropic rearrangement has been coined to cover those cases of rearrangements of organometallic complexes where an ML_n unit changes its connectivity (hapto number) to some ligand with multicoordinate site possibilities.[25] In general, these reactions can be described as $(\eta^n\text{-L'})ML_x \rightarrow (\eta^m\text{-L'})ML_y$ ($n \neq m$, $x \neq y$), in which the ligand L' changes its coordination number to the metal M from n to m. Haptotropic rearrangements can be divided into two classes. Ring slippage reactions cover those cases in which the metal remains coordinated to the same ring, whereas in inter-ring metal migrations the metal fragment changes coordination between adjacent rings in a multi-fused ring system.

1.2.1 Ring slippage reactions

For a number of years it was believed that the bonding in all η^5-C_5H_5 transition-metal complexes involved a uniform interaction between the five carbon atoms of the cyclopentadienyl ring and the metal atom.[26] However, in 1963 Dahl and Wei reported structural evidence for inequivalent metal-C_5H_5 bonds in $(\eta^5$-$C_5H_5)Ni[C_7H_5(CO_2CH_3)_2]$.[27] The following year Bennett made similar observations for a number of π-cyclopentadienyl transition-metal complexes.[28] In succeeding years many complexes were described as containing the C_5H_5 ligand, bonded in a η^3 fashion. Most of the compounds were formulated to be η^5 coordinated on the basis of the 18 VE rule. However, in all cases, X-ray diffraction studies disproved the existence of an η^3-cyclopentadienyl ligand.

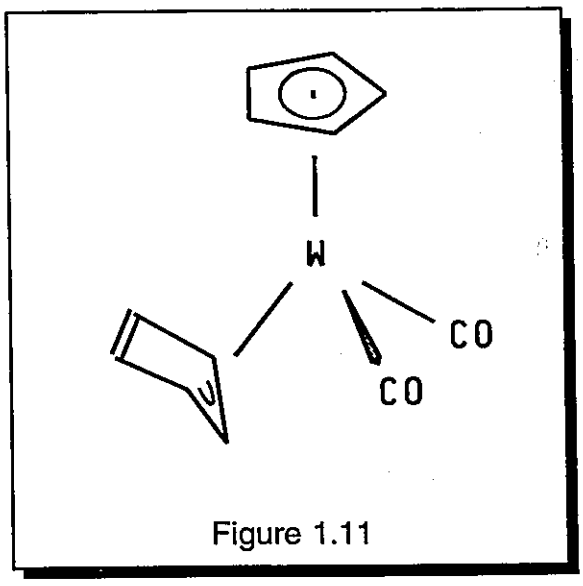

Figure 1.11

It was not until 1978 when Huttner et al.[29,30] published the crystal structure of $(\eta^3$-$C_5H_5)(\eta^5$-$C_5H_5)W(CO)_2$ in which one of the C_5H_5 rings was found to be significantly bent (Figure 1.11). By reaction of $(\eta^5$-$C_5H_5)_2W(CO)$ with excess CO, ring slippage from η^5 to η^3 was observed for the first time.

Within 3 years of the determination of the structure of ferrocene, the first η^1-C_5H_5 complexes were reported in the literature, none of which were synthesized by ring slippage from η^5-C_5H_5 complexes.[31,32] In 1978 Hames, Legzdins and Martin reported the first case in which a η^5-C_5H_5 complex, $(\eta^5$-$C_5H_5)_2Cr$, was converted to an isolable, well characterized η^1-C_5H_5 complex, $(\eta^1$-$C_5H_5)(\eta^5$-$C_5H_5)Cr(NO)_2$ (Figure 1.12).[33]

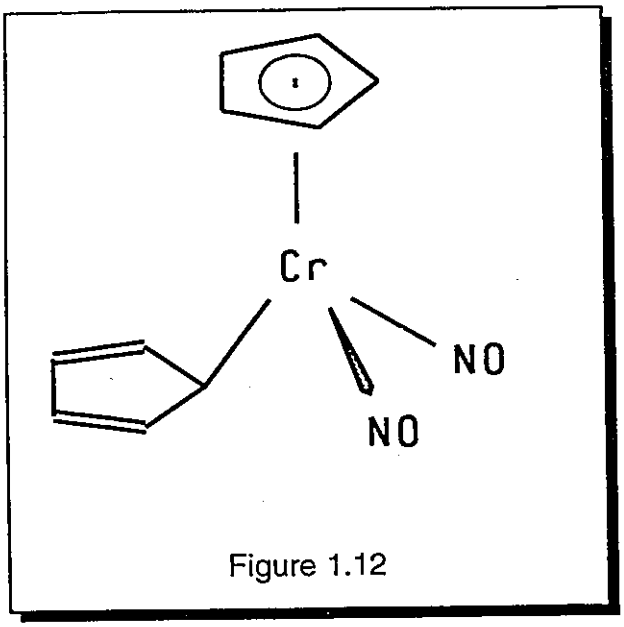

Figure 1.12

In the above cases, ring slippage is observed, a type of metal migration in which the metal fragment changes its coordination number to the ligand, but remains bonded to the same ring. Ring slippage has played an important role in the explanation of the facile replacement of carbonyl ligands by phosphines in indenyl complexes of rhodium.[34] Addition of phosphines to $(\eta^5\text{-}C_9H_7)Rh(CO)_2$ is believed to proceed via the trihapto transition state (or short-lived intermediate) $(\eta^3\text{-}C_9H_7)Rh(CO)_2(PR_3)$, which possesses a conjugated six-membered ring. This stabilization can not occur in the analogous C_5H_5 complex and has been termed the *indenyl effect* (Scheme 1.5).

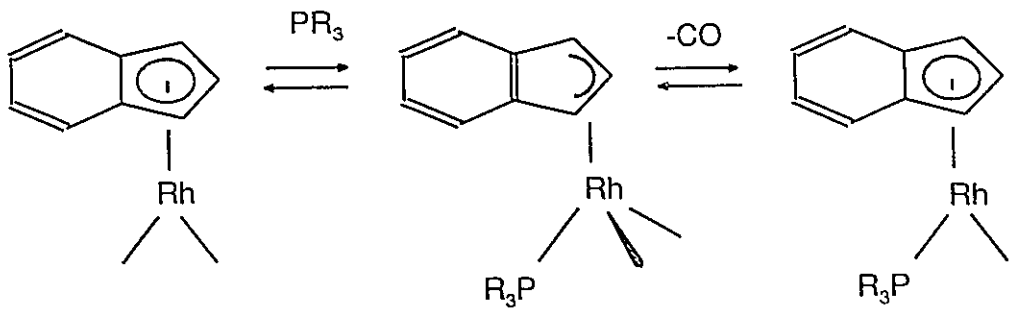

Scheme 1.5

1.2.2 Inter-ring metal migrations

As mentioned above, the term haptotropic rearrangement has been coined to cover those cases of rearrangements of organometallic complexes where an ML_n unit changes its connectivity (hapticity) to some ligand with multicoordinate site possibilities.[25] In the majority of the cases, inter-ring metallotropic rearrangements of transition-metal π-complexes of polycyclic aromatic systems have been studied (Figure 1.13).

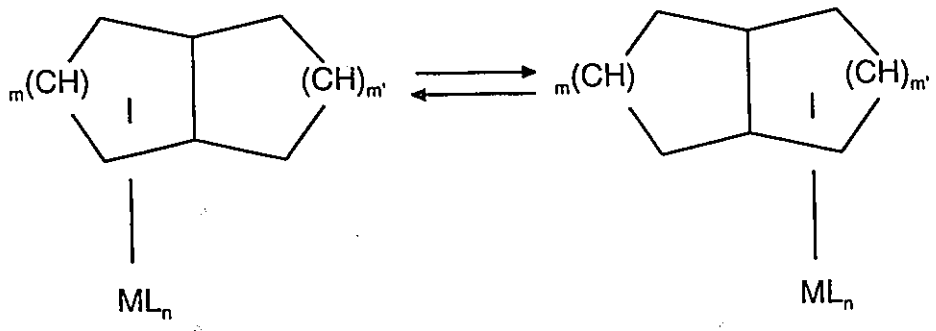

m = 1, 2, 3; m' = 1, 2, 3

Figure 1.13 Inter-ring metal migrations

The first publication of a haptotropic inter-ring rearrangement was presented by Müller et al. in 1969.[35] Upon irradiation of (bis-benzo[ae]cyclooctatetraene) $Cr(CO)_4$, the irreversible migration of chromium from the eight- to the six-membered ring was observed (Scheme 1.6).

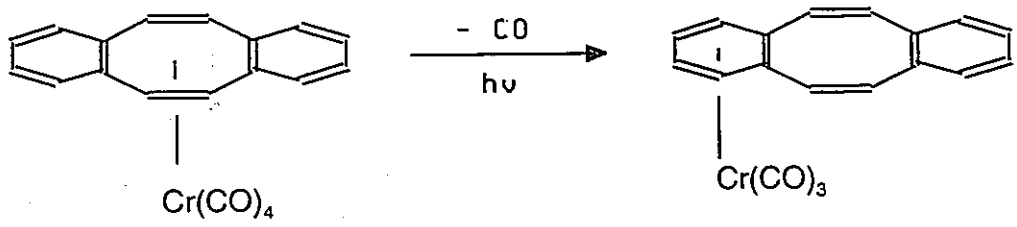

Scheme 1.6

Among the most intensively studied aromatic systems are organometallic complexes of naphthalene, anthracene, indene and fluorene. In the case of naphthalene transition-metal complexes, rearrangement between two six-membered rings can only be observed if one of the rings is substituted so they become different[36] (Scheme 1.7).

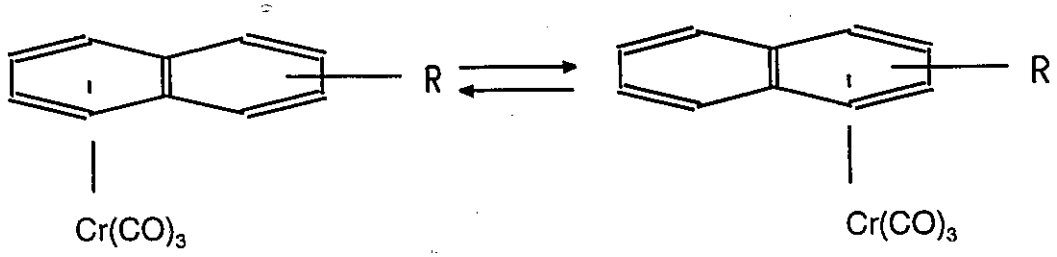

Scheme 1.7

Complexes of naphthalene have been reported for Ni,[37-39] Co,[40] Cr,[41-43] Rh[45] and Ir.[44,45] A few examples of haptotropic rearrangements in metal complexes of anthracene are known for Co[40] and Ni.[39,46] Recent studies on the metal migration in the case of Ni suggest that it involves η^2 and η^4 complexes (Scheme 1.8).

However, synthesis of these complexes is not trivial and the rearrangement behaviour has not been fully understood.

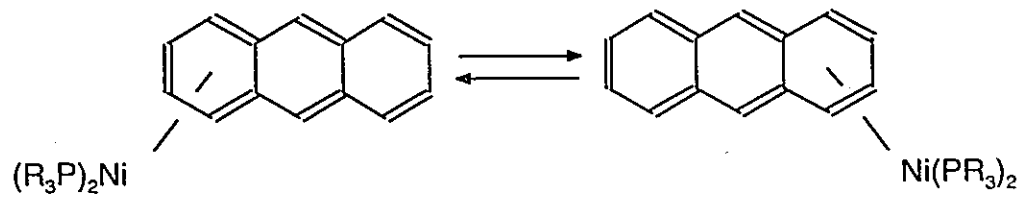

Scheme 1.8

Rearrangements in complexes of the indenyl ligand are the simplest cases of metal migrations between rings of different sizes. Complexes of indene and indenyl have been studied for Fe,[47] Re,[48] Rh,[45] Ir,[44,45] Cr,[49] Mo[49,50] and W.[49,50]

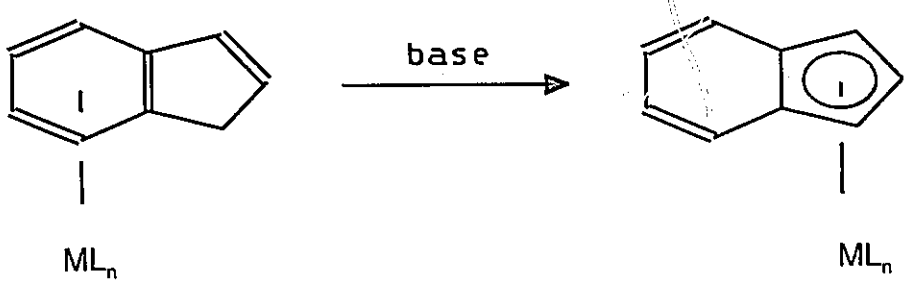

Scheme 1.9

Most of the rearrangements are of the type $\eta^6 \rightarrow \eta^5$ in which η^6 complexes of indene are treated with base to yield the η^5 isomers. These rearrangements are particularly well understood for complexes of $Cr(CO)_3$, $Mo(CO)_3$, $W(CO)_3$ and $Mn(CO)_3^+$ (Scheme 1.9). The reverse rearrangement was observed upon protonation of bis(η^5-indenyl)iron. This led to the isolation of (η^5-indenyl) Fe (η^6-indene)$^+$. The protonation was believed to take place at the metal, with subsequent proton migration to the ligand[47] (Scheme 1.10). Moreover, protonation of (η^5-indenyl)Rh(C_2H_4)$_2$, **3a**, or (η^5-indenyl)Rh(1,5-cyclooctadiene), **3b**, yields the

corresponding cationic η^6-complexes, **4a** and **4b**, respectively.[51] Interestingly, use of deuterated acids leads to incorporation of deuterium into the ethylene ligands of **3a**; this provides strong evidence that the initial protonation occurs at the metal center (Scheme 1.11).

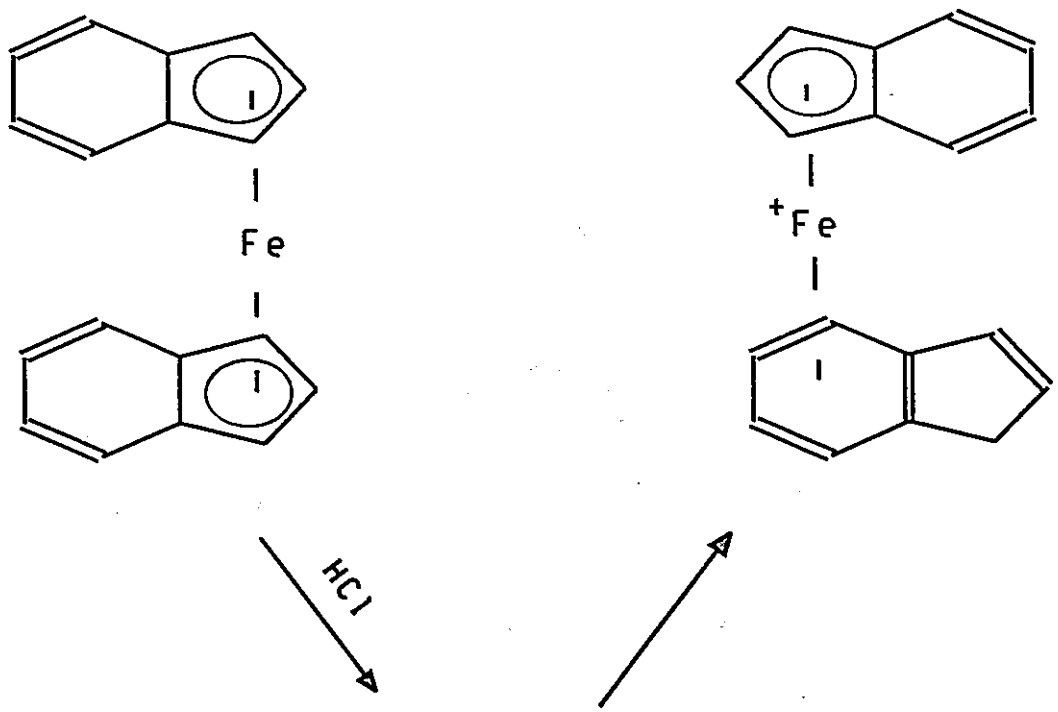

Scheme 1.10

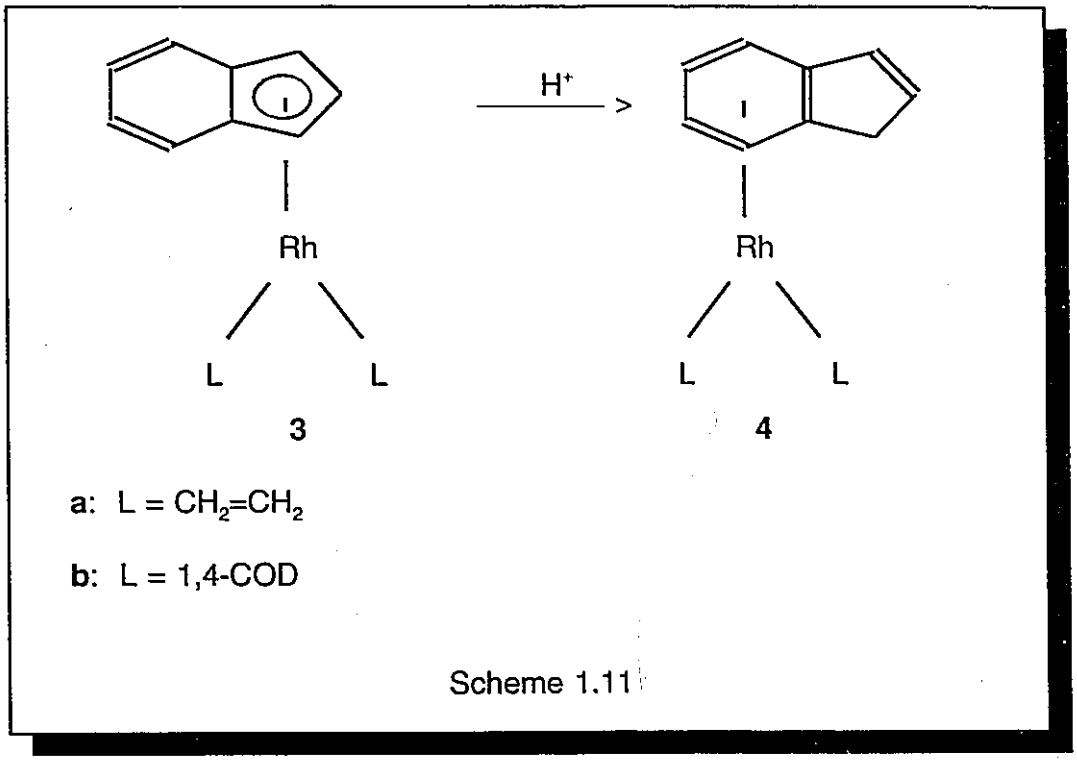

Scheme 1.11

Recently, a study by Siebert et al.[52] expanded the chemistry of haptotropic rearrangements to mixed iso/hetero-aromatic systems.

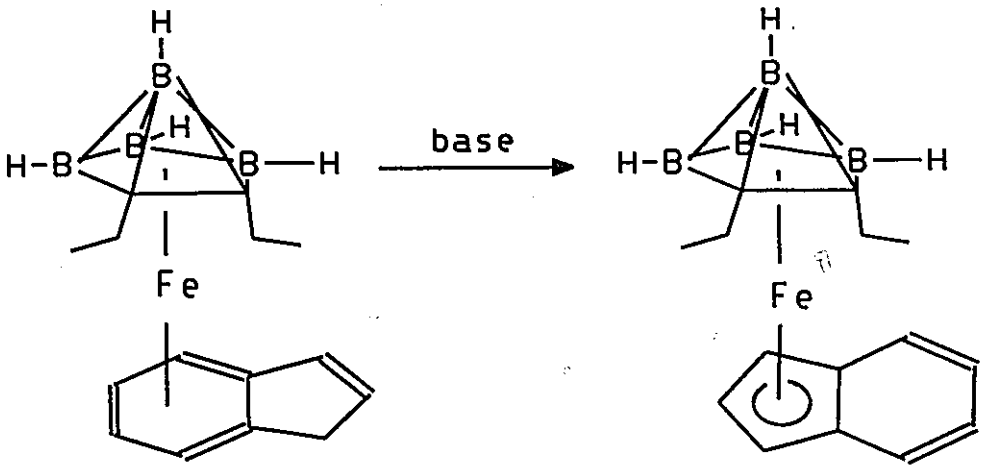

Scheme 1.12

Employing the isolobal replacement of $C_5H_5^-$ by the carborane cluster $(CR)_2(BH)_4$ led to the investigation of the rearrangement behaviour of the first carborane ferrocene analogue (Scheme 1.12).

The most intensively studied and best understood rearrangements are the ones of fluorenyl transition-metal complexes. Fluorenyl complexes of Cr,[49,53] Mo,[49] W,[49] Rh,[45] Ir,[44,45] Co,[40] Mn,[54] and Fe[55] have been prepared. However, studies on haptotropic rearrangements have mainly concentrated on complexes of Cr, Mn and Fe.

Nicholas and co-workers described the haptotropic rearrangement of $(C_{13}H_9)Cr(CO)_3^-$ in 1971.[54] Upon deprotonation of $(C_{13}H_{10})Cr(CO)_3$, a rapid equilibration was observed (Scheme 1.13).

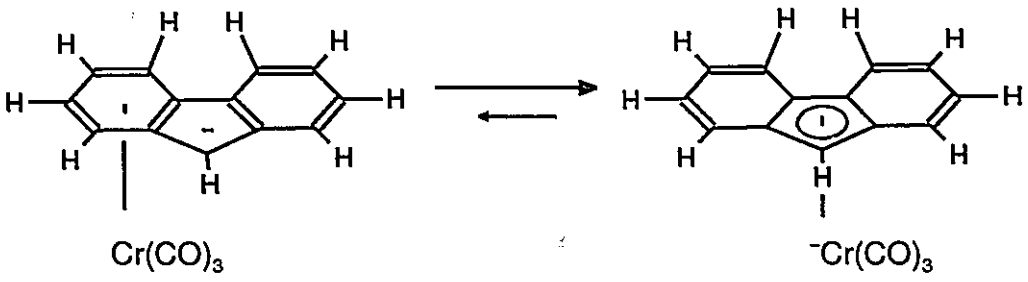

Scheme 1.13

The complexes were found to be very labile and sensitive towards heat, moisture and air. Attempts to isolate the K or Na salts of $(C_{13}H_9)Cr(CO)_3^-$ were unsuccessful and the compounds could only be studied in solution. A more practical approach was used by Treichel et al. in 1976. Starting from cationic fluorene complexes of Mn and Fe, deprotonation yielded the neutral compounds $(\eta^6\text{-}C_{13}H_9)Mn(CO)_3$ and $(\eta^6\text{-}C_{13}H_9)Fe(\eta^5\text{-}C_5H_5)$ (Scheme 1.14). The crystal structures of both molecules revealed that although the metals are coordinated to

the six-membered ring, they were displaced away from one of the ring junction carbons.[55] Moreover, the plane containing the five-membered ring and the non-complexed six-membered ring is folded away from the plane of the five metal-bonded carbons by approximately 10°.[56,57]

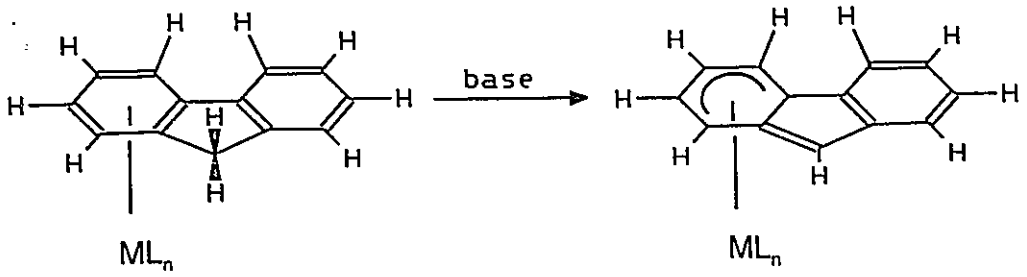

$ML_n = Mn(CO)_3$, $Fe(C_5H_5)$

Scheme 1.14

This important observation probes the question as to whether these complexes may be seen as a zwitterion **5a**, in which the metal would be centrally coordinated, or as a compound bearing a double bond in the five-membered ring, **5b** (Figure 1.14).

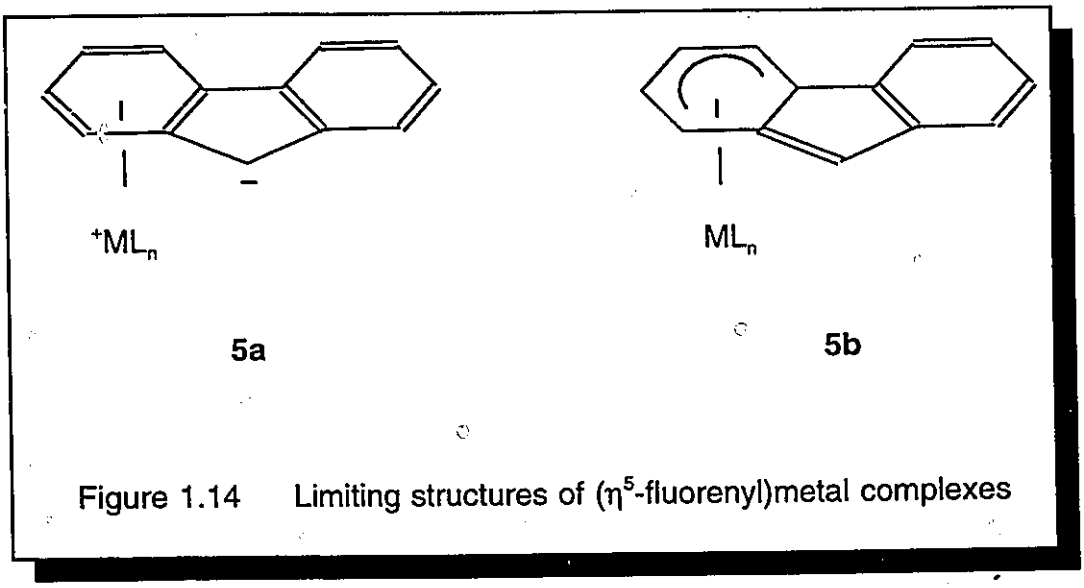

Figure 1.14 Limiting structures of (η^5-fluorenyl)metal complexes

The crystal structures suggested that these complexes employ a bonding pattern best described as η^5, **5b**. However, in order to differentiate between complexes in which the metal is η^5 bonded to the five-membered ring, the η^5 nomenclature is used exclusively for compounds in which the metal is coordinated to a five-membered ring.

It is relevant to note that the simplest (benzyl)Fe(η^5-C_5H_5) complex to have been crystallographically characterized is Astruc's ($C_5Me_5C{=}CH_2$)Fe(η^5-C_5H_5) system in which the exocyclic methylene group is folded away from the plane of the five-membered ring by 33°.[58] EHMO calculations favour a bend of only 10°, but the steric hindrance attributable to the presence of the methyl groups can account for this anomaly.[59]

The η^6-fluorenyl complexes of Mn and Fe did not rearrange at ambient temperatures. However, upon heating (η^6-$C_{13}H_9$)$Mn(CO)_3$ in refluxing hexane for 1h, (η^5-$C_{13}H_9$)$Mn(CO)_3$ was obtained (Scheme 1.15).[56a]

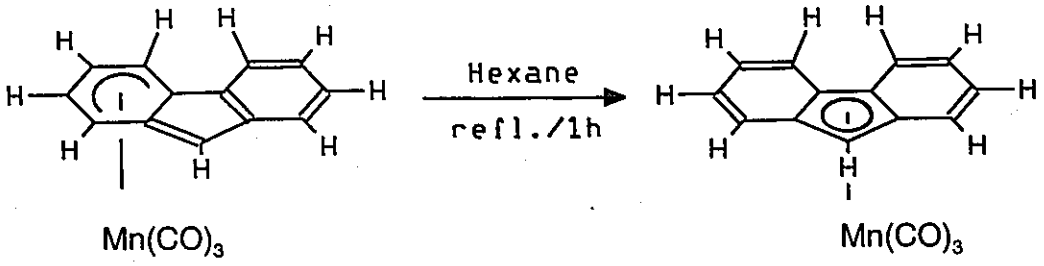

Scheme 1.15

It could be shown that for sufficiently high concentrations of strong organic acids, the η^6 to η^5 rearrangement of the complex can be reversed.[60]

Since then, attempts have been made to prepare (η^5-$C_{13}H_9$)Fe(C_5H_5) from (η^6-$C_{13}H_9$)Fe(C_5H_5) by thermal rearrangement, but no reliable evidence has proven

the existence of the ferrocene analogue. Treichel et al. reported the decomposition of the iron complex upon thermal treatment, [56b] whereas Ustynyuk published a communication on the successful rearrangement in 1986.[61] Unfortunately, the spectral evidence is not convincing, even though the same research group reported two more synthetic approaches to prepare $(\eta^5\text{-}C_{13}H_9)Fe(\eta^5\text{-}C_5H_5)$. This point remains unresolved.

This particular area of organometallic research has also attracted attention in other aspects, besides synthetic exploitation. The main interest has been focused on the mechanisms of haptotropic rearrangements. On the basis of kinetic data, a unimolecular mechanism has been proposed [62] and indeed the process has been shown to be intra-molecular by means of cross-over experiments.[63] In this light, inter-ring migrations have been subject of considerable theoretical interest, notably by Albright, Hoffmann and their colleagues.[25] In particular, it has been shown that the ability of organometallic fragments to migrate across the surfaces of polycyclic systems can be rationalized in terms of the interactions between the frontier orbitals of the ML_n moiety and of the π system. For example, the metallotropic shift of a $(\eta^5\text{-}C_5H_5)Fe$ unit in the indenyl anion, shown in Figure 1.15a, is calculated to proceed not via a least-motion pathway from ring center to ring center (route **A**) but rather via an exocyclic η^3 transition state **B**.[25] In contrast, EHMO calculations on the $[(\text{pentalene})Fe(\eta^5\text{-}C_5H_5)]^+$ system, shown in Figure 1.15b, suggest that a $(C_5H_5)Fe$ moiety can move across the common bond between the two rings; however, even in this case, the trajectory does not follow the least-motion pathway.[25]

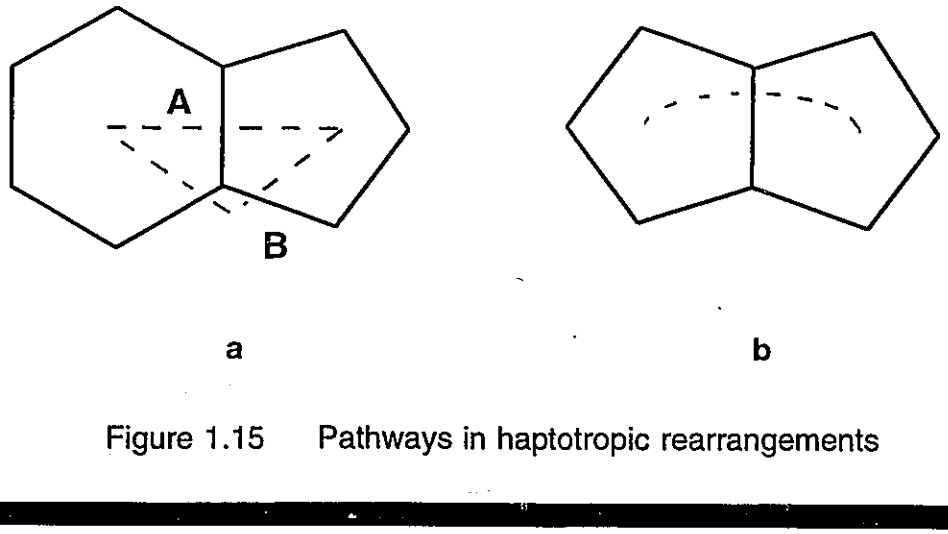

Figure 1.15 Pathways in haptotropic rearrangements

Chapter 2: The ligand

The molecule 4H-cyclopenta[def]phenanthrene (cppH), **6**, contains the carbon skeletons of indene, acenaphthylene, phenanthrene and fluorene (see Figure 2.1).

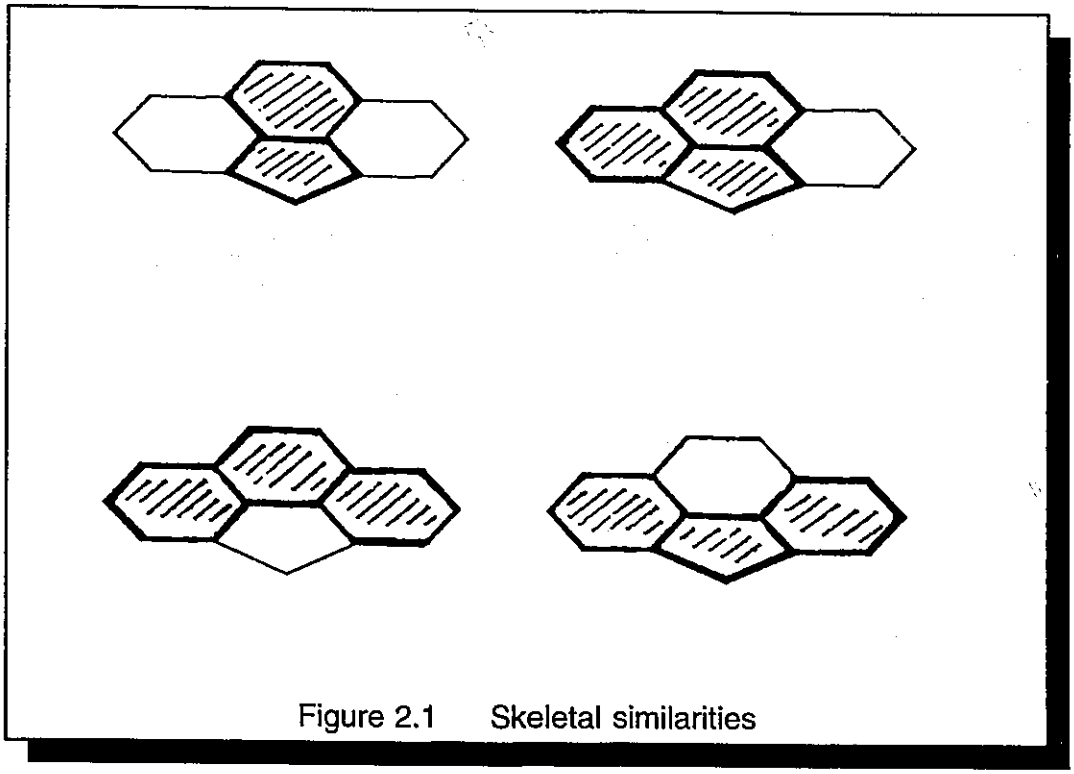

Figure 2.1 Skeletal similarities

Transition-metal complexes of these ligands exhibit quite different chemical behaviour and one might speculate whether complexes of the cppH ligand might adopt the characteristics of complexes of one of the aforementioned ligands, or instead whether its behaviour would not resemble any of the known multi-fused ring systems. Analyzing the π-orbitals of cppH, **6** and cpp^-, **7**, it appears that the

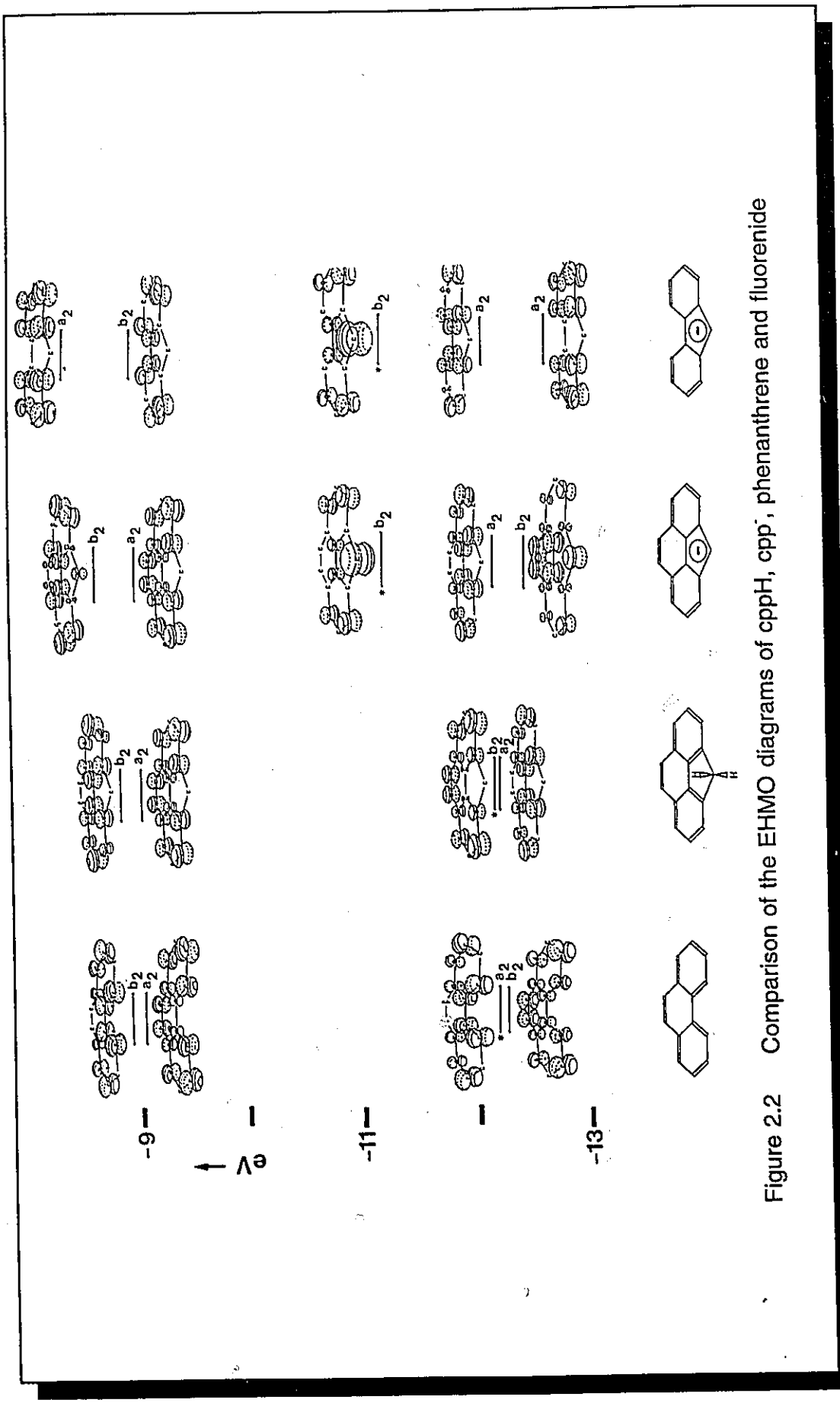

Figure 2.2 Comparison of the EHMO diagrams of cppH, cpp$^-$, phenanthrene and fluorenide

molecular orbital pattern of cppH itself closely resembles that for phenanthrene; in contrast, the frontier orbitals of $C_{15}H_9^-$, *i.e.* the cpp anion, match those of the fluorenide anion in that the HOMO has a large p_z coefficient at the C(4) position (Figure 2.2). One can deduce from these calculations that the organometallic chemistry of cppH itself will be rather similar to that of phenanthrene, whereas the chemistry of cpp^- should be analogous to that of fluorenide.

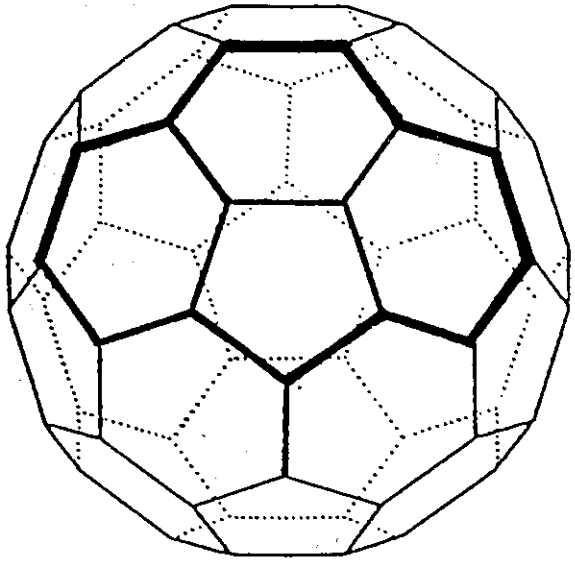

Figure 2.3 CppH represents 25% of the C_{60} skeleton

Furthermore it should be noted that cpp represents 25% of the C_{60} framework (Figure 2.3). Only a few metal complexes of C_{60} are known, in all of which the metal binds in a η^2-fashion.[64] Rearrangements in these complexes have

not so far been observed. CppH is the largest multi-fused ring system available for organometallic synthesis, in which the skeleton is part of the C_{60} framework. Corannulene which represents ⅓ of the C_{60} framework, can only be prepared on a very small scale, insufficient for organometallic research (Figure 2.4).[65,66]

CppH is an attractive ligand because it offers multiple sites for the attachment of organometallic moieties which can potentially bind in an η^6-, η^5-, η^4-, η^3-, η^2- or η^1- fashion. To our knowledge, no transition metal complexes of this ligand have been reported.

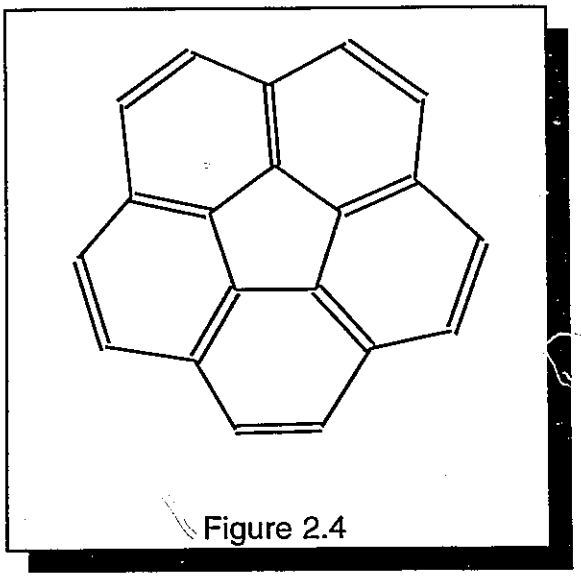

Figure 2.4

Moreover, deprotonation of η^6-complexes of the cppH ligand provides the opportunity for haptotropic shifts by ML_n units from (or through) six-membered rings to a five-membered ring. Of particular significance here is the fact that the π-electron count in the 4H-cyclopenta[def]phenanthrene system can be conveniently reduced by two merely by hydrogenating the C(8)=C(9) double bond. Thus one can make direct comparisons between polycyclic molecules possessing the same skeletal geometry but with different frontier orbital patterns.

It may appear somewhat simplistic to assume that merely closing the structure of fluorene by means of a 1,2-ethylidene bridge, to obtain the tetracyclic cppH ligand, should bring about different chemical behaviour of the ligand complexes. However, indenyl and fluorenyl complexes show different behaviour and the behaviour of tetracyclic versus di- and tricyclic ring systems as ligands in

metal migration reactions can not be predicted easily. It is noteworthy that there are very few literature reports in which a system that had considerable potential to undergo haptotropic rearrangements did not in fact exhibit fluxional properties.

Chromium complexes of multi-fused organic ligands are known to undergo rapid rearrangement even at very low temperature.[67] One exception was found in (fluoradene) $Cr(CO)_3$. Deprotonation of the neutral complex did not lead to the expected η^5-fluoradene compound (Scheme 2.1).[68]

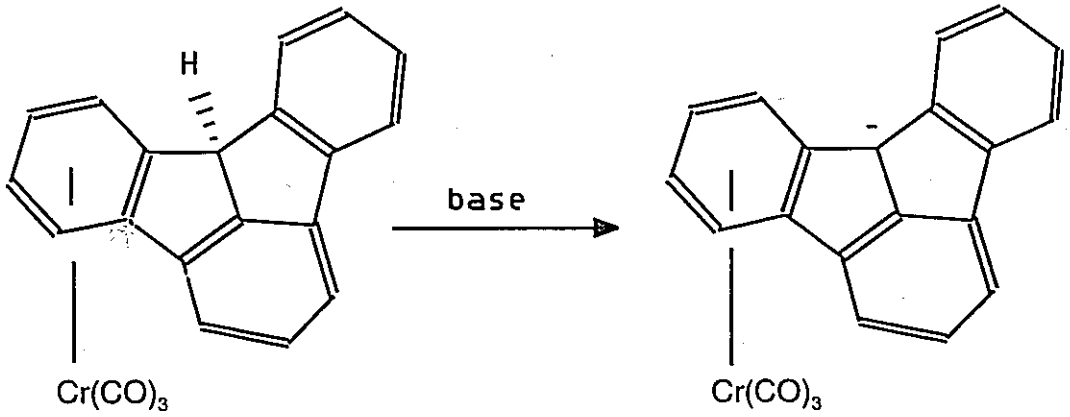

Scheme 2.1

A very interesting paper on the structural dependence of rearrangements was published in 1990 by Ustynyuk and co-workers.[69] Comparing the behaviour of $Mn(CO)_3$ complexes of cis- and trans-indenoindene, it was found that a haptotropic rearrangement can only be observed for the cis isomer (Scheme 2.2).

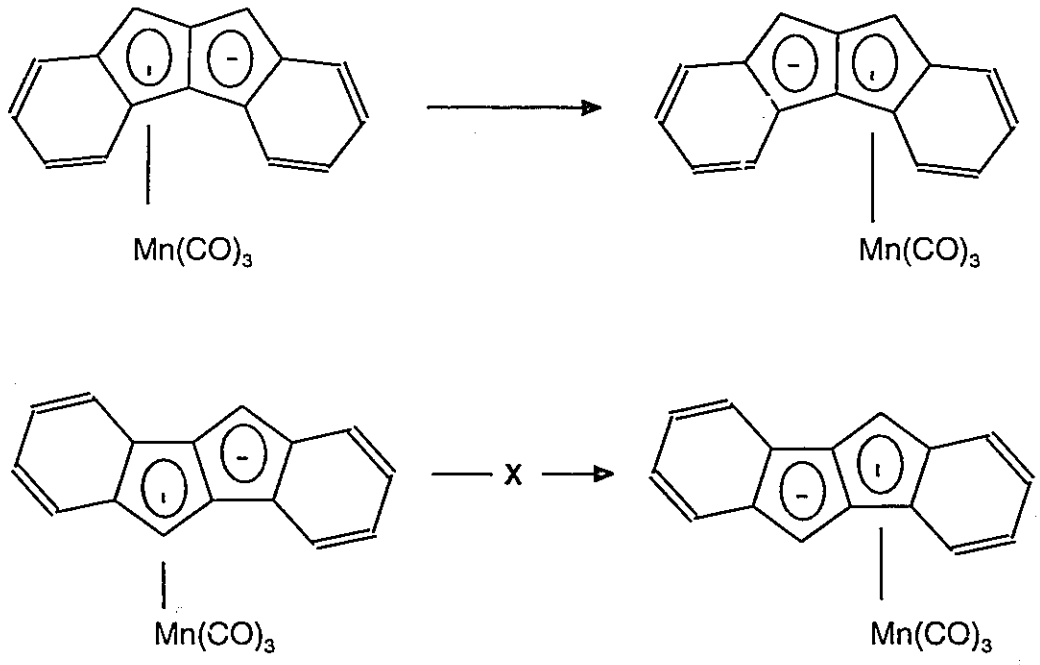

Scheme 2.2

Only a few bi- or tri-metallic polycyclic complexes have been prepared. Examples include $[(naphthalene)Cp_2Fe_2]^{2+}$ and $[(phenanthrene)Cp_2Fe_2]^{2+}$ or $(fluorene)[Cr(CO)_3]_2$. A very interesting system, trans-$[Mn(CO)_3]_3$-truxene is shown in Scheme 2.3.[70]

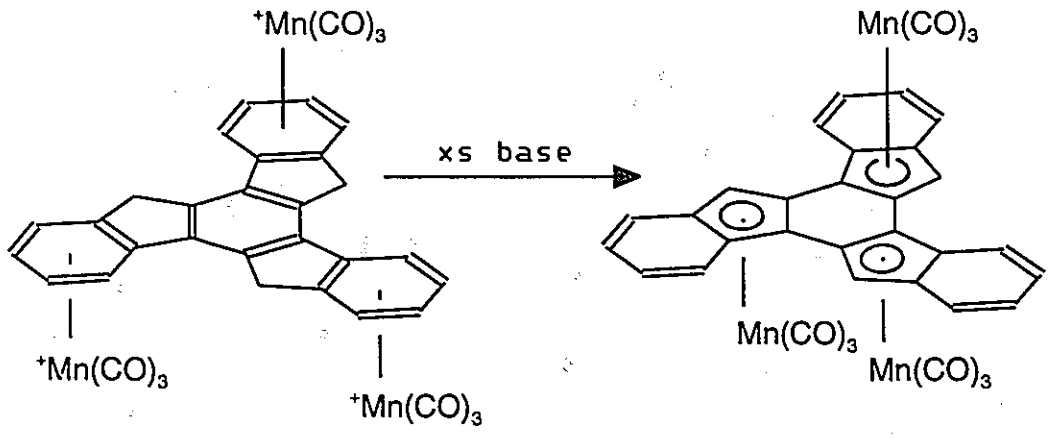

Scheme 2.3

Unfortunately, the all η^6-isomer (i.e., the initial organometallic compound) was not isolated and a stepwise rearrangement using equimolar amounts of base not attempted. Therefore, information about the rearrangement mechanism is not available and a concerted mechanism can not be excluded. These few examples are the only ones where investigations of haptotropic rearrangements of transition-metal complexes of large multifused ring systems have been undertaken. The results suggest that even small changes to the molecular geometry of the hydrocarbon ligands can have a significant influence on the metal migrations in the corresponding transition-metal complexes. A particularly fascinating feature of the cppH / H_2-cppH ligand system is that it offers the possibility of comparing haptotropic rearrangements in fluorene metal complexes with a tetracyclic ring system that contains the fluorene skeleton of variable electron count (14π versus 12π).

As mentioned previously, no transition metal complexes of cpp or cppH have been reported in the literature. Furthermore, very little is known about the organic chemistry of cppH, as well as the molecular and crystal structure of this ligand. Growing crystals of X-ray quality appeared to be a severe problem. The molecule crystallizes in thin plates of very little scattering power. Crystals grown from the melt, by vapour diffusion techniques and slow evaporation of the solvent were unsuitable for crystal structure refinement. The carbon atom positions were found to be disordered which could not be modeled and the structure could not be refined properly. Only crystals grown by chilling a saturated hexane solution for a period of several weeks could be used to obtain a data set that gave a satisfactory refinement. Further improvement by obtaining a data set at low

temperature failed as the crystals shattered upon cooling the sample. There are two independent molecules in the unit cell and, moreover, there is a disorder problem (which is further discussed on p. 39 and p. 99); the crystal structure of one of these molecules is shown in figure 2.5.

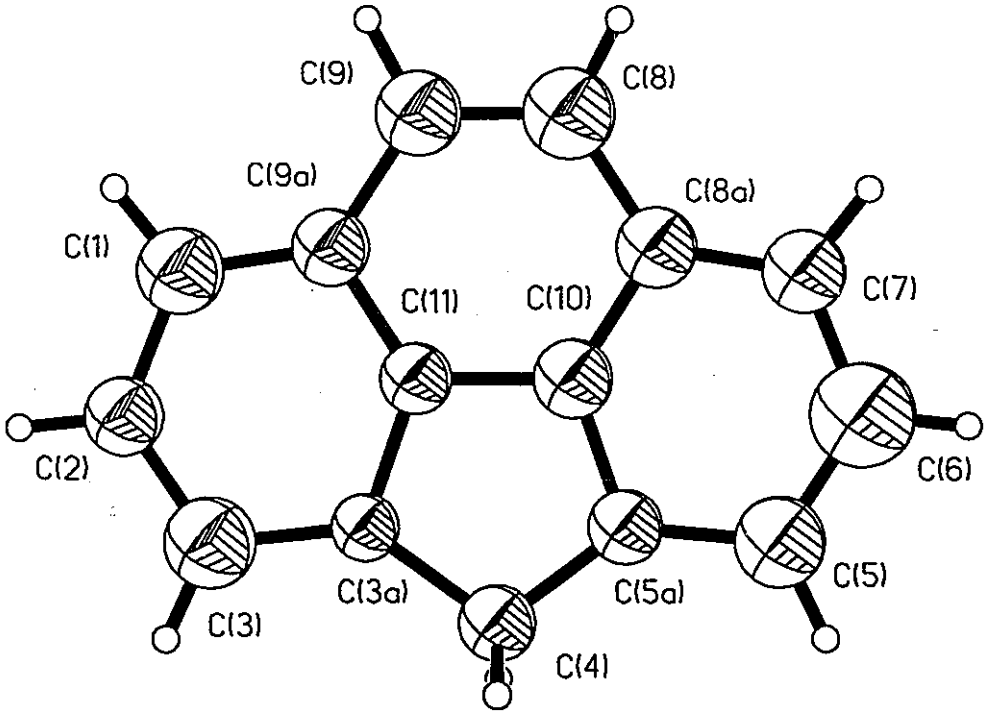

Figure 2.5 X-ray crystal structure of cppH, **6**

Chapter 3: Synthesis and Characterization of η^6-complexes of cppH

Haptotropic rearrangements have been studied for a variety of ligands and metal fragments. With very few exceptions, these systems have been investigated starting from η^6-complexes. Our first goal in this project was to prepare a number of organometallic derivatives of cppH.

3.1 Chromium complexes of cppH

The reaction of 4H-cyclopenta[def]phenanthrene (cppH), **6**, with chromium hexacarbonyl following standard procedures yields the complex (η^6-cppH)$Cr(CO)_3$, **8**, in which the tripodal fragment is attached to a terminal six-membered ring (Scheme 3.1).

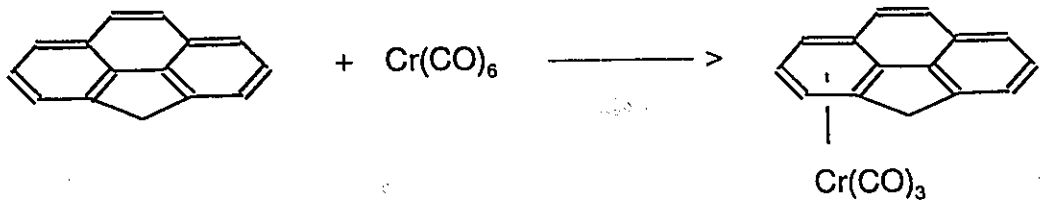

8

Scheme 3.1

Formation of this isomer parallels the behaviour of other polyaromatic complexes in which the metal binds preferentially to an outer ring of the polycyclic system (see Chapter 1, p. 13).[71] Although the assignments of the ^{13}C and ^{1}H NMR

resonances of **8** were made by standard one- and two-dimensional techniques, the attribution of the *exo* and *endo* methylene protons at C(4) was not so trivial. This was achieved by taking advantage of the anisotropic solvent-induced shift (ASIS) effect.[72] As depicted in Figure 3.1, successive addition of aliquots of benzene to a $CD_2C\ell_2$ solution of **8** led to a greater increase in shielding of one of the aforementioned methylene protons. It is the *exo* hydrogen which is the more exposed to the anisotropic solvent and so the attributions are evident.

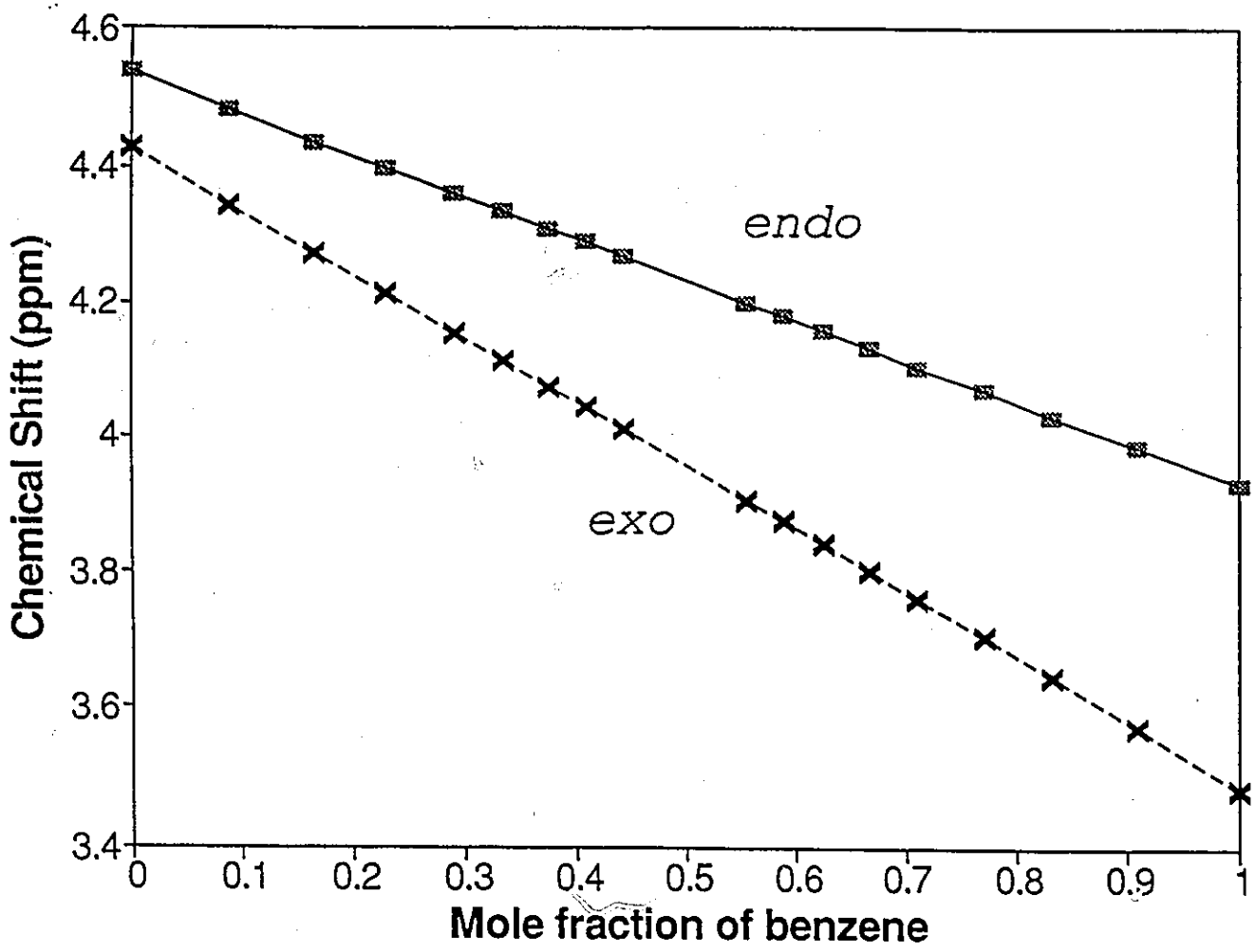

Figure 3.1 ASIS titration for $(\eta^6\text{-cppH})Cr(CO)_3$, **8**

The analogous dihydro- and octahydro-complexes can be prepared in a

similar fashion. Hydrogenation of cppH on Pd/C yielded 8,9-dihydro-4H-cyclopenta[def]phenanthrene, H_2cppH, **9**, and the octahydro derivative H_8cppH, **10**. Reaction with $Cr(CO)_6$ yielded the complexes (η^6-H_2cppH)$Cr(CO)_3$, **11**, and (η^6-H_8cppH)$Cr(CO)_3$, **12** (Scheme 3.2).

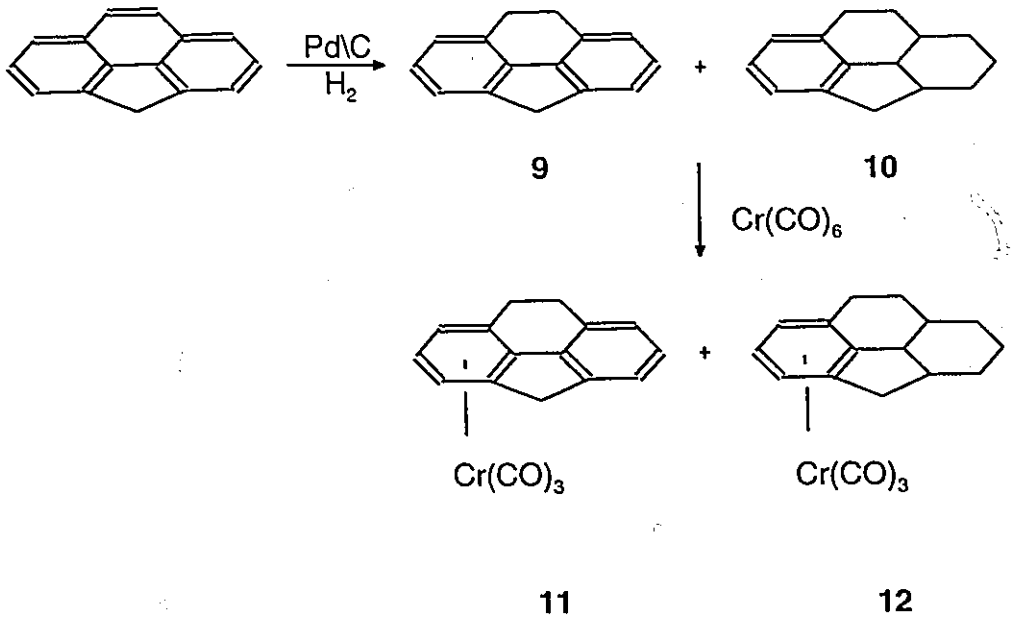

Scheme 3.2

Again, the assignments of the ^{13}C and ^{1}H NMR resonances of **11** were made by standard one- and two-dimensional NMR techniques. Examining the ASIS effect on **11** for different concentrations of benzene, it is apparent that it is necessary to obtain a complete series of spectra in order to eliminate misinterpretation of data. In many cases,[72b] ASIS effects are only investigated using two data points (*i.e.* 100% $CH_2C\ell_2$ and 100% benzene). As can be seen in Figure 3.2, the curves for the *exo* and *endo* protons cross, and this can only be observed if the spectra are measured over a full range of concentrations.

The assignments of the peaks in (η^6-H_8cppH)$Cr(CO)_3$, **12**, required a more

thorough NMR investigation. The assignments of the ^{1}H and ^{13}C NMR resonances were made on the basis of 1D and 2D NMR techniques.[73]

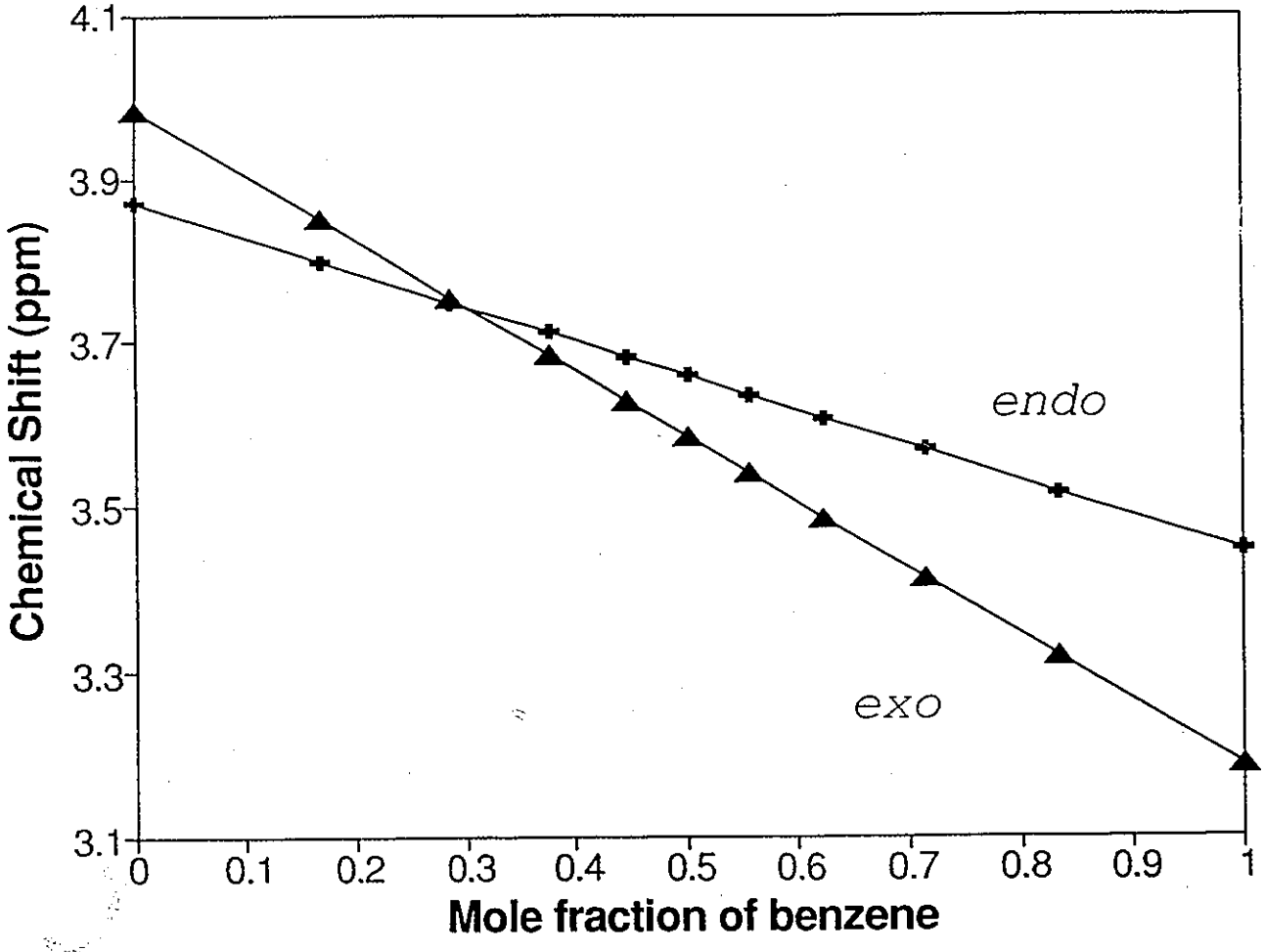

Figure 3.2 ASIS titration for (η^6-H_2cppH)Cr(CO)$_3$, **11**

The structure of the complex (η^6-cppH)Cr(CO)$_3$, **8**, was readily deduced from its ^{1}H and ^{13}C NMR spectra but the establishment of the orientation of the tripodal substituent required an X-ray crystallographic determination. The preferred orientation of the tripod has been calculated in (phenanthrene)Cr(CO)$_3$, **13**, and X-ray data are in accord with this prediction (Figure 3.3) in that the tripod adopts the

orientation **13b**.[71c] Our EHMO calculations on $(\eta^6\text{-cppH})Cr(CO)_3$, **8**, indicate that it should mirror the behaviour of **13**. The X-ray crystallographically determined structure of **8** appears as Figure 3.4 and reveals that the tricarbonylchromium tripod adopts the EHMO-predicted orientation.

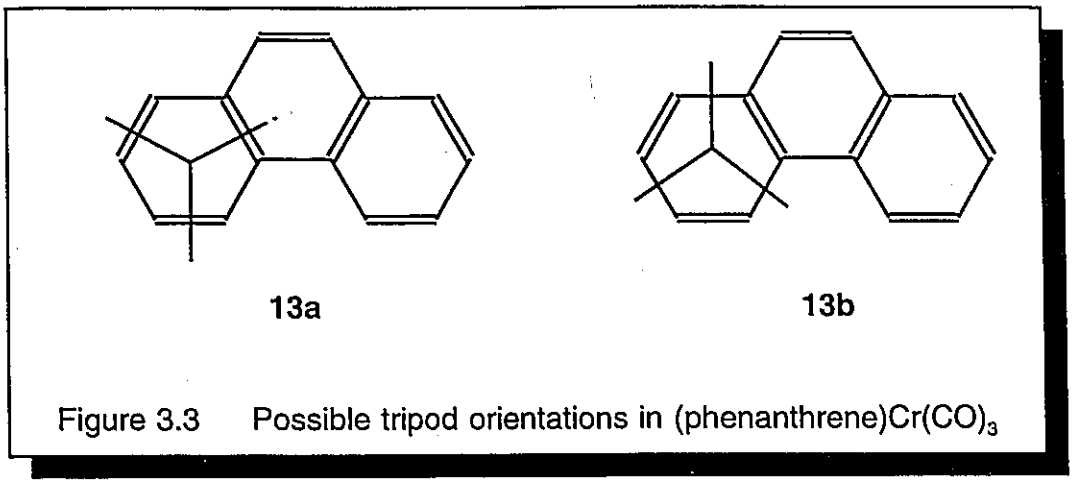

Figure 3.3 Possible tripod orientations in (phenanthrene)$Cr(CO)_3$

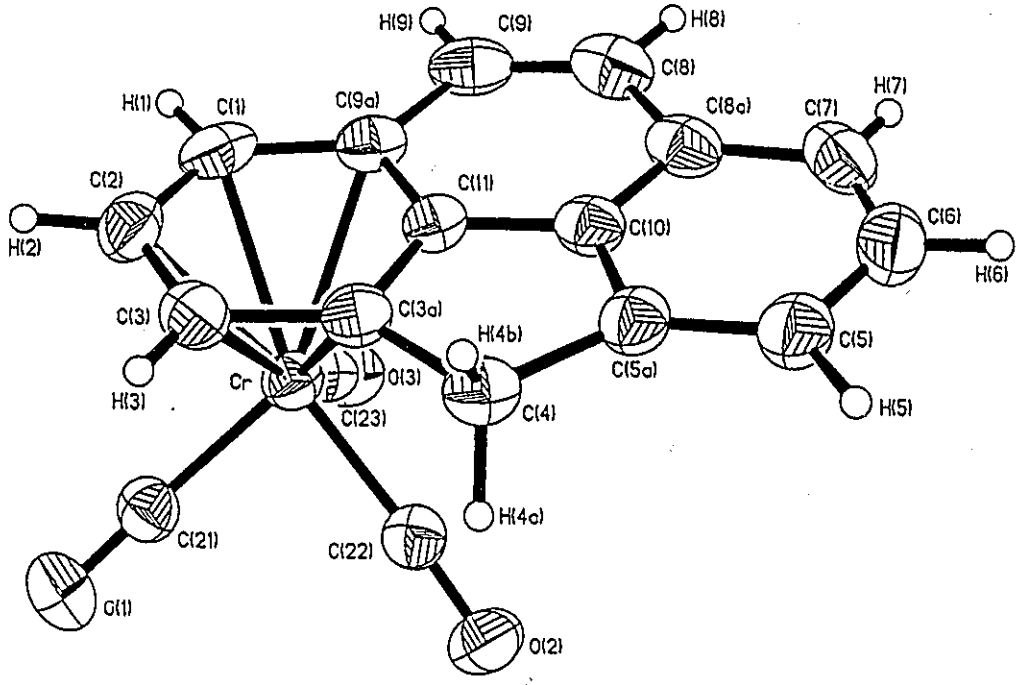

Figure 3.4 X-ray crystal structure of $(\eta^6\text{-cppH})Cr(CO)_3$, **8**

It is noteworthy that the tetracyclic ring system in **8** is not planar but instead bends in a gentle arc away from the organometallic fragment. The interplanar angle between the two external six-membered rings is 5.2°. The free ligand cppH, **6**, crystallizes in thin plates in which the atom positions were found to be disordered so the extent of deviation from planarity is unknown.

The deviation from planarity can be compared with the crystal structure of (η^6-dihydroanthracene)$Cr(CO)_3$ in which the metal is bonded to the concave face of the ligand;[74] a view of which appears as Figure 3.5. This result should be compared with the molecular and crystal structure of the analogous 9,10-dihydro complex (η^6-H_2-cppH)$Cr(CO)_3$, **11**, a view of which appears as Figure 3.6. The most obvious point is that the ligand is no longer a flat molecule with a gentle arc but instead the external arene rings are twisted through 7.1° relative to each other. The C(8)-C(9) bond is no longer coplanar with the "fluorene-like" tricyclic unit but rather adopts a half-chair conformation such that the benzylic methylene unit bonded to the chromium-complexed ring is *exo* with respect to the metal fragment. This has the effect of twisting the non-complexed half of the molecule. (We note that a preliminary report on the molecular structure of (9,10-dihydrophenanthrene)$Cr(CO)_3$ appeared a number of years ago[75] and the non-planarity of the tricyclic ligand was detected.) It is also instructive to look at the packing of the molecules in the unit cell.

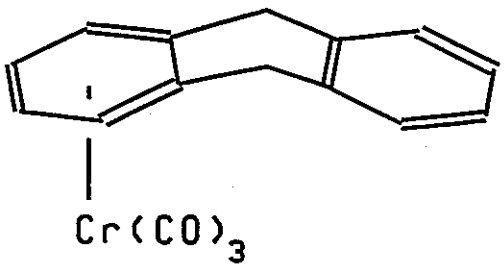

Figure 3.5

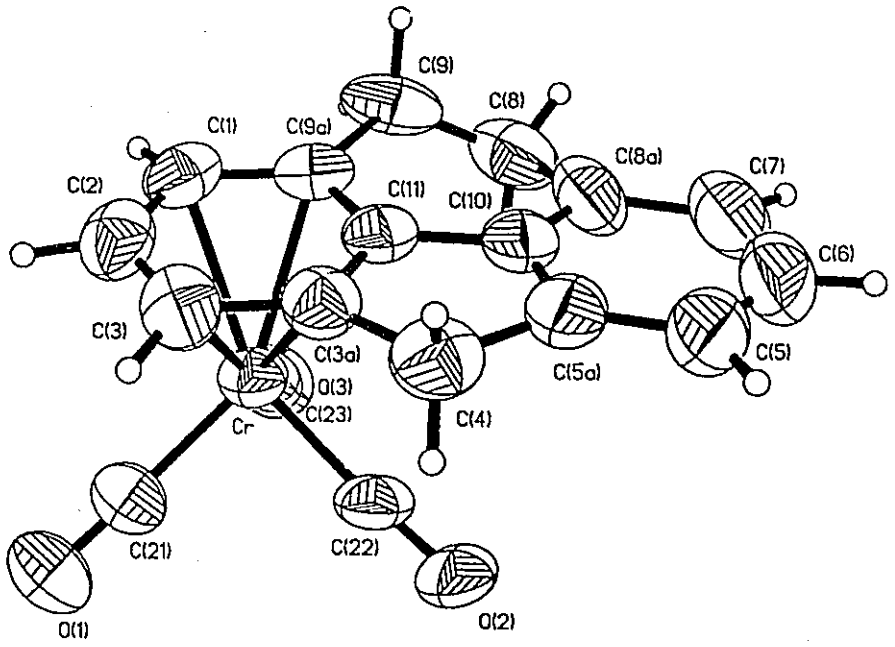

Figure 3.6 X-ray crystal structure of $(\eta^6\text{-}H_2\text{cppH})Cr(CO)_3$, **11**

The molecules of **8** are arranged in a head-to-head manner such that closest neighbors have their tetracyclic ligands aligned parallel to each other at an inter-plane distance of 3.45 Å. From a comparison of the crystal packing of $(\eta^6\text{-}H_2\text{-cppH})Cr(CO)_3$, **11**, with $(\eta^6\text{-cppH})Cr(CO)_3$, **8**, it appears superficially (see Figure 3.7) that the two are rather similar. However, a view along an orthogonal direction (Figure 3.8) reveals that in the dihydro-complex **11** there has been a slippage of one molecule relative to its nearest neighbor. The net result of hydrogenating the C(8)-C(9) bond is not only an increase in the inter-plane distance from 3.45 Å in **8** to 3.6 Å in **11** but also in the volume of the unit cell by 5.5% relative to that of **8**.

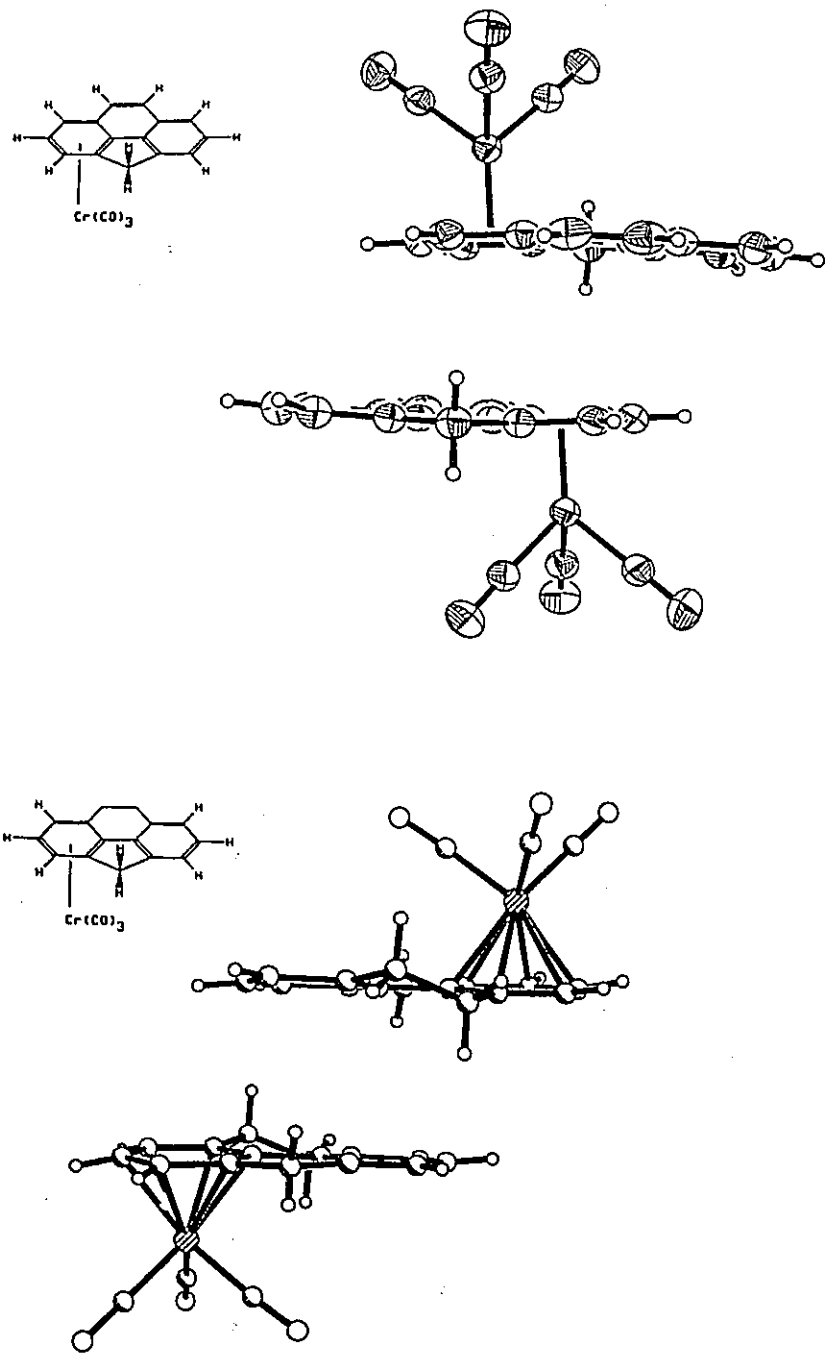

Figure 3.7 $(\eta^6\text{-cppH})Cr(CO)_3$ and $(\eta^6\text{-}H_2\text{cppH})Cr(CO)_3$, view 1

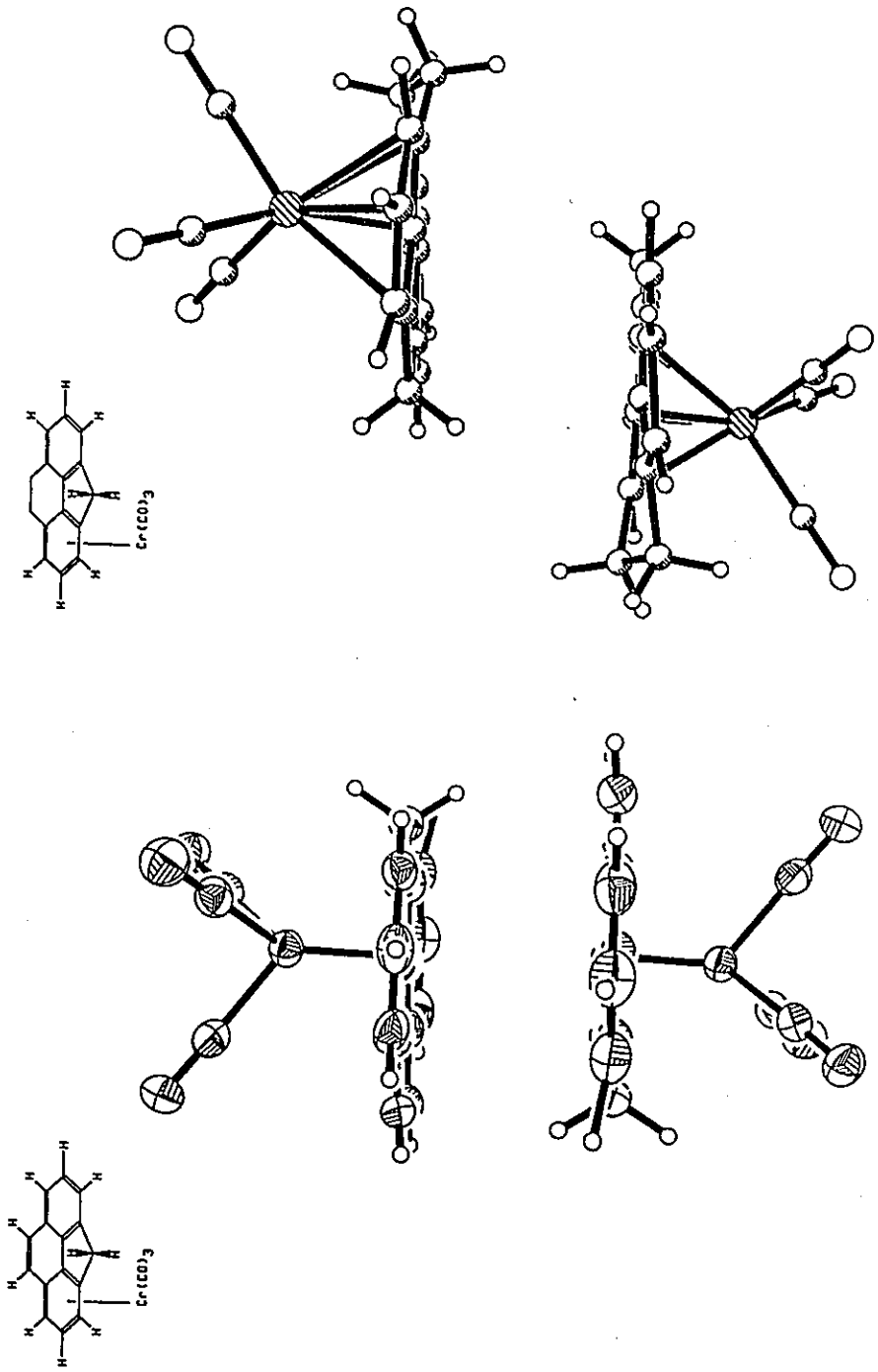

Figure 3.8 (η^6-cppH)$Cr(CO)_3$ and (η^6-H_2cppH)$Cr(CO)_3$, view 2

The corresponding inter-planar separations in $(\eta^5\text{-cpp})Mn(CO)_3$ and in $[(\eta^6\text{-cppH})Fe(\eta^5\text{-}C_5H_5)]^+ PF_6^-$ are 3.40 Å and 3.35 Å, respectively (the structures of these molecules will be discussed in following chapters).

A very intriguing structure was determined for $(\eta^6\text{-}H_8\text{cppH})Cr(CO)_3$, **12**, in which only one of the rings remains unsaturated. This aromatic ring, to which the $Cr(CO)_3$ fragment is coordinated, was found to be planar. The other terminal six-membered ring is in a chair conformation, the internal six-membered ring in a half-chair conformation and the five-membered ring is in an envelope conformation (Figure 3.9). This pattern of ring conformations is reminiscent of steroidal systems in which the A ring is planar and aromatic (in the estrogens), the B ring adopts a half-chair, and the C and D rings have chair and envelope conformations (for example, in cholesterol).

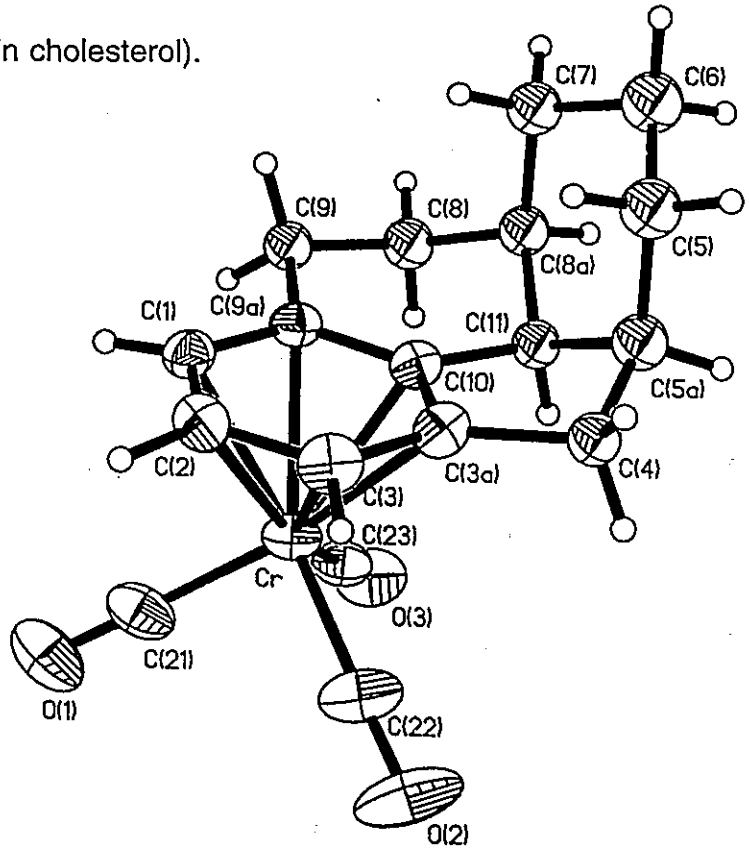

Figure 3.9 X-ray crystal structure of $(\eta^6\text{-}H_8\text{cppH})Cr(CO)_3$, **12**

3.2 Iron complexes of cppH

In contrast to the synthesis of the cation $[(\eta^6\text{-phenanthrene})Fe(C_5H_5)]^+$ which is always accompanied by much hydrogenation of the C(8)=C(9) double bond,[76] this is not a particular problem with $[(\eta^6\text{-cppH})Fe(\eta^5\text{-}C_5H_5)]^+ PF_6^-$, **14**. The reaction of cppH with ferrocene in the presence of $A\ell C\ell_3$ yields the cation **14** (Scheme 3.3).

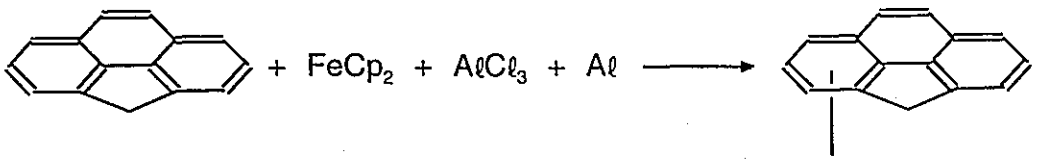

14

Scheme 3.3

Crystal structures of the analogous complexes $(\eta^6\text{-indene})Fe(C_5H_5)PF_6$, **15**, and $(\eta^6\text{-fluorene})Fe(C_5H_5)PF_6$, **16** (Figure 3.10), have not been reported in the literature. Even though a data set was obtained for the fluorene complex, Treichel[56b] and co-workers were unable to solve the highly disordered structure.

15 **16**

Figure 3.10 (indene)- and $(fluorene)Fe(C_5H_5)PF_6$

We were able to grow X-ray quality crystals of **14** by vapour diffusion techniques[77] by using 1,2-dichloroethane and n-heptane. The x-ray crystal structure of the cation is shown in Figure 3.11. The structure determination was complicated by the disorder found for the PF_6 anion and also for the (C_5H_5) ring. Only the restriction of a general isotropic refinement of the fluorine atoms in two independent sets of PF_6 anions gave an acceptable model. Also, the thermal motion of the C_5H_5 ligand was corrected employing librational rigid-body motion analysis.[78]

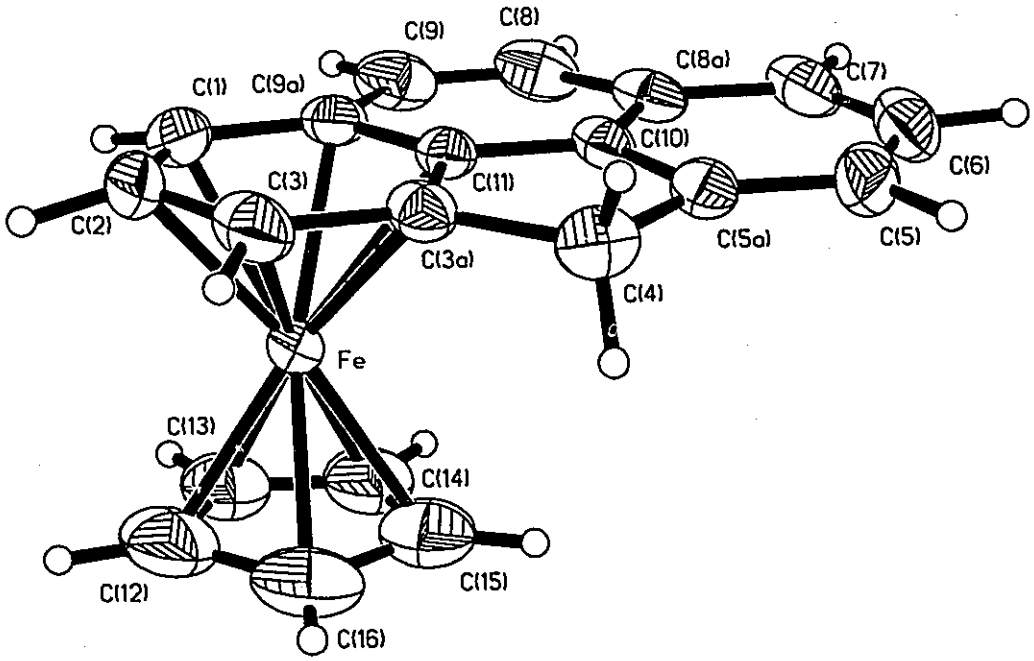

Figure 3.11 X-ray crystal structure of (η^6-cppH)Fe(C_5H_5)PF_6, **14**

3.3 Manganese complexes of cppH

The preparation of $(\eta^6\text{-cppH})Mn(CO)_3^+$, **17**, was attempted following the procedures reported for the analogous fluorene complex (Scheme 3.4).[56a]

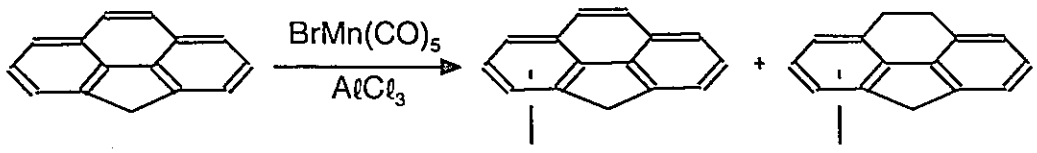

17 **18**

Scheme 3.4

The synthesis yielded the desired product, but in unacceptably low yields (2%). The major compound was identified as $(\eta^6\text{-}H_2\text{cppH})Mn(CO)_3PF_6$, **18**, obtainable in a yield of 20%. The hydrogenation might be explained by hydrogen transfer from (a) another cppH ligand or (b) the solvent. Abstraction of hydrogen from another cppH ligand would yield a radical and, subsequently, the coupling product ($C_{15}H_9\text{-}C_{15}H_9$). Ligand dimerization, followed by H_2 elimination would lead to the very stable fluorenylidene-type molecule **19** (Scheme 3.5). Indeed, the attempted synthesis of $(\eta^5\text{-fluorenyl})Rh(C_2H_4)_2$ by treatment of $[(C_2H_4)_2RhCl]_2$ with fluorenide ion gave good yields of bis-fluorenylidene.[79]

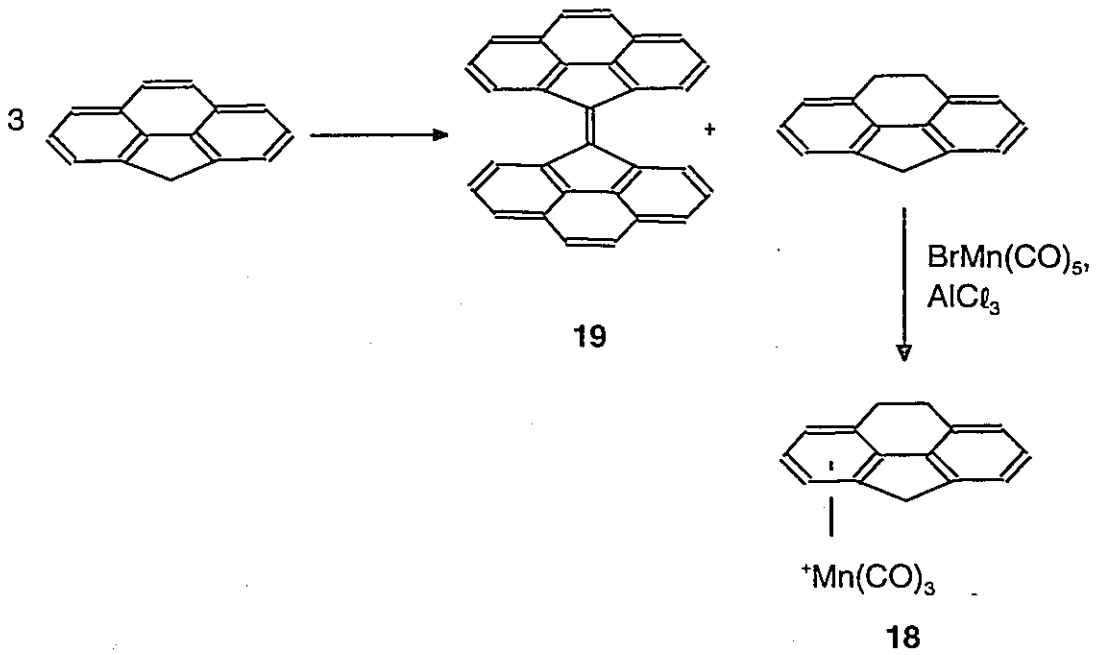

Scheme 3.5

If such a mechanism were operative, this hydrogen might be available to react with the free ligand or with $(\eta^6\text{-cppH})Mn(CO)_3^+$ to give the hydrogenated product **18.**

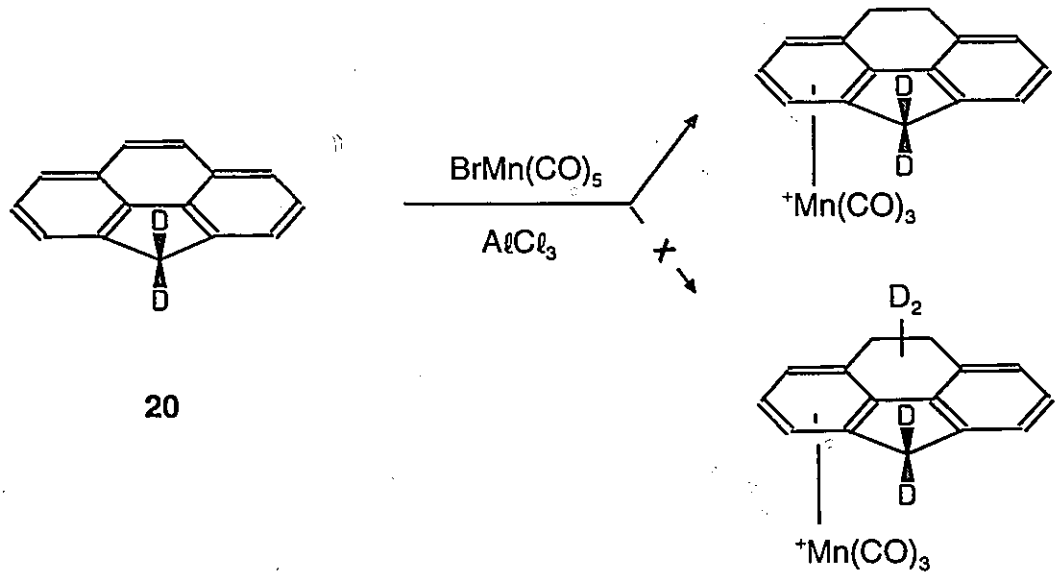

Scheme 3.6

However, labelling studies, using cppH-d_2, **20**, did not lead to any uptake of deuterium in the (dihydro-cppH)manganese complex (Scheme 3.6). Only (η^6-cppH-d_2)$Mn(CO)_3^+$ was detected using ^1H, ^2H and ^{13}C NMR as well as mass spectrometry. It would seem, therefore, that one can exclude the cppH ligand as the origin of the extra hydrogen atoms in the product.

Solvent induced hydrogenation has been observed in solvents such as decalin (decahydronaphthalene - from which loss of hydrogen yields the stable aromatic molecule, naphthalene), but seems to be very unlikely in n-hexane which was used in the preparation of the manganese complexes. However, one could readily imagine traces of moisture as the source of the hydrogen, and indeed thorough drying of the solvent over NaH for two days and distillation prior to use increased the yields to 65%. Moreover, the material was now contaminated with the hydrogenation product to a much lesser degree (5%). Even though these yields indicate an improvement over the original synthesis, the excellent yields of 85% that Treichel had reported in his work on the fluorene system were never obtained. One could make other efforts to improve the yield by rigorously drying of the starting materials cppH, $BrMn(CO)_5$ and $A\ell C\ell_3$. CppH was used as received from the supplier and $BrMn(CO)_5$ was sublimed prior to use and both compounds can be considered dry. $A\ell C\ell_3$ on the other hand is known to be hygroscopic. Interestingly, Nesmeyanov has noted that the use of very dry $A\ell C\ell_3$ in the preparation of [(arene)$Fe(C_5H_5)]^+$ complexes leads to extremely poor yields; apparently, traces of water are necessary for the reaction to proceed satisfactorily.[80]

Chapter 4: Haptotropic rearrangements of cpp complexes

As expected from the published data for the analogous fluorene complex,[54] deprotonation of $(\eta^6\text{-cppH})Cr(CO)_3$, **8**, at ambient temperature yields a complex whose NMR spectra reveal that the $Cr(CO)_3$ fragment has migrated onto the cyclopentadienyl ring. The NMR spectra are consistent only with a molecule **22** possessing a single mirror plane, and the aromatic resonances are typical for non-complexed arene rings. Moreover, the appearance of the C(4) and $Cr(CO)_3$ resonances at δ 60.4 and 245.8, respectively, provide compelling evidence for an η^5-complex. The corresponding complex $(\eta^6\text{-cpp})Cr(CO)_3$, **21**, where deprotonation of the starting material resulted in a compound in which the metal fragment is still coordinated to terminal six-membered ring can be accomplished at low temperatures. Using 15-crown-5 to increase the solubility of the Na salts, deprotonation of $(\eta^6\text{-cppH})Cr(CO)_3$, **8**, can be carried out at -78°C. Rearrangement to the symmetrical η^5-complex can be followed using ^1H NMR at temperatures between -25°C and -10°C (Scheme 4.1).

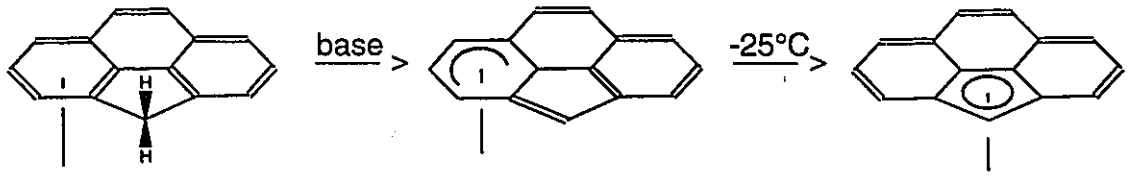

21 **22**

Scheme 4.1

As a consequence of the ionic nature of the resulting products, these air- and moisture-sensitive complexes could not be isolated and our studies on the species **21** and **22** were restricted to spectroscopic investigations in solution; however, we anticipated that use of cationic η^6 precursors should yield neutral η^5 complexes which might be more readily amenable to X-ray diffraction techniques.

In his pioneering studies on fluorenyl complexes, Treichel showed that deprotonation of the cationic complexes bearing such η^6-bonded fragments as $Mn(CO)_3^+$, **23a**, or $(C_5H_5)Fe^+$, **23b**, yields isolable intermediates in which the metal remains attached to the six-membered ring, **24**.[56] In the manganese case, the reaction continues whereby the $Mn(CO)_3$ moiety eventually moves into the five-membered ring. In the (cyclopentadienyl)iron analogue, Treichel was unable to detect (η^5-fluorenyl)(η^5-cyclopentadienyl)iron, **25b**, but Ustynyuk *et al.* have claimed that this ferrocene analogue is produced.[61]

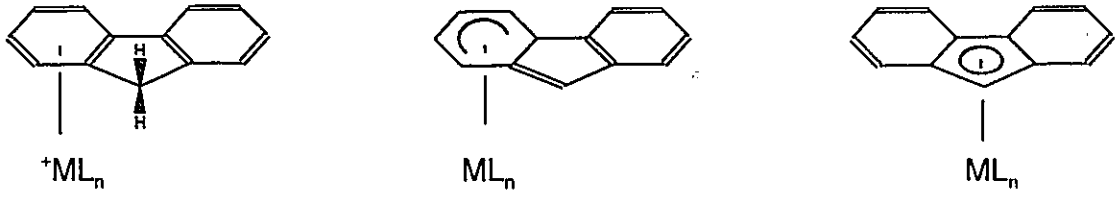

23 **24** **25**

a : $ML_n = Mn(CO)_3$

b : $ML_n = Fe(C_5H_5)$

Figure 4.1 η^6- and η^5-fluorene complexes of Mn and Fe

Reaction of the ionic complex $(\eta^6\text{-cppH})Fe(C_5H_5)^+PF_6^-$, **14**, yields the unstable complex $(\eta^6\text{-cpp})Fe(C_5H_5)$, **26**. Attempts to thermally induce metal migration to obtain the η^5-complex failed. Heating of complex **26** in $CH_2C\ell_2$ to

reflux did not lead to haptotropic rearrangement, whereas heating in 1,2-dichloroethane resulted in decomposition and the ferrocene analogue was not observed (Scheme 4.2).

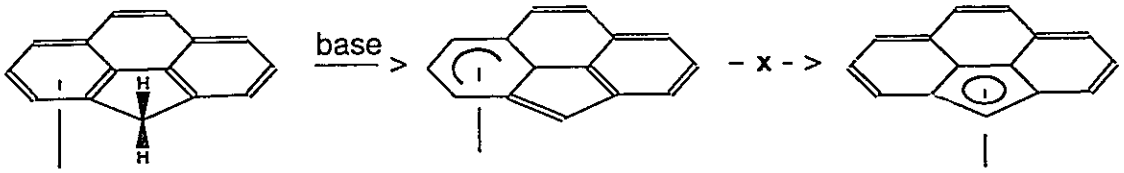

$^{+}Fe(C_5H_5)$ $Fe(C_5H_5)$ $Fe(C_5H_5)$

14 **26** **27**

Scheme 4.2

In contrast, deprotonation of the cation **17** at room temperature leads to (η^5-cpp)$Mn(CO)_3$, **29**, with no detectable intermediacy of **28** (Scheme 4.3).

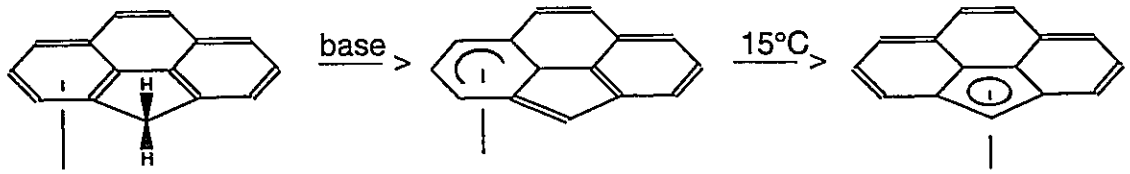

$^{+}Mn(CO)_3$ $Mn(CO)_3$ $Mn(CO)_3$

17 **28** **29**

Scheme 4.3

However, generation of **28** can be accomplished readily at -40°C by treatment of a dichloromethane solution of **17** with 1,8-bis-(dimethylamino)-naphthalene (Proton Sponge). Rearrangement to the η^5-isomer **29** is evident at temperatures above 15°C. In contrast, prior reduction of the C(8)=C(9) double bond of cppH, to give H_2-cppH, **9**, followed by complexation with $Mn(CO)_3^+$ yields **18**. Subsequent deprotonation of **18** results in metal migration, but this process

clearly occurs in a stepwise manner. Indeed, **30** is stable at room temperature in acetone solution for at least 24 h or in the solid state for several weeks at -20°C. However, upon heating a hexane solution of **30** for an hour, it is slowly transformed into the centrally-bonded isomer **31** and therefore mirrors the behaviour of the analogous fluorenyl system (Scheme 4.4).[56]

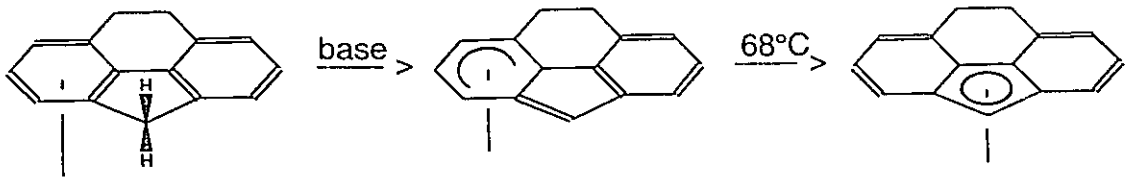

18 **30** **31**

Scheme 4.4

The pentahapto complex **29** can be independently synthesised in surprisingly good yield via the reaction of the cpp anion, $C_{15}H_9^-$, with bromo(pentacarbonyl)manganese;[81] presumably, the reaction proceeds via the initially formed η^1-species **32** but this was not isolable (Scheme 4.5).

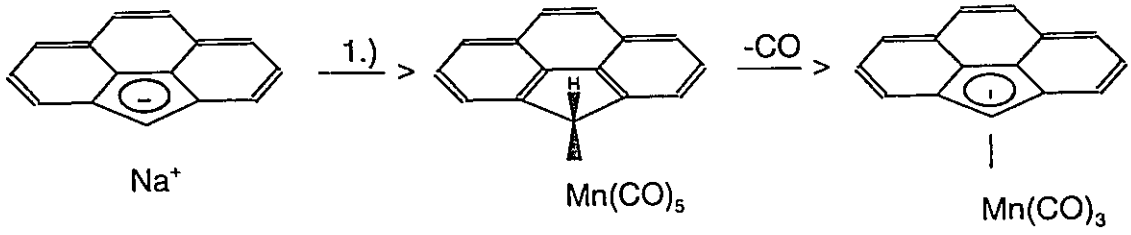

1 : $BrMn(CO)_5$, $A\ell C\ell_3$ **32** **29**

Scheme 4.5

The molecule (η^5-cpp)$Mn(CO)_3$, **29**, poses several interesting structural questions. One might wonder whether the metal binds in a genuinely pentahapto fashion, or does it perhaps have a tendency towards trihapto bonding, as has been found for (indenyl)$Rh(C_2H_4)_2$ and related systems?[82,83] Moreover, the recently published structure of bis(fluorenyl)barium-tetrakis(ammonia) reveals that the metal is considerably displaced from the ring centers.[84] Extended Hückel molecular orbital calculations on **29** tell us not only that the metal fragment should be situated at a position displaced ≈ 0.1 Å from the center of the five-membered ring towards C(4) but also that the tripod is preferentially oriented such that a carbonyl ligand is trans to the C(4) carbon. This situation arises as a result of the very considerable localization of the HOMO of the cpp anion at C(4) (see figure 2.2 in chapter 2, p. 27). Analogously, in (η^5-fluorenyl)$Cr(CO)_2NO$ the chromium is displaced slightly towards the unique ring carbon; furthermore, it is the nitrosyl ligand which is found trans to the CH unit of the five-membered ring thus aligning the most strongly donating site with the best π-acceptor ligand.[85] Crystals of (η^5-cpp)$Mn(CO)_3$, **29**, were grown from 1,2-dichloroethane / heptane by using solvent diffusion techniques,[77] and the structure was determined by X-ray crystallography. In accord with the NMR data, the $Mn(CO)_3$ moiety is indeed bonded to the five-membered ring, as shown in Figure 4.2. However, the metal is not attached centrally but rather is displaced towards the C(4) position such that the manganese—ring carbon distances are found to be Mn-C(4) 2.121 (2) Å, Mn-C(3a/5a) 2.204 (2) Å, Mn-C(10/11) 2.206 (2) Å. Furthermore, the orientation of the metal-tripod was found to be that predicted from the EHMO calculations; that is, one of the carbonyl ligands is trans to the C(4) carbon, placing the metal in a pseudo-octahedral environment.

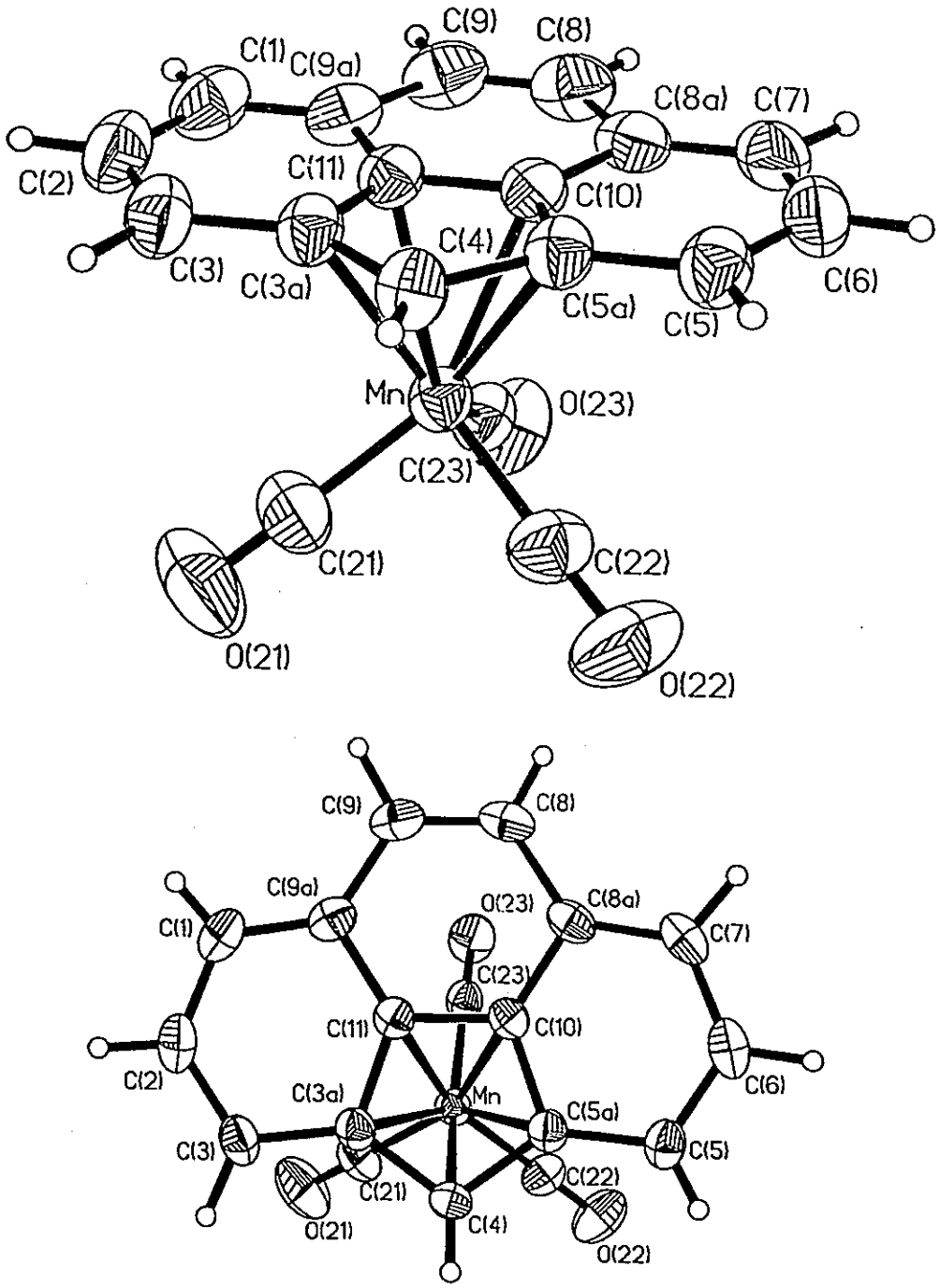

Figure 4.2 X-ray crystal structure of (η^5-cpp)Mn(CO)$_3$, **29**

However, the barriers to tripod rotation in **29** are not high enough to allow investigations on the NMR time scale; *i.e.* splitting of the carbonyl signals in the ^{13}C NMR at low temperature. A further noteworthy structural result is the fact that the three six-membered rings attached to the cyclopentadienyl moiety are slightly folded away from the $Mn(CO)_3$ tripod. The interplanar angle between the two external six-membered rings is 4.9°. This mirrors the behaviour previously found for $(\eta^6\text{-cppH})Cr(CO)_3$ (5.2°) and $(\eta^6\text{-cppH})Fe(C_5H_5)^+$ (2.7°).

Chapter 5: Theoretical considerations

5.1 General

After the discovery of sandwich and half-sandwich complexes, many theoretical concepts about the binding schemes in molecules like ferrocene, $(C_6H_6)_2Cr$ or $(C_6H_6)Mn(CO)_3^+$ were considered. Inspired by the unique chemical and physical behaviour of these compounds, especially their high stability, computational investigations led to the calculation of very sophisticated molecular orbital diagrams and, therefore, the understanding of the bonding modes in π-complexes. Early experiments concerning haptotropic rearrangements focussed on the mechanism of the reactions. It was established that the rearrangements proceed in a unimolecular fashion[62] and were proven to be intramolecular.[63] Taking these important results into account, haptotropic rearrangements can in fact be described as metal migrations over the surface of the organic ligand. Based on this assumption, EHMO calculations by Hoffman, Albright and their colleagues led to the first theoretical approach to describe haptotropic rearrangements.[86] A very thorough investigation was carried out for the metal migration in the complex (indenyl)Fe(C_5H_5).[25] It was found that rearrangements from the six- to the five-membered ring will not occur via the least-motion pathway **A** (Figure 5.1). Most of the bonding interaction between the metal frontier orbitals and the indenyl π-system is lost in the η^2-transition state. It requires about 58 kcal mol^{-1} for the least-motion shift going from the η^6 to the η^5 isomer. This is in the neighborhood of dissociation energies for Fe-Cp bonds.[86] Interestingly, using an EHMO

approach, we determined dissociation energies for (indenyl)Fe(C_5H_5) to be approximately 47 kcal mol^{-1}.

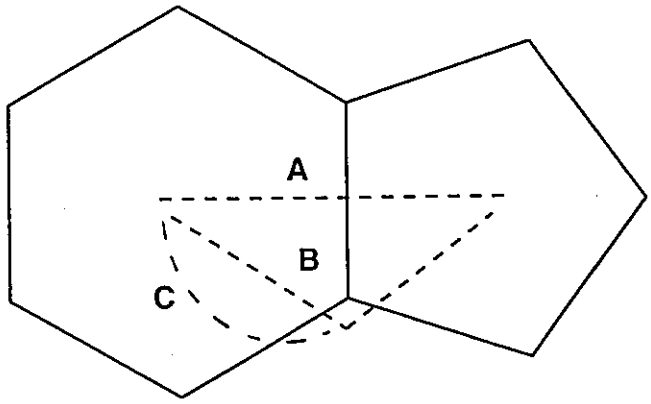

Figure 5.1 Rearrangement pathways in (indenyl)Fe(C_5H_5)

The loss of orbital overlap in the η^2-position from filled ligand orbitals into empty metal orbitals (donation) is accompanied by an repulsive interaction between filled ligand orbitals and filled metal orbitals, thus leading to a very unfavourable interaction between metal and ligand. Metal-ligand separation is actually favoured over the interaction required by a least-motion pathway. A viable alternative was found in the non-least-motion pathways **B** and **C** (Figure 5.1). Computing the potential energy surface for (indenyl)Fe(C_5H_5), the authors found two minimum energy pathways, both joining in a η^3-transition state. Surprisingly, Hoffman et al. did not investigate pathway **C** further as it was felt that *path **C** may well be an artifact of the computational method and may disappear at a more sophisticated level* even though the barrier appears to be 4.5 kcal mol^{-1} lower than the corresponding maximum in the trajectory **B**. Nevertheless, following the non-

least-motion pathway **B**, it requires 35 kcal mol^{-1} to proceed from the η^6-position to the η^5-position, considerably less than the 58 kcal mol^{-1} required for the least-motion pathway.

Extending this type of theoretical strategy to the less symmetric fluorenide system, a similar situation was found, in that the least-motion pathway requires an unacceptably high barrier of 57 kcal mol^{-1}. The discussion of non-least-motion pathways in (fluorenyl)Fe(C_5H_5) is more complicated than in the analogous indenyl system since the two η^3-transition states are no longer equivalent. There is some confusion in this particular paper concerning the barriers of migration. In this particular case, the entire potential surface was not published, instead some of the barrier values are mentioned in the discussion. Unfortunately, the barriers for the $\eta^6 \rightarrow \eta^3$ shift are not equivalent to the barriers of the $\eta^3 \rightarrow \eta^5$ shift. It turns out that the higher barrier, and therefore the most significant one, is for the initial migration of the metal fragment from the six-membered ring to the allylic transition state; this barrier was not reported.

5.2 Migrations in (fluorenyl)Fe(C_5H_5) and (cpp)Fe(C_5H_5)

EHMO calculations were carried out for migrations of $(C_5H_5)Fe^+$ over the surfaces of fluorenyl$^-$ and cpp$^-$ with a constant distance of 1.59 Å between the metal and the ligand. The center of the six-membered ring was chosen as the starting points for the metal migrations and assigned an arbitrary energy of zero. All energies are reported in kcal mol^{-1} relative to this origin. The choice of computing the haptotropic rearrangements of $(C_5H_5)Fe^+$ rather than $(CO)_3Mn^+$ or $(CO)_3Cr$ alleviates the problem of ligand orientation relative to the metal fragment.

As Albright et al.[25] reported for similar calculations on naphthalene and fluorenyl systems, orientation of the tripod relative to the hydrocarbon plays an important role in maximizing orbital overlap, whereas for the isolobal $(C_5H_5)Fe^+$ fragment a fixed orientation of the Cp-ring is justified by its low barriers to rotation.

In accord with their calculations on indenyl and fluorenyl complexes,[25] we find that there will be an unacceptably high barrier to the least-motion pathway (route **A**) of an $Fe(C_5H_5)$ unit directly across the C(3a)-C(11) bond in the cpp system. The barriers were calculated to be 50.3 kcal mol^{-1} for $cppFe(C_5H_5)$ and 56.0 kcal mol^{-1} in the fluorenyl system.

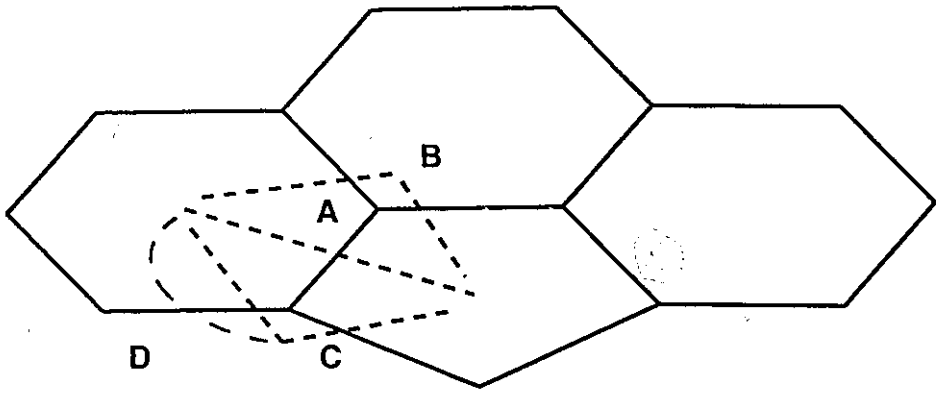

Figure 5.2 Rearrangement pathways in $(cpp)Fe(C_5H_5)$

As shown in Figure 5.2, the transit through the central six-membered ring (route **B**) provides a lower activation energy pathway, but the favoured route (**C**) proceeds via an exocyclic π-allylic structure. The calculated barriers for these migration pathways are 39.3 and 32.5 kcal mol^{-1}, respectively. These compare with EHMO-derived values of 38.2 and 36.8 kcal mol^{-1}, respectively, for the

analogous migrations in the fluorenyl case (Figure 5.3). In both systems the metal migration leads to a strongly favoured η^5-isomer. The stabilization for the cpp complex is -13.4 kcal mol^{-1} and -10.5 kcal mol^{-1} in the case of the fluorenyl ligand. Experimental results clearly show that no haptotropic rearrangement is observed upon thermal treatment of $(\eta^6\text{-cpp})Fe(C_5H_5)$; however, rearrangement in the complexes $(\eta^6\text{-cpp})Mn(CO)_3$ and $(\eta^6\text{-cpp})Cr(CO)_3^-$ to their corresponding $(\eta^5\text{-cpp})$ analogues was found to be rather facile.

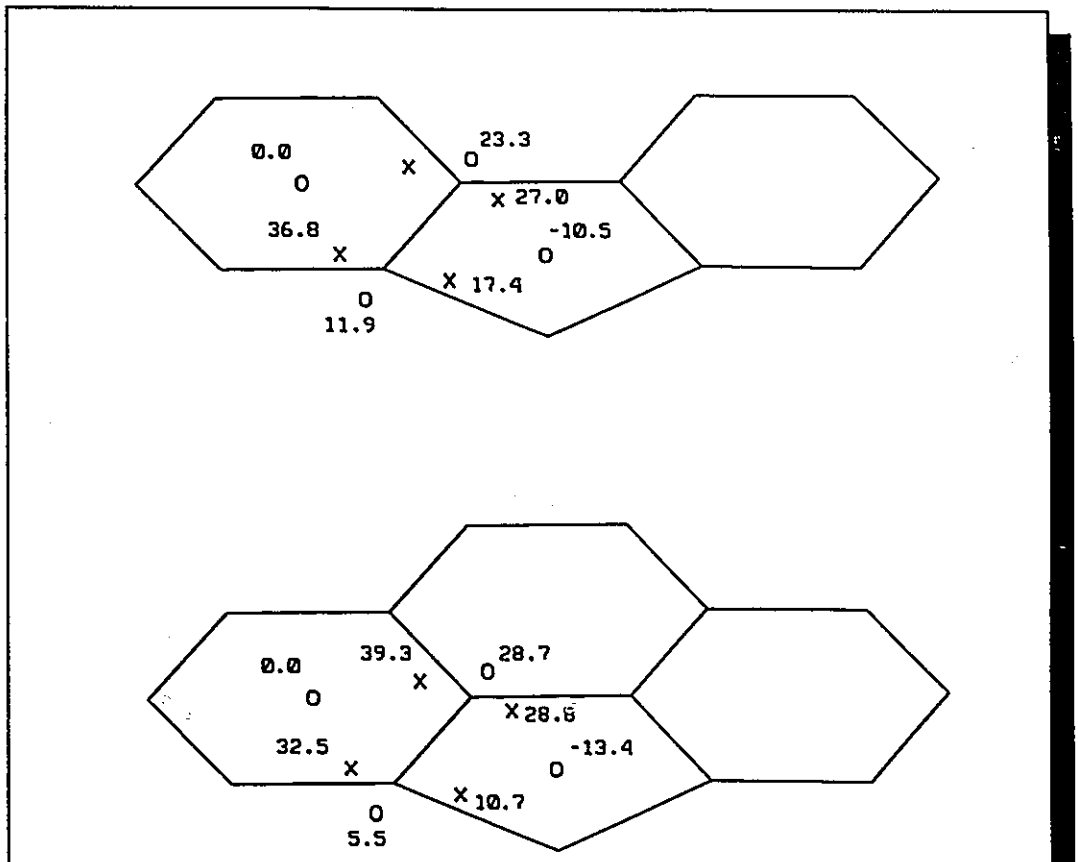

Figure 5.3 Selected energies for the migration of $Fe(C_5H_5)$

Furthermore, it was found that the rearrangements in $(\eta^6\text{-cpp})Mn(CO)_3$ and $(\eta^6\text{-cpp})Cr(CO)_3^-$ occur at much lower temperatures than was observed for the corresponding complexes of fluorenide and H_2-cpp. EHMO calculations for metal shifts in complexes of $Fe(C_5H_5)$ reveal that the barriers to migration can be expected to be much lower in the cpp complex than in the fluorenyl case. Assuming a linear, non-least-motion trajectory, the barriers in the cpp complex were found to be 32.5 kcal mol^{-1}, whereas a barrier of 36.8 kcal mol^{-1} was computed for the fluorenide complex. The same scheme can be found for a non-linear, non-least-motion over the ligand surfaces (pathway **D** in figure 5.2). The required energy for a $\eta^6 \rightarrow \eta^5$ shift in cpp is 30.0 kcal mol^{-1}, as opposed to the 38.0 kcal mol^{-1} Albright calculated for the fluorenide. Therefore, the barriers to migration for $Fe(C_5H_5)$ are expected to be lower in the case of cpp in comparison to fluorenide by 4.3 kcal mol^{-1} considering a linear, non-least motion pathway and 8.0 kcal mol^{-1} for a non-linear, non-least motion pathway. A comparison of the energies for the linear and non-linear pathways in the $Fe(C_5H_5)$ migrations over the cpp surface appears as figure 5.4. The reaction coordinate represents the pathway from the η^6- to the η^5 position, in each case at 10 points / Å resolution. The above data were extracted from a 3D plot (Figure 5.5) which was obtained by moving a $Fe(C_5H_5)$ fragment over the surface of cpp at a constant distance of 1.59 Å and colorcoding the obtained energies as shown in the legend.

The enhanced ease of migration in cpp complexes can be explained either on the basis of these molecular orbital calculations or, more straightforwardly, by using the simple bonding pictures **A** and **B** (Figure 5.6). It is only in the cpp complexes, if the migration proceeds via the exocyclic π-allylic transition state **A**,

that one can maintain the 10π (naphthalene-like) aromatic character of two rings throughout the course of the reaction.

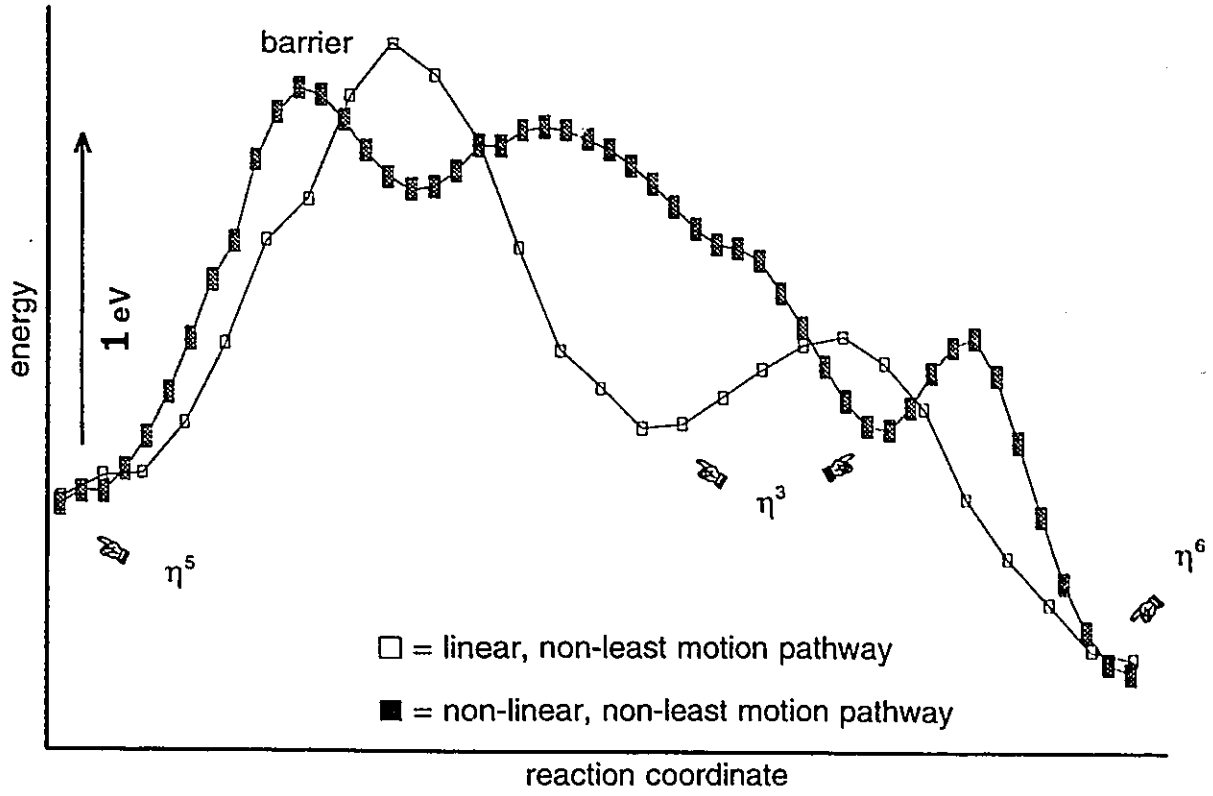

Figure 5.4 Energy diagram, for the migration pathways of (cpp)Fe(C_5H_5)

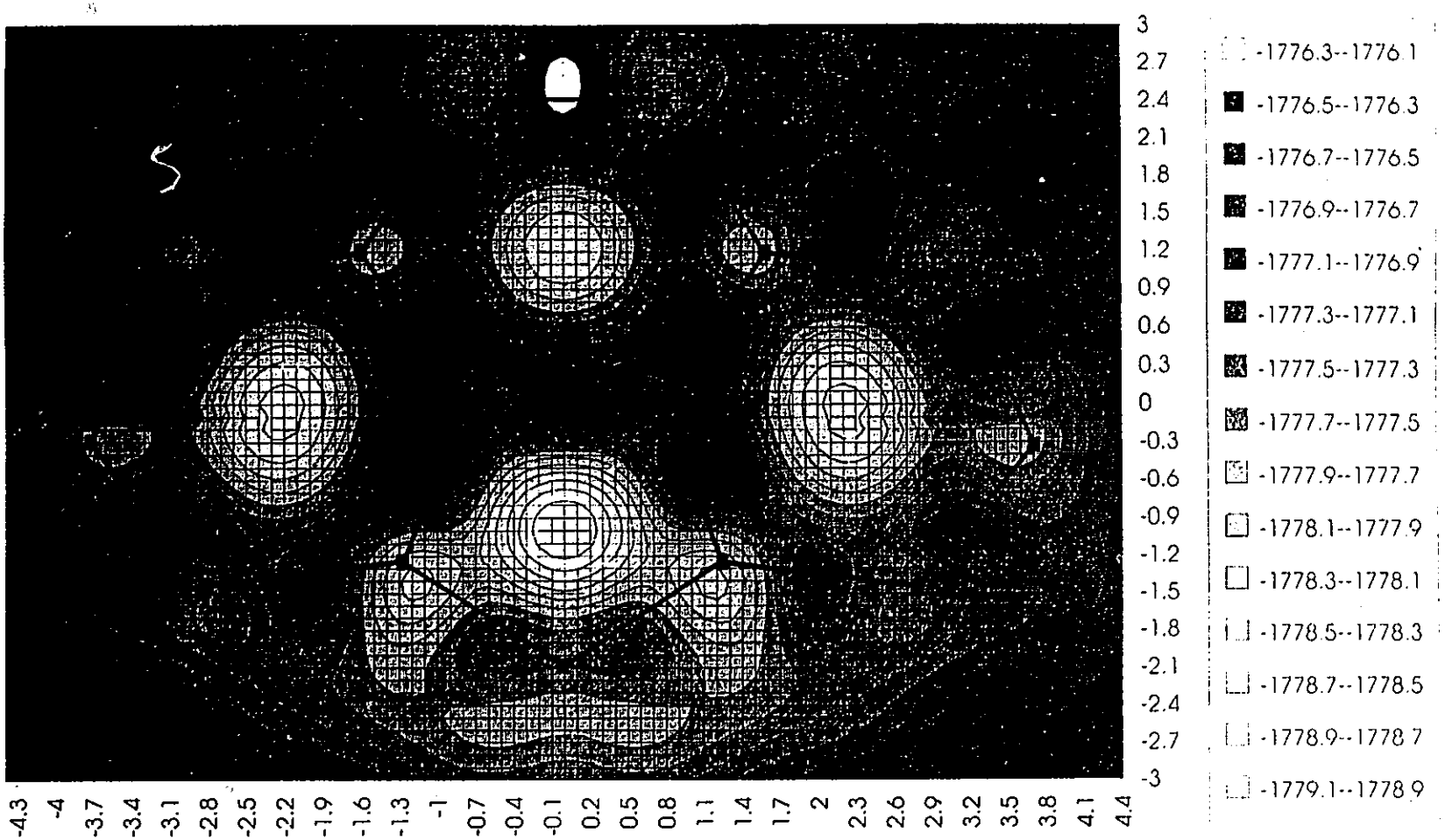

Figure 5.5 3D plot for the rearrangement of (cpp)Fe(C_5H_5)

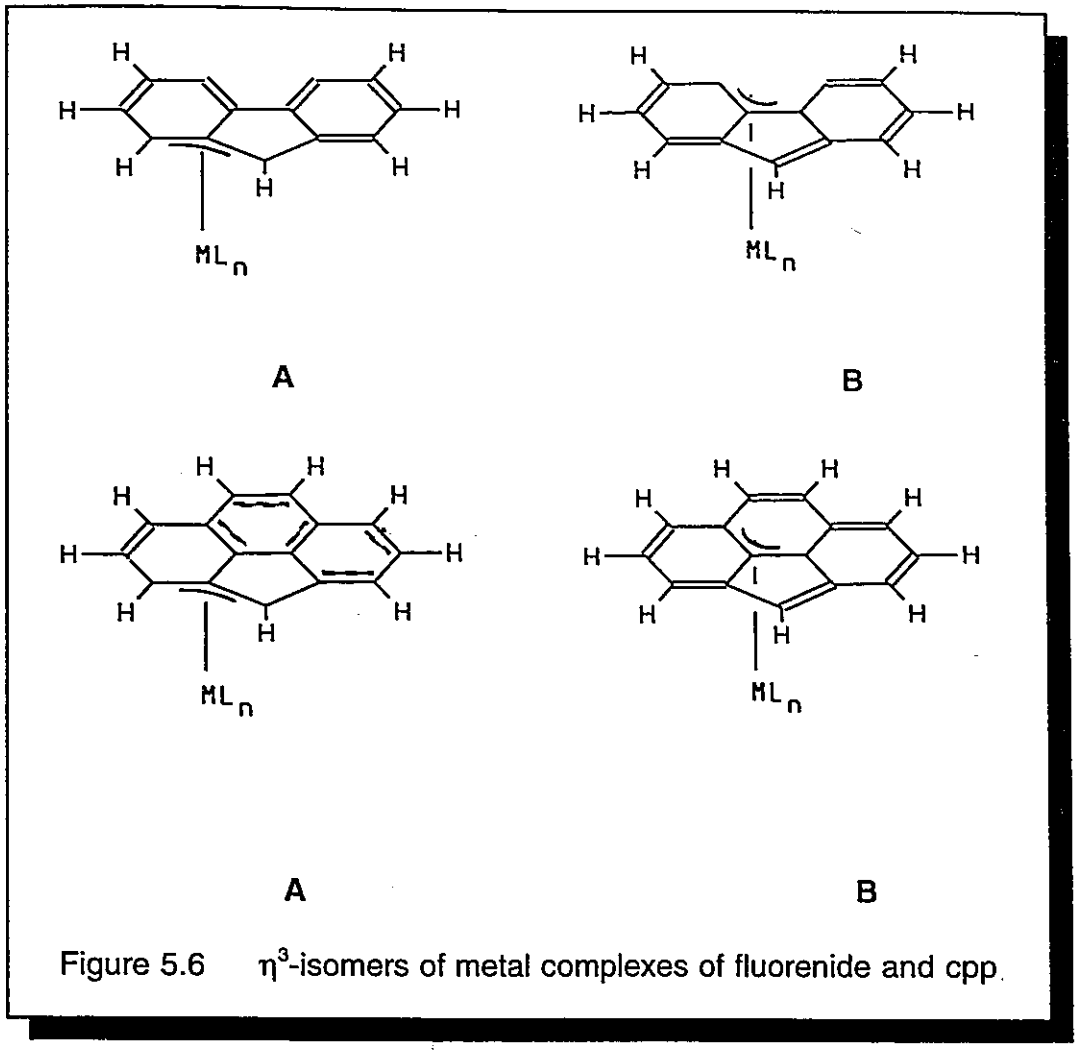

Figure 5.6 η^3-isomers of metal complexes of fluorenide and cpp.

This proposal gains support from the observation that the migration of an $Mn(CO)_3$ group upon deprotonation of the cppH complex **17** is very facile, whereas the corresponding reactions using the dihydro-cppH complex **18** are rather slow; moreover, the intermediate (η^6-H_2-cpp)$Mn(CO)_3$, **30**, can be isolated.

5.3 Migrations in (cpp)$Mn(CO)_3$

It would be desirable to compare the obtained barriers for metal migration in (cpp)$Fe(C_5H_5)$ to those where the metal fragment is $Mn(CO)_3$ and $Cr(CO)_3^-$. EHMO calculations for $M(CO)_3$ tripods can not be carried out the same way the $Fe(C_5H_5)$ rearrangement was approached. As mentioned before, the orientation of the tripod relative to the hydrocarbon plays an important role in maximizing orbital overlap as Albright et al.[25] reported for similar calculations on naphthalene and fluorenyl systems, whereas for the isolobal $(C_5H_5)Fe$ fragment a fixed orientation of the Cp-ring is justified by its low barriers to rotation. EHMO calculations were carried out for migration of an $Mn(CO)_3$ fragment over the surface of the cpp ligand. In this case the importance of the tripod orientation was taken in account by rotating the metal fragment in 10° steps over a range of 120° at each point of the surface. Choosing the minimum energy for each point, a 3D plot similar to that for the $Fe(C_5H_5)$ migration was obtained and is shown as figure 5.7. The most important difference compared to the 3D plot for the migrations of $Fe(C_5H_5)$ over the cpp surface can be found by comparing the possible trajectories for the metal shifts of the two isolobal metal fragments (Figure 5.8). In the case of $Fe(C_5H_5)$ we were able to identify three local minima; the η^6 starting point, the η^5 end point and the η^3 transition state. For the analogous $Mn(CO)_3$ system we were not able to identify a η^3 transition state. This has a significant implication for the trajectory in that the linear, non-least-motion and the non-linear, non-least-motion pathways for the $Mn(CO)_3$ shift become indistinguishable.

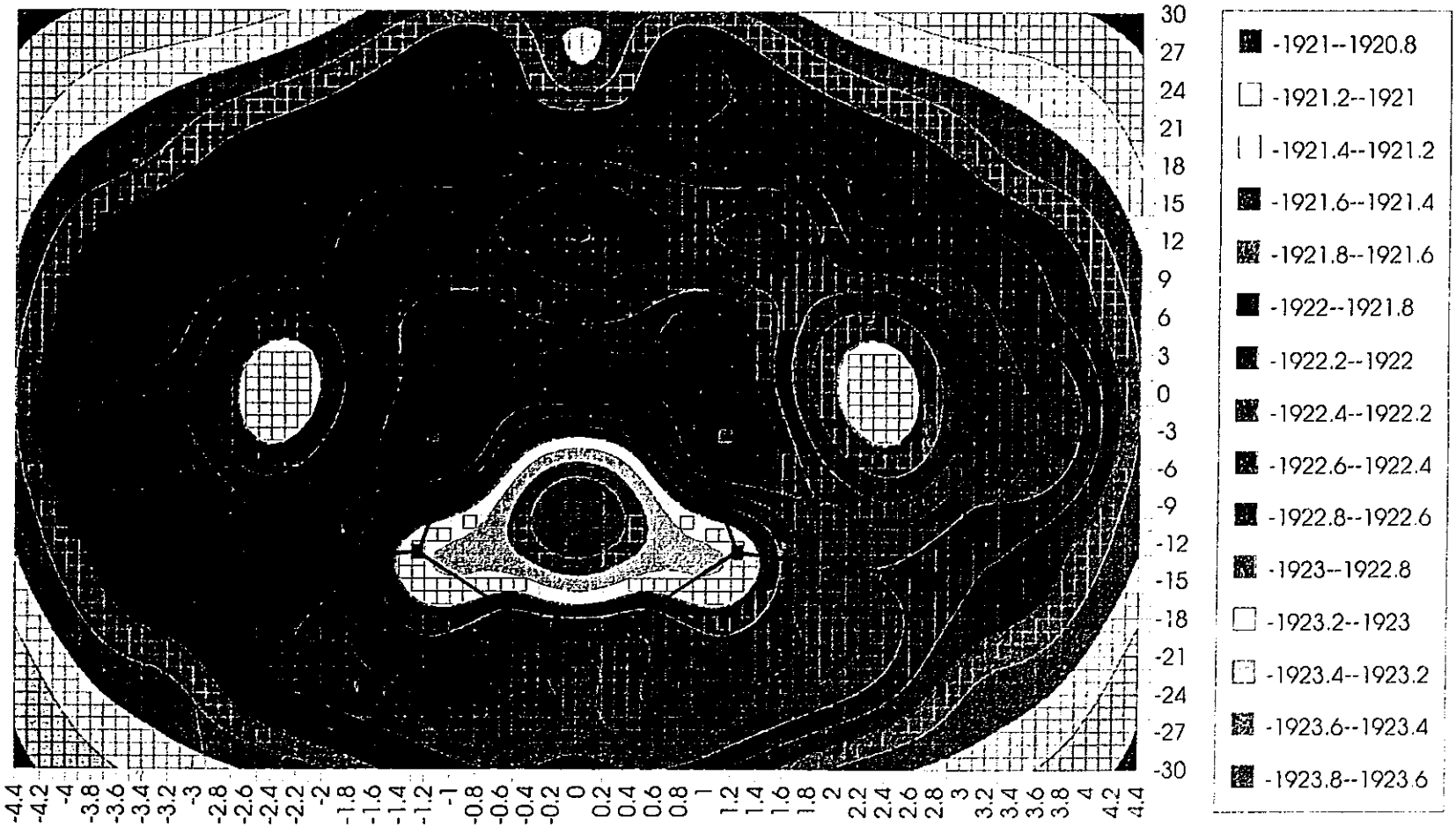

Figure 5.7 3D plot for the rearrangement of (cpp)$Mn(CO)_3$

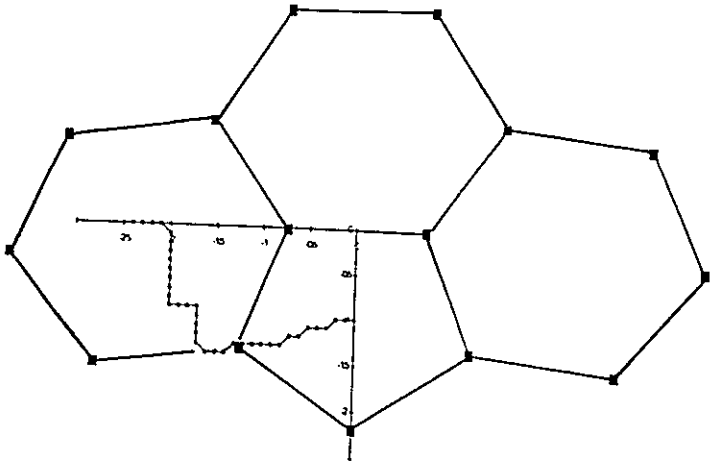

Trajectory for the (cpp)$Mn(CO)_3$ rearrangement

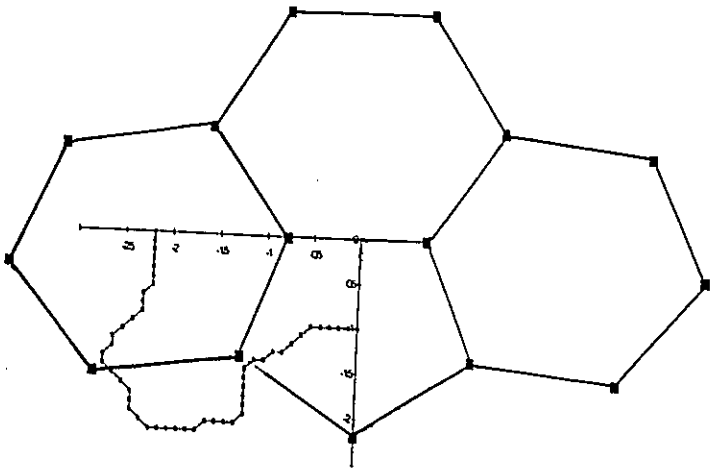

Trajectory for the (cpp)$Fe(C_5H_5)$ rearrangement

Figure 5.8

The energetically most favoured pathway in the metal migration of $Mn(CO)_3$ requires 17.5 kcal mol^{-1} to proceed, a barrier that can be compared to the 30.0 kcal mol^{-1} for the analogous migration for the $Fe(C_5H_5)$ fragment. Also, the η^5 position is favoured over the η^6 position by -16.0 kcal mol^{-1} as supposed to only

-13.4 kcal mol^{-1} in the $Fe(C_5H_5)$ rearrangement. The barrier found for the $Mn(CO)_3$ migration appears to be about 50% lower than for the $Fe(C_5H_5)$ migration. These findings mirror the behaviour found experimentally in that no haptotropic rearrangement was observed in $(\eta^6\text{-cpp})Fe(C_5H_5)$ even at elevated temperatures, whereas the analogous $(\eta^6\text{-cpp})Mn(CO)_3$ system rearranges at ambient temperatures. An energy diagram for the migration of $Mn(CO)_3$ and $Fe(C_5H_5)$ over the surface of cpp is shown as figure 5.9 and the angle dependence throughout the rearrangement appears as figures 5.10 and 5.11.

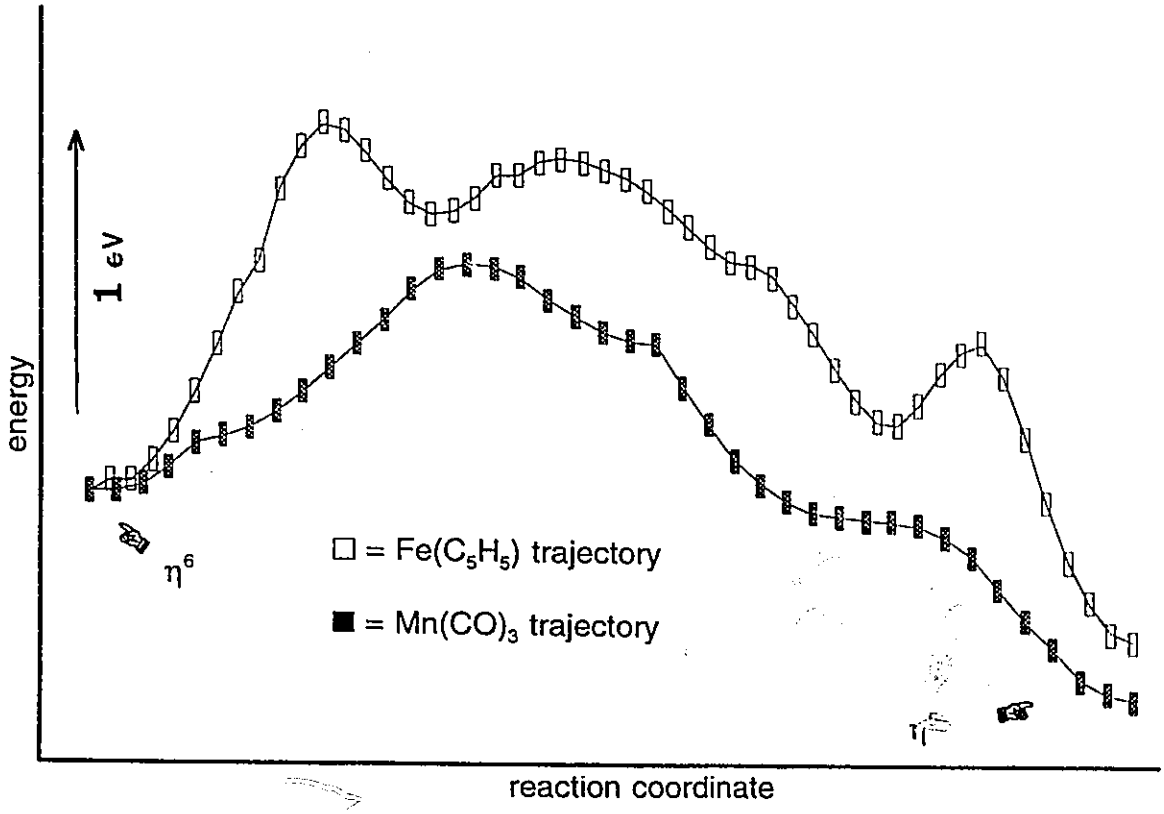

Figure 5.9 Energy diagram for the migration in cpp complexes

The angles are reported relative to the orientation determined in the X-ray crystal structure of (η^5-cpp)$Mn(CO)_3$, **29**, and positive values correspond to a counter clockwise rotation of the metal-tripod during the shift as presented in figure 5.8. It appears that the tripod rotates by 70° during the metal shift, especially in the vicinity of the barrier, a dramatic change in tripod orientation can be assumed.

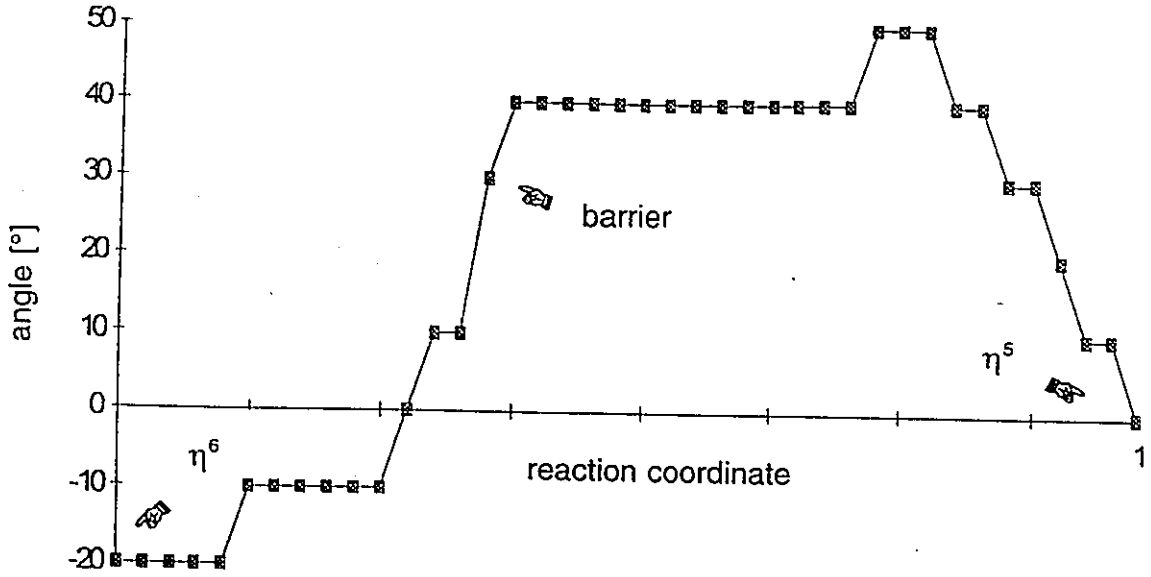

Figure 5.10 $Mn(CO)_3$ tripod orientation during the course of rearrangement

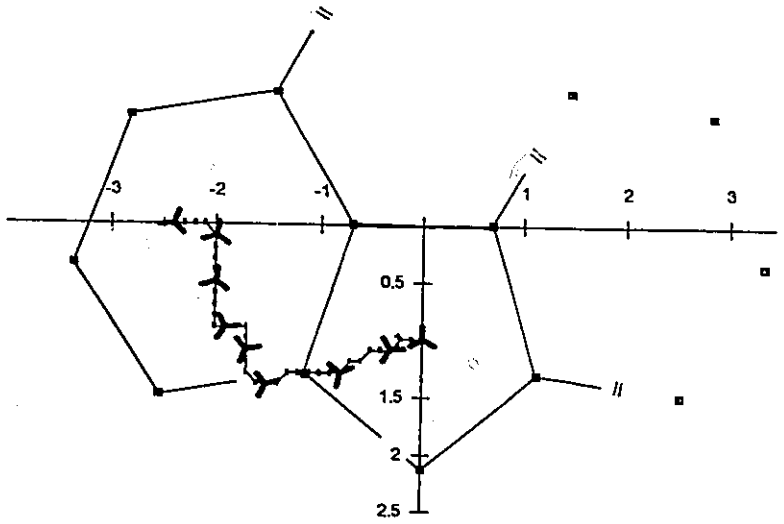

Figure 5.11 $Mn(CO)_3$ orientation during rearrangement

Chapter 6: The η^3-transition state.

As outlined in chapter 5, haptotropic rearrangements in metal complexes of fluorene, cppH and H_2-cppH are expected to proceed via an allylic η^3-transition state. The question arises, whether one might be able to experimentally prove the calculated trajectory by trapping or isolating a compound in which the metal-vertex is coordinated to the ligand in a η^3-fashion.

Many publications suggest η^3-species as intermediates, especially in carbonyl replacement reactions. As mentioned in Chapter 1, Basolo et al. observed an increased rate of reaction by a factor of 10^8 for CO substitution by phosphines in (η^5-indenyl)$Rh(CO)_2$ in comparison to (η^5-C_5H_5)$Rh(CO)_2$.[34] The *indenyl ligand effect* invoked a (η^3-indenyl)$Rh(CO)_2PR_3$ transition state to explain the dramatic increase in the rate of reaction. Numerous other authors use Basolo's proposal to explain their experimental results.[26] However, spectroscopic evidence is limited in most of the cases, and the assignment of the intermediates is based on IR spectroscopy of reaction mixtures. Only in a few cases were the authors able to structurally characterize compounds bearing a η^3-indenyl ligand using NMR techniques[87-89] or single crystal X-ray diffraction.[87,90] (η^3-Fluorenyl) transition-metal complexes have not been structurally characterized to date. Ji, Rerek and Basolo compared the kinetics of the phosphine substitution reactions of the indenyl complex (η^5-C_9H_7)$Mn(CO)_3$ and the fluorenyl complex (η^5-$C_{13}H_9$)$Mn(CO)_3$.[91] Phosphine substitution with P(n-Bu)$_3$ at 140°C occurs 250

times faster with the fluorenyl ligand than with the indenyl ligand to produce the monophosphine complexes $(\eta^5\text{-}C_9H_7)Mn(CO)_2P(n\text{-}Bu)_3$ and $(\eta^5\text{-}C_{13}H_9)Mn(CO)_2\text{-}P(n\text{-}Bu)_3$, **34**. The related cyclopentadienyl complex $(\eta^5\text{-}C_5H_5)Mn(CO)_3$ is inert to thermal CO substitution. The rates of reaction depend on both size and basicity of the incoming ligand. These results support an associative mechanism in which ring slippage to form an $(\eta^3\text{-}C_{13}H_9)$ mono(phosphine) intermediate, **33**, occurs in the rate determining step (Scheme 6.1).

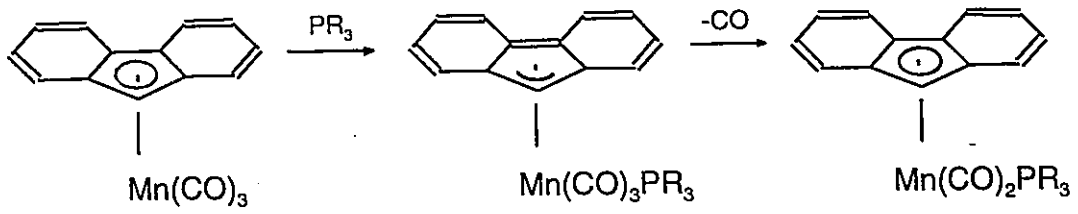

33 **34**

Scheme 6.1

Upon irradiation of $(\eta^1\text{-}C_{13}H_9)Re(CO)_5$, Wrighton and co-workers detected an intermediate which they claim is $(\eta^3\text{-}C_{13}H_9)Re(CO)_4$, **35**.[92] This material was not obtained in a pure form and its IR spectrum is obscured by the absorption of the starting material. The final product was identified as $(\eta^5\text{-}C_{13}H_9)Re(CO)_3$, **36**, (Scheme 6.2).

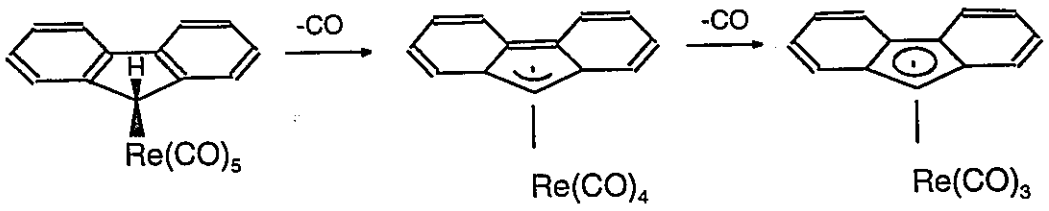

35 **36**

Scheme 6.2

Both reports considered the intermediate to be the symmetrical η^3-isomer, **37** rather than the exocyclic isomer **38**. Considering the extra stabilization of the transition state in the CO replacement by phosphine in the fluorenyl complex $(\eta^5\text{-}C_{13}H_9)Mn(CO)_3$ over that in the analogous indenyl complex $(\eta^5\text{-}C_9H_7)Mn(CO)_3$ leading to an increase in the rate of reaction by a factor of 250 does, in our opinion, not provide unequivocal evidence for the existence of the isomer **37**. The π-system in this isomer is significantly disturbed in that no aromaticity is retained in the transition state. In contrast, isomer **38** involves a 6π arrangement in the uncomplexed six-membered ring leading to a relatively stable aromatic system (Figure 6.1). However, spectroscopic evidence for either of the isomers is insufficiently conclusive and a η^3-fluorenyl transition-metal complex has not been identified so far.

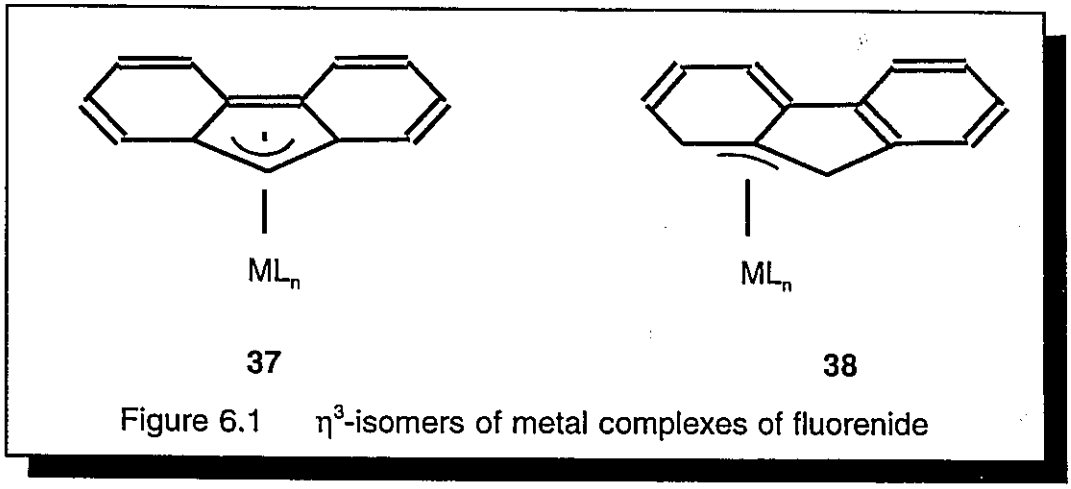

37 **38**

Figure 6.1 η^3-isomers of metal complexes of fluorenide

Isolating a metal complex in which the cppH ligand is coordinated in a η^3-fashion would substantially support our EHMO calculations and for the first time give direct evidence for an allylic transition state. Several different synthetic approaches were considered:

a.) *Thermal trapping of the intermediate complex in the course of a rearrangement.* EHMO calculations suggest that the barriers for the rearrangement from a η^6-complex to a η^3-complex are much higher than for a η^3-complex to a η^5-complex. Once a metal has reached the allylic transition state it will be impossible to stop the metal migration. Starting in the η^5 position, it will be very difficult to provide just enough potential energy to selectively overcome the smaller barrier. No experiments were carried out using this approach.

b.) *Direct preparation of η^3-complexes.* η^3-indenyl complexes have been reported for Pd and Pt. However, only one paper describes the synthesis of these rather unstable organometallic compounds.[88] Attempts to adopt the literature procedure to cppH complexes were unsuccessful. Furthermore, Pd and Pt complexes of multi-fused ring systems are not known to undergo haptotropic rearrangements and the preparation of η^3-cpp complexes of Pd and Pt would not necessarily prove the trajectory in metal migrations of Cr and Mn systems.

c.) *From η^5-complexes.* Addition of a ligand to (η^5-cpp)$Mn(CO)_3$ (the appropriate Fe complexes are unknown and the Cr complexes very unstable) should lead to the desired η^3-complexes via ring slippage. In 1984, Basolo reported on kinetic studies concerning phosphine substitution reactions of the fluorenyl complex (η^5-$C_{13}H_9$)$Mn(CO)_3$, **25a**, (Scheme 6.3).[91] In the course of their investigations they proposed the intermediacy of the diphosphine addition product (η^1-$C_{13}H_9$)$Mn(CO)_3(PR_3)_2$, **40**. This molecule was later isolated by Biagioni and co-workers,[93] however, NMR and IR spectroscopic data did not agree with the data published by Basolo. Biagioni concluded that a *trans-meridional* complex was obtained (trans with respect to the phosphine groups), but failed to prove their

proposal with an X-ray crystal structure determination of this very interesting molecule. The reaction mechanism was believed to proceed via the monophosphine complex (η^3-$C_{13}H_9$)$Mn(CO)_3PEt_3$, **39**. With high concentrations of phosphine, the fluorenyl complex **25a** is converted to the bis(phosphine) substitution product **43**. To explain the rapid bis substitution of **25a**, the sequential formation of the η^3-$C_{13}H_9$ mono(phosphine), **39**, η^1-$C_{13}H_9$ bis(phosphine), **40**, and η^3-$C_{13}H_9$ bis(phosphine), **42**, intermediates were proposed.[91,93]

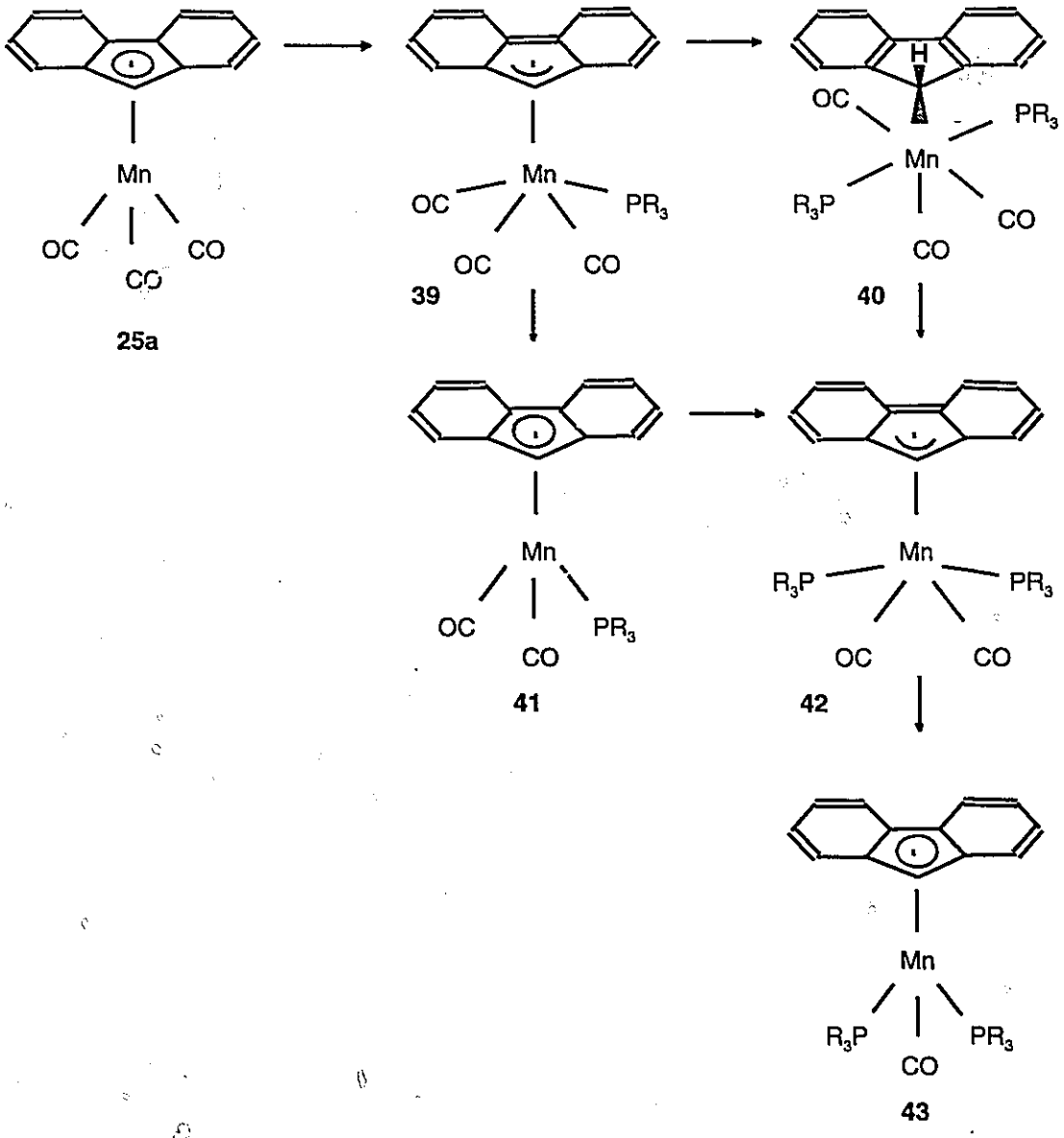

Scheme 6.3

The (η^5-$C_{13}H_9$)-mono(phosphine) complex **41**, however, is not an intermediate in the formation of **43** from **25a** under these conditions, since the conversion of **41** to the final product **43** is 70 times slower than the direct formation of **43** from **25a**.[91] Unfortunately, the publications do not contain any information on the possibility of isolating the η^3-$C_{13}H_9$ isomers **39** and **42**.

d.) *From η^1-complexes.* The most promising approach might be the selective abstraction of a ligand from a η^1-complex of cpp. As carbonyl abstractions from metal complexes using Me_3NO or by UV irradiation are widely used, it should be possible to selectively remove one CO ligand from complexes such as (η^1-cpp)Mn(CO)($Ph_2PCH_2PPh_2$)$_2$, (η^1-cpp)Mn(CO)$_3$(PMe_3)$_2$ or (η^1-cpp)Fe(CO)$_2$Cp.

6.1 The (η^1-cpp)Mn(CO)($Ph_2PCH_2PPh_2$)$_2$ system

As mentioned in chapter 4, the complex (η^5-cpp)Mn(CO)$_3$, **29**, can be prepared in unexpectedly high yields from cpp$^-$ and $BrMn(CO)_5$. One can assume that the reaction proceeds via the monohapto complex (η^1-cpp)Mn(CO)$_5$, **32** (Figure 6.2).

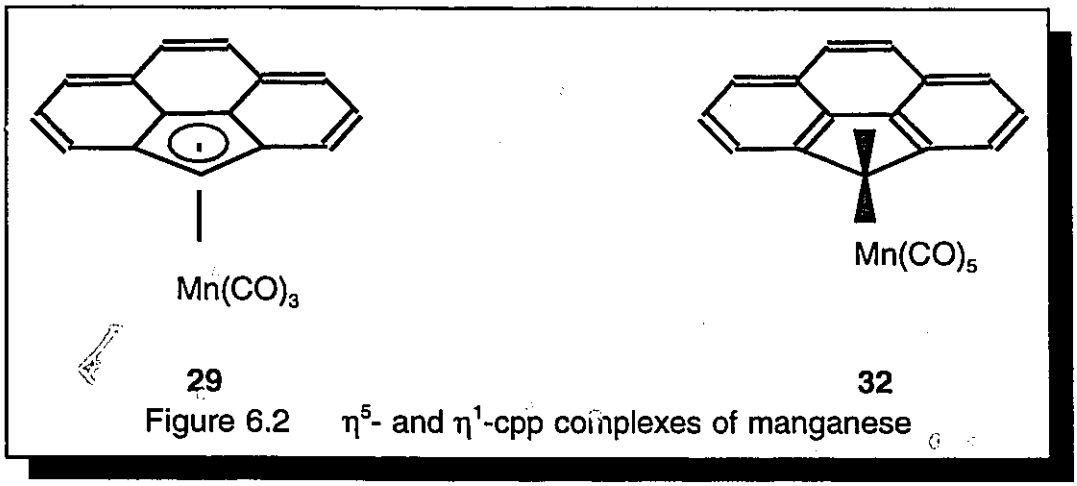

Figure 6.2 η^5- and η^1-cpp complexes of manganese

Repeating this experiment with $BrMn(CO)(Ph_2PCH_2PPh_2)_2$, **44**, should lead to the complex $(\eta^1\text{-cpp})Mn(CO)(Ph_2PCH_2PPh_2)_2$, **45**, which may rearrange to the allylic species $(\eta^3\text{-cpp})Mn(Ph_2PCH_2PPh_2)_2$, **46**, after removal of the carbonyl ligand (Scheme 6.4). Unfortunately, we were not able to synthesize the manganese starting material **44**. Following the literature procedure of Singleton,[94] we were able to isolate the mono substitution product $BrMn(CO)_3(Ph_2PCH_2PPh_2)$, **47**. Attempts to replace two more CO ligands with a diphosphine using different UV wavelengths only led to recovery of the starting material.

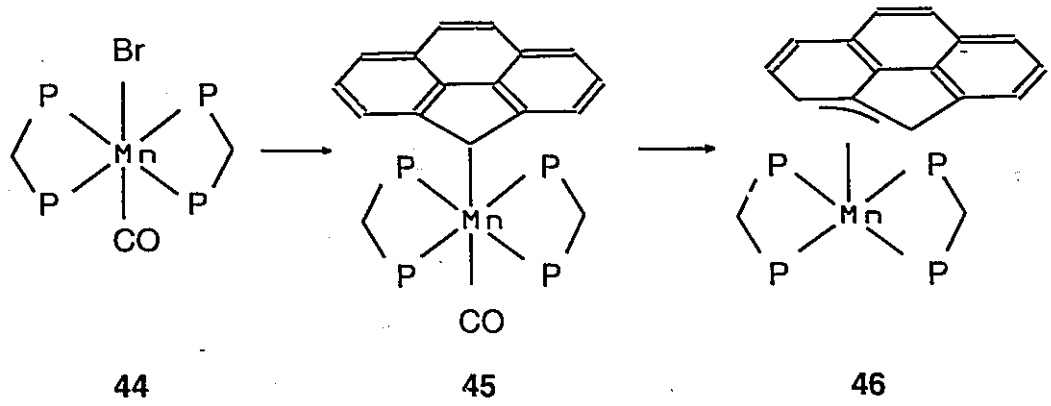

44 **45** **46**

Scheme 6.4

We were, however, able to prepare the interesting Mn complex **48**, either from $BrMn(CO)_5$[95] or $BrMn(CO)_3(Ph_2PCH_2PPh_2)$ by thermal ligand replacement (Scheme 6.5). By treatment of this complex with cppNa we intended to prepare the η^1-cpp complex **49**, which upon reaction with Me_3NO or by UV irradiation could result in CO loss to yield the complexes **50** and **46** (Scheme 6.6).

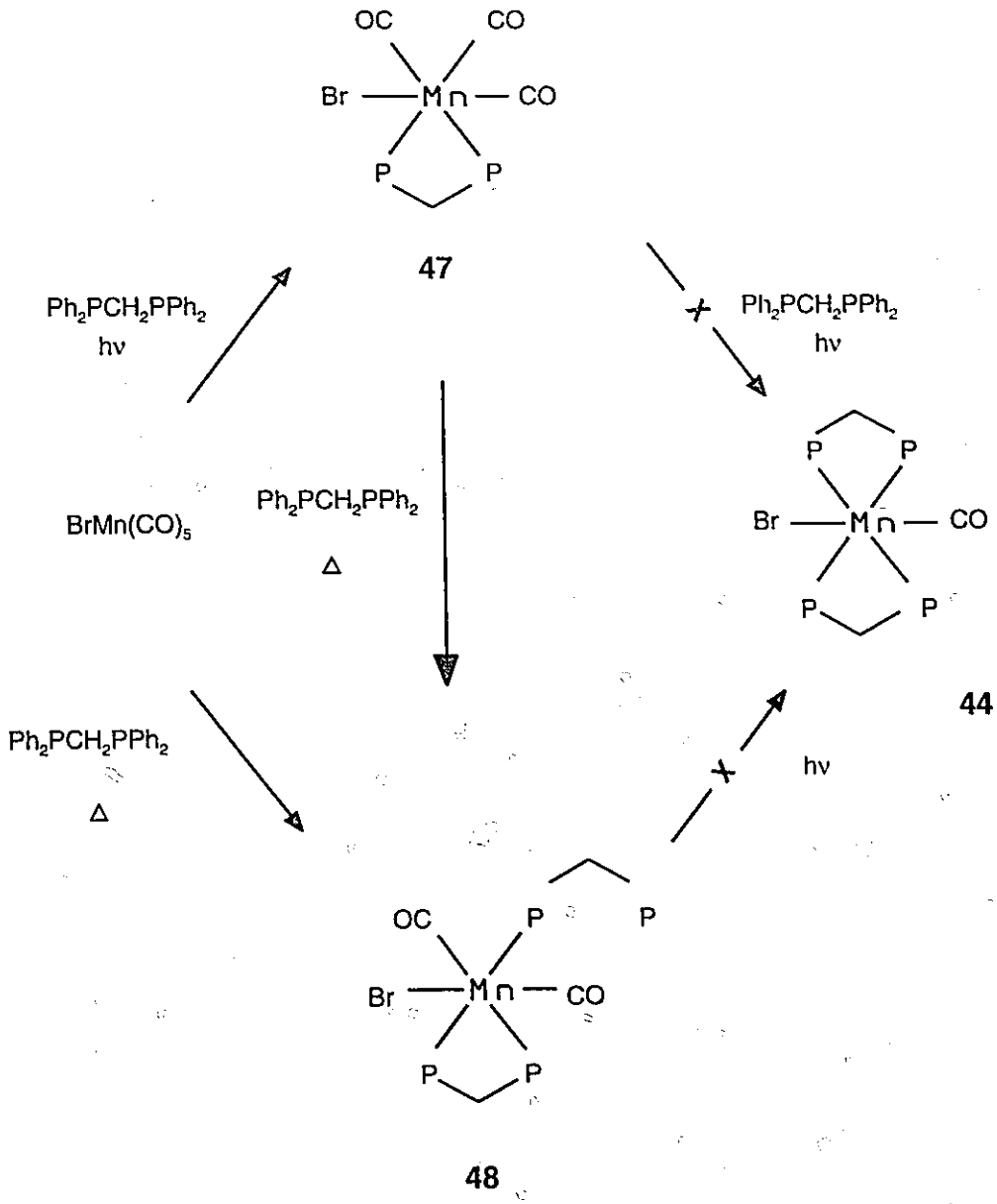
OC
CO
Br
Mn
CO
P
P
47
Ph2PCH2PPh2
hν
Ph2PCH2PPh2
hν
BrMn(CO)5
Ph2PCH2PPh2
Δ
P
P
Br
Mn
CO
P
P
44
Ph2PCH2PPh2
Δ
hν
OC
P
P
Br
Mn
CO
P
P
48

Scheme 6.5

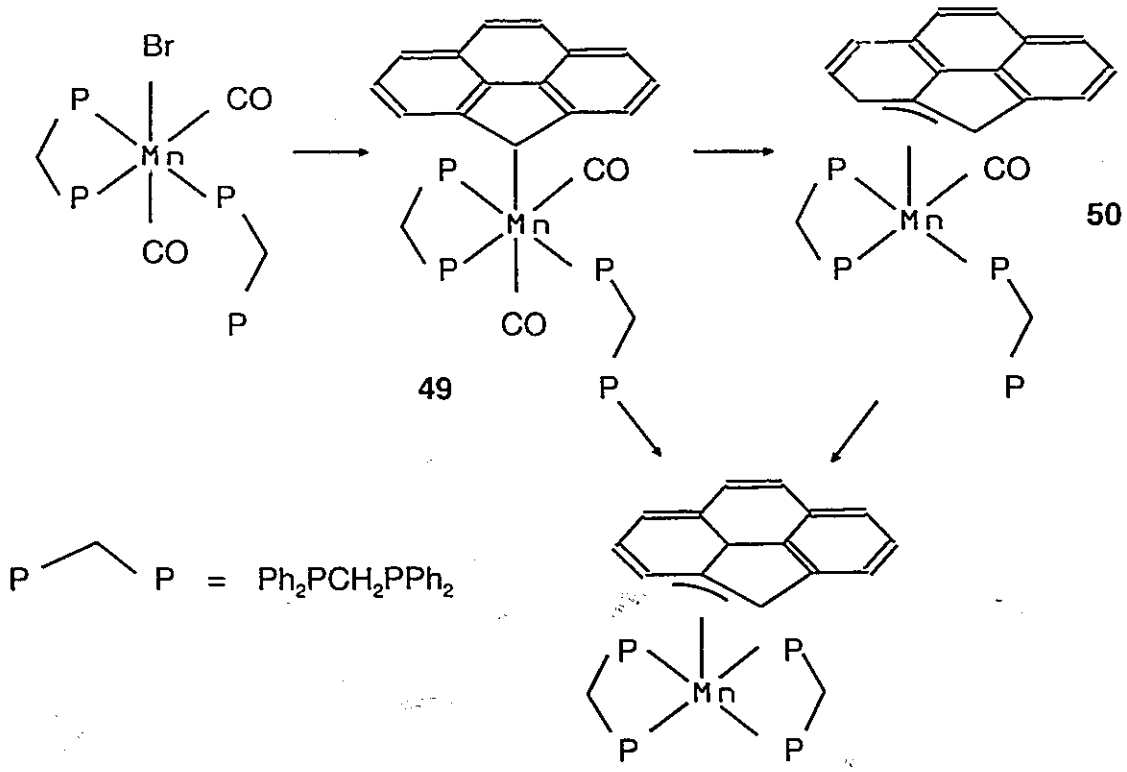

Scheme 6.6

However, after separation of the reaction mixture it became apparent that a cpp complex of Mn had not been prepared. Instead, the cpp *trimer* **52** and the bis-Mn complex **53**[96] were isolated.

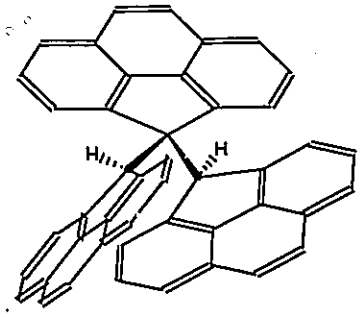

52

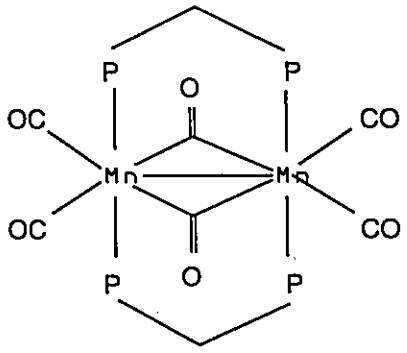

53

6.2 The $(\eta^1\text{-cpp})Fe(CO)_2(\eta^5\text{-}C_5H_5)$ system.

In 1956, Piper and Wilkinson reported on the synthesis of $(\eta^1\text{-}C_5H_5)Fe(CO)_2(\eta^5\text{-}C_5H_5)$, **53**, from the interaction of CpNa and $IFe(CO)_2(\eta^5\text{-}C_5H_5)$ (Scheme 6.7).[97] The molecule attracted considerable interest since it appeared to be fluxional. The ^1H NMR of the molecule changes with temperature and it was rationalized by rapid 1,5-sigmatropic rearrangement of the $(\eta^5\text{-}C_5H_5)Fe(CO)_2$ unit around the σ-coordinated cyclopentadienyl ring.[98] The authors noted that, although fairly stable, the material slowly lost carbonyls and reverted to the very stable ferrocene.

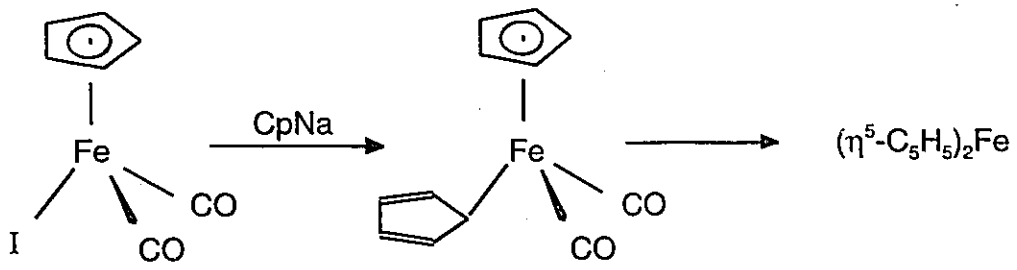

53

Scheme 6.7

Using NaCpp instead of NaCp, we had hoped to obtain the mono-hapto complex $(\eta^1\text{-cpp})Fe(CO)_2(\eta^5\text{-}C_5H_5)$, **54**. Selective removal of CO using Me_3NO or by UV irradiation was expected to yield the η^3-cpp complex **55** or the ferrocene analogue $(\eta^5\text{-cpp})Fe(\eta^5\text{-}C_5H_5)$, **27** (Scheme 6.8). Reaction of NaCpp with $IFe(CO)_2(\eta^5\text{-}C_5H_5)$ yielded the η^1-cpp derivative **54** in surprisingly good yields.[99] The complex turned out to be very stable. Attempts to remove CO with Me_3NO following the procedures described by Black et al.[100] did not yield the desired products **55** or **27** but resulted in decomposition of the organometallic compound.

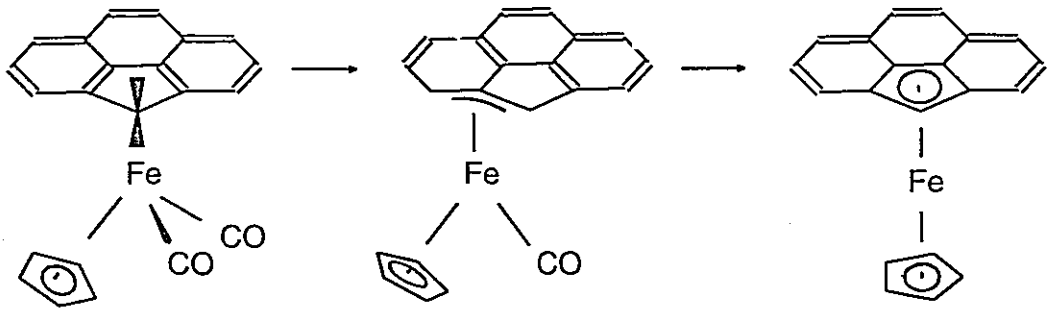

54 **55** **27**

Scheme 6.8

Furthermore, in the hope that (η^1-cpp)Fe(CO)$_2$(η^5-C_5H_5) would mirror the behaviour of the analogous (η^1-C_5H_5) complex,[97] (η^1-cpp)Fe(CO)$_2$(η^5-C_5H_5), **54,** was dissolved in $CH_2C\ell_2$ and left for several weeks. Rearrangement to the η^3- and η^1-species **55** and **27** was not observed. Instead, trimerization of the cpp ligand yielded the molecule **52** (Figure 6.3).

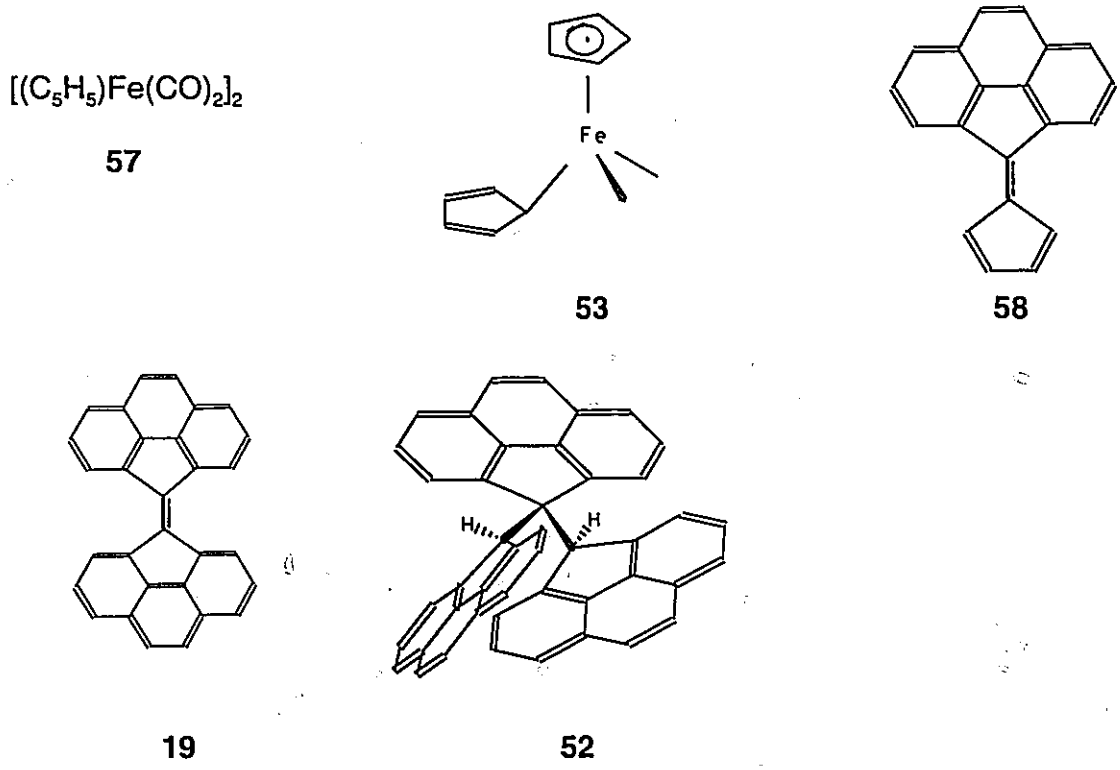

Figure 6.3 Side products in the preparation of (η^1-cpp)Fe(CO)$_2$(η^5-C_5H_5), **54**

Though the synthesis of $(\eta^1\text{-cpp})Fe(CO)_2(\eta^5\text{-}C_5H_5)$ was surprisingly facile, isolation of the orange product was complicated since a number of by-products were obtained and had to be separated. Flash chromatography of the crude reaction mixture yielded a series of pure compounds, illustrated in figure 6.3, as well as the starting materials cppH and $IFe(CO)_2(\eta^5\text{-}C_5H_5)$. The cpp *trimer* $C_{45}H_{26}$, **52**, has been reported in the literature, although characterized extremely poorly.[101] It is believed to be the product the reaction of cppH with the ylid **19**. The *trimer* was identified by ^1H and ^{13}C NMR as well as MS. This material could be of potential interest for X-ray crystal structure determination. Single crystals of cppH, **6**, were obtained but appear to be highly disordered. Several data sets were obtained but a structure determination did not allow satisfactory refinement. From this data it can not be concluded whether the free ligand cppH is a planar molecule or whether it is arched. In all metal complexes of cppH we have found that the ligand gently arches away from the metal fragment (see Chapters 2 and 3 for a more detailed discussion). The cpp *trimer* may allow an X-ray structure determination and the deviation from planarity in the central $C_{15}H_8$ fragment and the terminal $C_{15}H_9$ fragments could be compared with the deviation from planarity in the cppH complexes $(\eta^6\text{-cppH})Cr(CO)_3$, **8**, $(\eta^6\text{-cppH})Fe(\eta^5\text{-}C_5H_5)PF_6$, **14** and $(\eta^5\text{-cppH})Mn(CO)_3$, **29**.

6.3 The (η^5-cpp)$Mn(CO)_3$ system.

Ligand removal from η^1-complexes of cpp as in (η^1-cpp)Mn(CO)-$(Ph_2PCH_2PPh_2)_2$ and (η^1-cpp)$Fe(CO)_2(\eta^5-C_5H_5)$ to yield η^3-complexes of cpp were not successful. We were not able to prepare the Mn complex, whereas the Fe complex was found to be too stable and CO removal using Me_3NO was not achieved.

Starting from a η^5-complex of cpp it might be possible to add a two electron donor ligand such as PR_3 and $P(OR)_3$ to induce migration of the metal fragment and so lead to the isolation of an allylic isomer of the cpp ligand. The ideal starting material for such an attempt would be (η^5-cppH)$Mn(CO)_3$. Following the procedures described by Biagioni[93] for the addition of phosphines to the fluorenyl complex ($\eta^5-C_{13}H_9$)$Mn(CO)_3$ we were hoping to obtain the mono(phosphine) products (η^3-cpp)$Mn(CO)_3PR_3$ (**58** or **59**) (Figure 6.4).

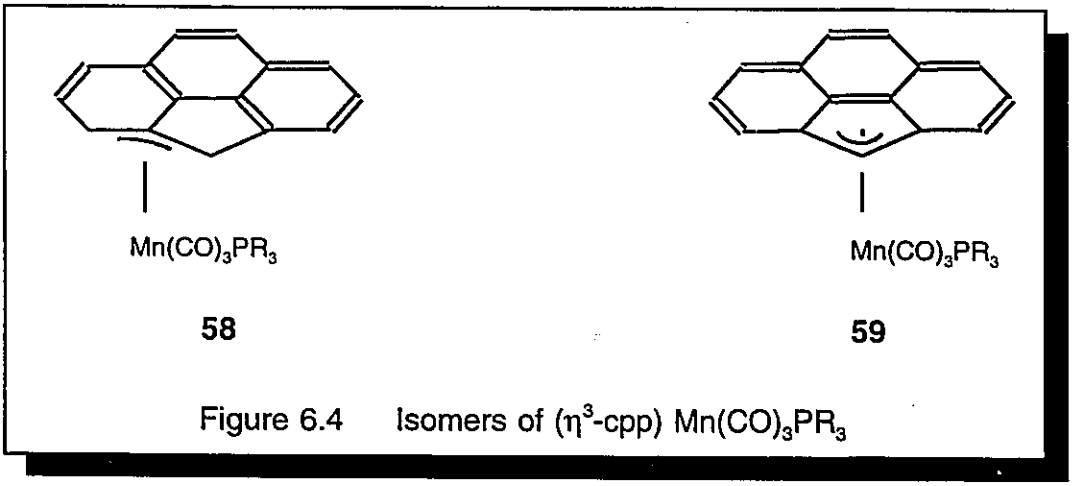

58 **59**

Figure 6.4 Isomers of (η^3-cpp) $Mn(CO)_3PR_3$

Modifying the literature procedure,[93] $P(C_2H_5)_3$ was added to a solution of ($\eta^5-C_{15}H_9$)$Mn(CO)_3$ in benzene, the mixture concentrated immediately and the product precipitated by addition of hexane. However, ^{31}P, ^1H and ^{13}C NMR, as well

as mass spectrometry suggested that we had isolated a bis(phosphine) addition product. The spectra are in agreement with the data published for $(\eta^1\text{-}C_{13}H_9)Mn(CO)_3(P(C_2H_5)_3)_2$[93] and contradict Basolo's findings.[91] The NMR data for our cpp complex suggested that the molecule contained two inequivalent phosphine groups. Three different isomers can theoretically be envisage for (Figure 6.5). The mer-cis(phosphine) isomer **60a** and the fac-cis(phosphine) isomer **60b** contain inequivalent phosphine groups, whereas the mer-trans(phosphine) isomer **60c** is expected to involve equivalent phosphine groups, based on the assumption of rapid rotation around the metal ligand σ-bond.

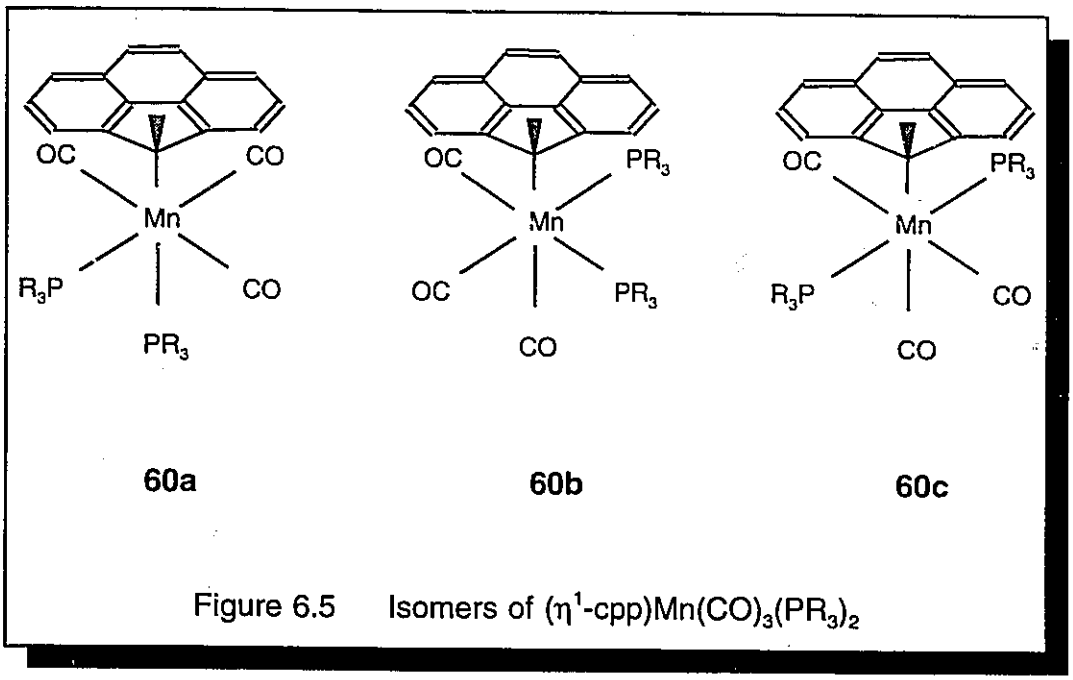

Figure 6.5 Isomers of $(\eta^1\text{-cpp})Mn(CO)_3(PR_3)_2$

Crystals of the material were grown by evaporation of a solution of **60** in a mixture of $CH_2C\ell_2$, 1,2-dichloroethane, hexane and heptane. The X-ray crystal structure appears as figure 6.6.

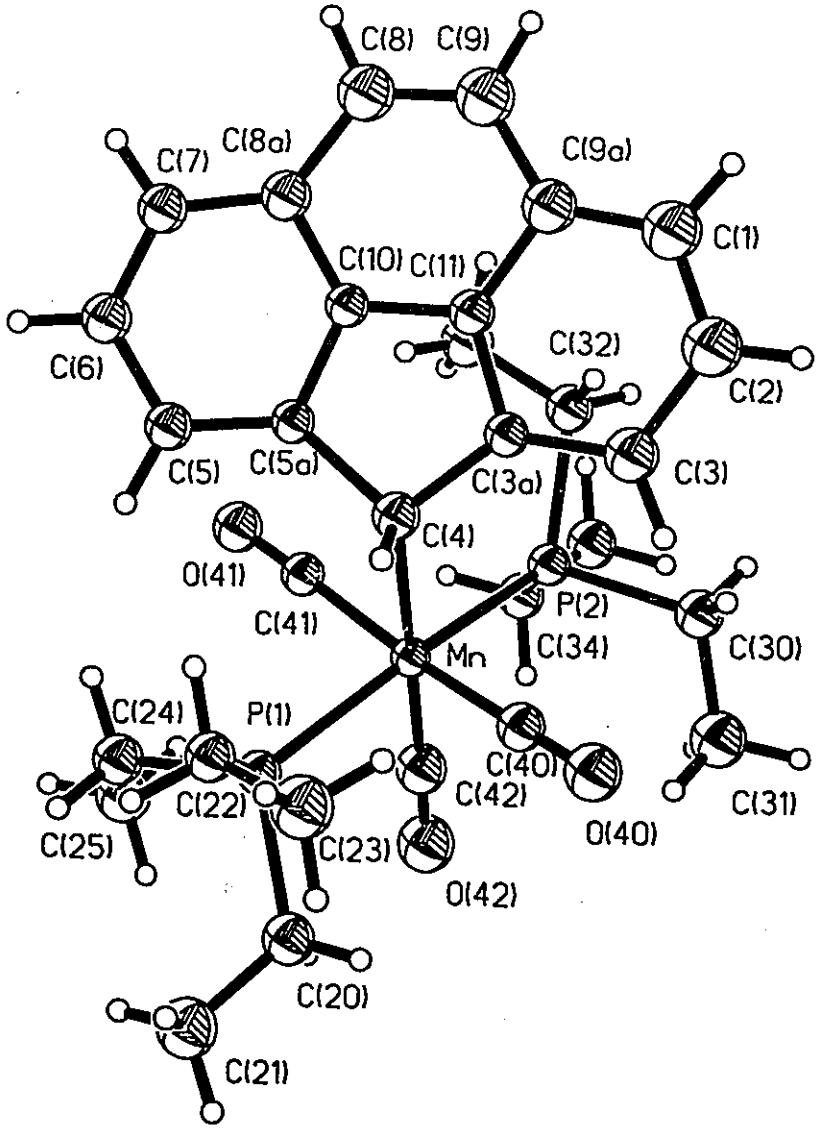

Figure 6.6 X-ray crystal structure of $(\eta^1\text{-cpp})Mn(CO)_3(PEt_3)_2$, **60**

As can be seen from the X-ray structure determination, the phosphine ligands are trans to each other and the molecule adopts the mer-trans(phosphine) arrangement **60c**, a structure that Biagioni et al. suggested for the fluorenide analogue.[93] The structure does not contain a single mirror plane as expected, but

rather contains one of the phosphine ligands displaced under the cpp ligand, whereas the second phosphine ligand points away from it. Therefore, the two phosphine groups become inequivalent. One can imagine rapid rotation around the metal-cpp σ-bond so that the phosphine groups appear to be equivalent on the NMR time scale. At ambient temperature it was found that the NMR reveals two sets of signals for the phosphorus (^{31}P NMR), the CH_2 groups (^{1}H and ^{13}C NMR) and the CH_3 groups (^{1}H and ^{13}C NMR) in the $P(CH_2CH_3)_3$ region. Interestingly, the cpp ligand itself exhibits only four signals in the uncomplexed CH region, suggesting a pseudo mirror plane bisecting C(4) and the bond between C(8) and C(9). These results imply that the complex is indeed fluxional, but a relatively high barrier to rotation and the large chemical shift separation of the two phosphine ligands allows the observation of two inequivalent ligands at ambient temperature. Unfortunately, not enough material was obtained to allow a variable temperature, multinuclear NMR investigation.

The above model assumes a relatively high barrier to rotation. In contrast, rotations around metal-C single bonds are generally expected to be quite facile and any divergence from this generalization would have to be based on steric hindrance. Careful investigation of the crystal structure of this molecule reveals that the ligand undergoes quite substantial twisting to accommodate the proximal PR_3 group. As can be seen from Figure 6.7, not only is the ligand located unsymmetrically between the two phosphines, it also bends away from the phosphine that is located underneath the cpp surface.

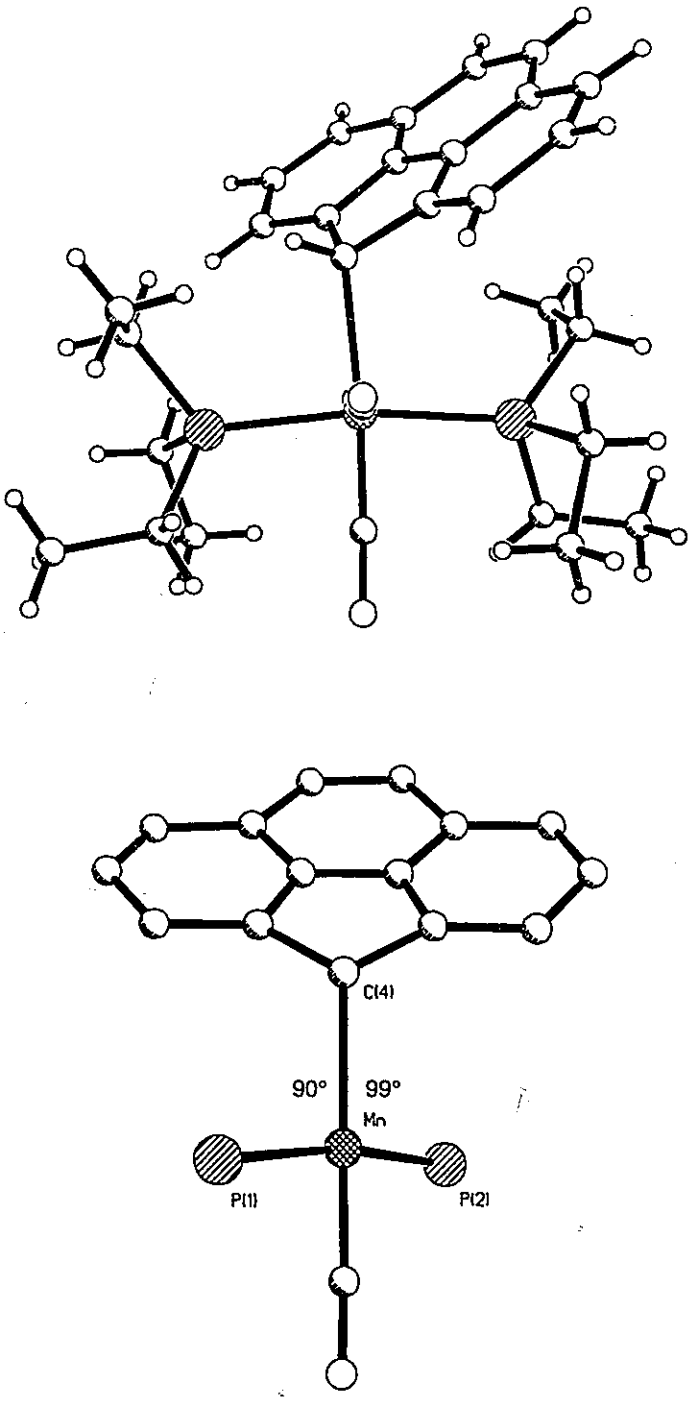

Figure 6.7 Views of the structure of $(\eta^1\text{-cpp})Mn(CO)_3(PR_3)_2$, **60**

Chapter 7: Future work

A very important question raised during the course of this thesis dealt with the quest to experimentally prove the trajectory calculated via the extended Hückel molecular orbital (EHMO) approach. So far, systems which yielded starting materials that can be obtained in high yields have failed to yield isolable η^3-complexes. However, many low yield synthesis to η^3 coordinated metal systems are known. Very stable compounds are usually obtained upon treatment of allyl halides with $Fe_2(CO)_9$. The appropriate starting material to adopt this approach for the preparation of (η^3-cpp)$Fe(CO)_3Br$, **62**, would be 4-Br, 4H-cyclopenta[def]phenanthrene, **61**, a molecule that can be obtained by interaction of cppH and N-bromosuccinimide (Scheme 7.1).

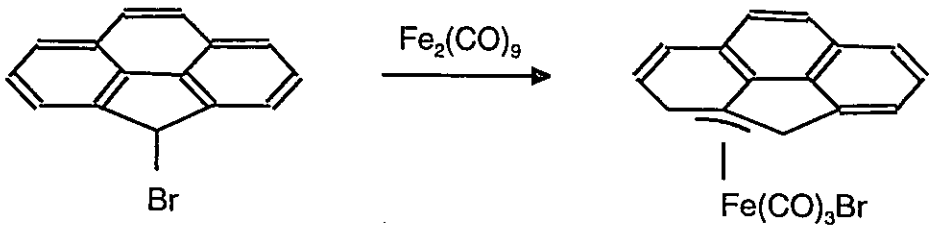

61 **62**

Scheme 7.1

Every approach mentioned in this thesis to trap or isolate a complex of cpp in which the ligand is bonded to a metal fragment in a η^3 fashion involves electronic control to afford an exocyclic allylic complex. Steric control might be achievable by blocking the C(4) position in cppH with a bulky group and therefore

eliminating the $\eta^6 \rightarrow \eta^5$ shift. Treating the alkyl substituted organometallic complexes **63** with base should yield compounds of the type **64**. Rearrangement to the corresponding allylic species **65** can be expected for $ML_n = Cr(CO)_3^-$ and $Mn(CO)_3$, whereas for $M = Fe(C_5H_5)$ a metal shift will be unlikely (Scheme 7.2).

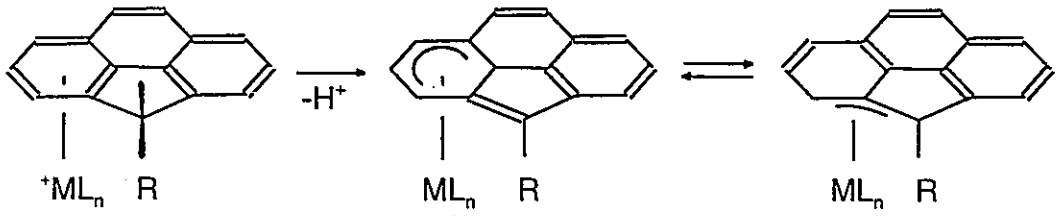

63 **64** **65**

R: $C(CH_3)_2H$, $C(CH_3)_3$

a: $ML_n = Cr(CO)_3^-$

b: $ML_n = Mn(CO)_3$

c: $ML_n = Fe(C_5H_5)$

Scheme 7.2

As fascinating as haptotropic rearrangements, especially inter-ring migrations, in metal complexes may be viewed, experimentally they have been based on the trial and error method. Metal migrations have been studied mostly in systems where the organic ligand is commercially, or at least easily, available. Failure or unexpected deviation from the expected rearrangement behaviour in complexes that are readily available does not present a major problem. However, haptotropic rearrangements in metal complexes of complicated, multi-fused ring systems has not been investigated thoroughly, mainly because of the uncertainty in the rearrangement behaviour. The possible failure to detect rearrangements in complexes of ligands that can only be obtained via a multi-step syntheses is a

concern and has hindered the expansion of research to interesting, but complicated ring systems. With the availability of cheap personal computers and software, the researcher is now able to predict the rearrangement behaviour of metal complexes.

A very interesting area of haptotropic rearrangements that has not been explored so far is that of multiple inter-ring migrations. One might wonder, whether deprotonation of complexes like **66** and **67** will lead to haptotropic rearrangement (Figure 7.1).

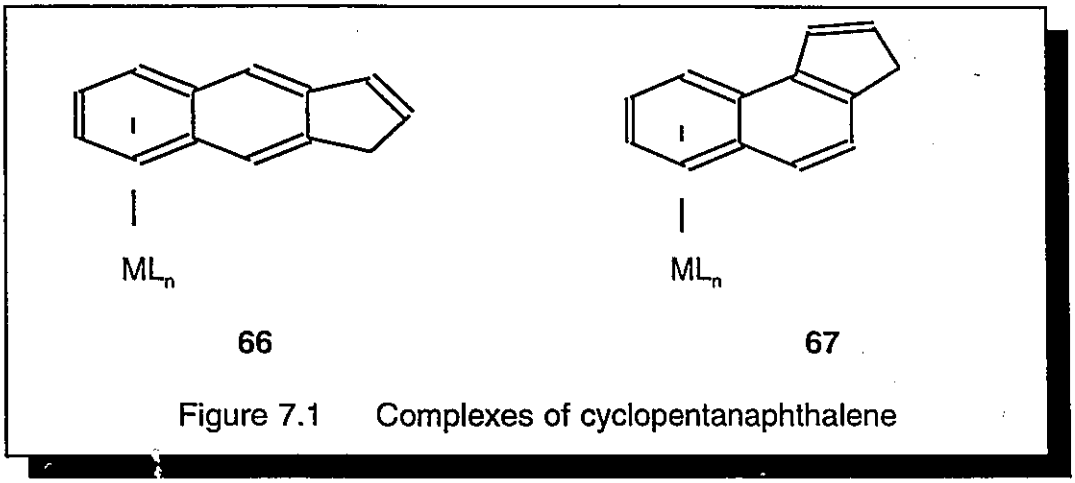

66 **67**

Figure 7.1 Complexes of cyclopentanaphthalene

Furthermore, one might speculate whether the rearrangements will lead to species in which the metal is bonded to the external six-membered ring, **68** and **71**, the internal six-membered ring, **69** and **72**, or the five-membered ring, **70** and **73** (Scheme 7.3).[102]

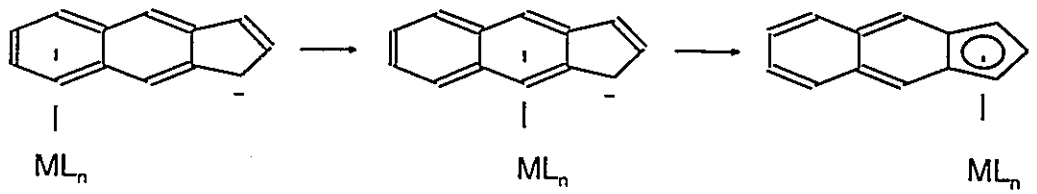

68 **69** **70**

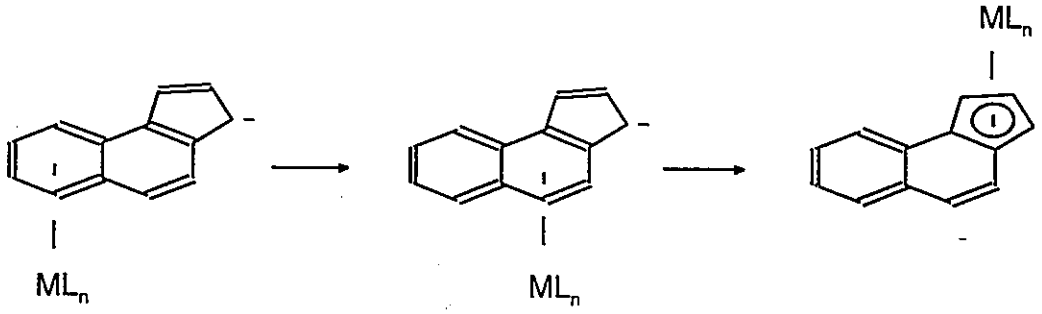

71 **72** **73**

Scheme 7.3

Another intriguing system is the tricyclic system shown in figure 7.2. It contains a five-, a six-, and a seven-membered ring. Preliminary studies on this particular system suggest that haptotropic rearrangements can be expected to proceed from the six-membered ring into the five-membered ring, **76**, upon deprotonation of the starting material. Metal shifts into the seven-membered ring, **75**, can be

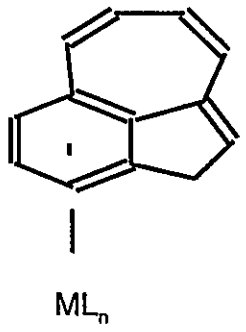

Figure 7.2

accomplished by hydride abstraction starting with the same complexes.[102]

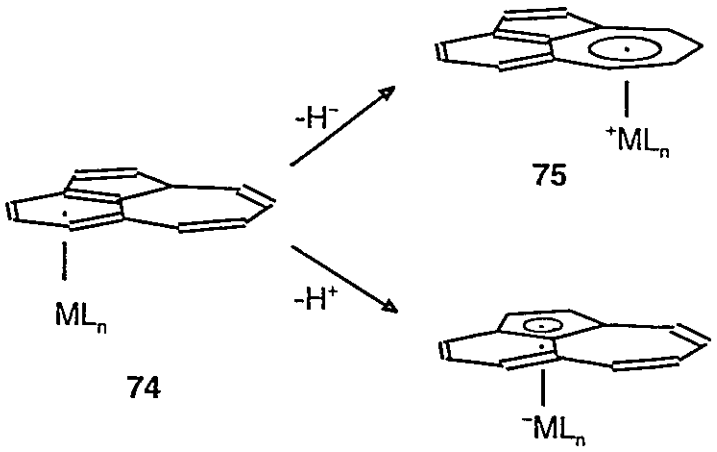

Scheme 7.4

Using the approach that we have used as outlined in chapter 5, one can calculate the barriers to migration simply by moving a metal fragment over the surface of the organic ligand. Computing the energies for the entire surface of a ligand permits the consideration of (a) least-motion, (b) linear, non-least-motion and (c) non-linear, non-least-motion pathways. In this case the less obvious non-linear pathways will not be missed and the overall lowest barrier to the particular rearrangement can be compared to calculated barriers in systems that have shown to rearrange. Molecules in which the barriers are calculated to be fairly low and therefore have the potential to undergo metal shifts are very attractive to the synthetic chemist even if the organic ligand requires a multi-step synthesis.

Chapter 8. Experimental

8.1 General procedures

All preparations were carried out under a dry atmosphere of nitrogen and solvents were dried according to standard procedures.[103] Ferrocene[104] and $BrMn(CO)_5$[105] were prepared according to standard procedures. Melting points were measured in open glass capillaries using a Thomas Hoover Unimelt capillary melting point apparatus. The melting points were not corrected.

8.2 NMR spectra

All NMR spectra were recorded on a Bruker AM-500, AC-300 or AC-200 spectrometer. Proton spectra obtained on an AM-500 spectrometer were acquired at 500.135 MHz using a 5 mm dual frequency ^1H - ^{13}C probe. Spectra were obtained in 8 scans in 32K data points over a 5.000 kHz spectral width (3.277 s acquisition time). Sample temperature was maintained at 30 °C by a Bruker BVT-1000 variable temperature unit. The free induction decays (FID) were processed using exponential multiplication (line broadening 0.3 Hz). The free induction decays of $(\eta^6\text{-}H_8cppH)Cr(CO)_3$, **12**, were acquired in 32K data points over a spectral width of 5.0 kHz. The data were processed using Gaussian multiplication for resolution enhancement (line broadening: -1.5 Hz, Gaussian broadening factor: 0.2) and were zero-filled to 64K before Fourier transformation. Proton spectra obtained on an AC-200 spectrometer were acquired at 200.133 MHz using a 5 mm dual frequency ^1H - ^{13}C probe. Spectra were obtained in 32 scans in 16K data

points over a 2.000 kHz spectral width (4.096 s acquisition time). The free induction decays (FID) were processed using exponential multiplication (line broadening 0.3 Hz).

Proton-proton NOE difference spectra obtained on an AM-500 spectrometer were acquired by subtraction of a control FID from an on-resonance FID. The decoupler in the control FID irradiated a position in the spectrum where there were no proton signals. The on-resonance FID was obtained with the proton of interest being selectively saturated. In both cases the same decoupler power and duration of saturation (5.0 s) were used. This saturation period also served as the relaxation delay for both the control and on-resonance FID's. The decoupler was gated off during acquisition. Eight scans were acquired for both the control and on-resonance FID's. The cycle of alternate acquisition of control and on-resonance FID's was repeated 4 times for a total of 32 scans for the complete difference FID. A 90° ^{1}H pulse width of 18.6 μs was used. The difference FID was processed using exponential multiplication (line broadening 4.0 Hz) and was zero-filled to 32K before Fourier transformation. The sample was not degassed.

Proton COSY 2-D NMR spectra were recorded in the absolute value mode using the pulse sequence 90° - t_1 - 90° - ACQ. Spectra were acquired in 8 scans for each of the 256 FID's that contained 2K data points in F2 over a 2.941 kHz spectral width. The ^{1}H 90° pulse width was 18.6 μs. A 1.0 s relaxation delay was employed between acquisitions. Zero-filling in the F1 dimension produced a 1K x 1K data matrix with a digital resolution of 2.872 Hz/point in both dimensions. During the 2-D Fourier transformation a sine-bell squared window function was applied in both dimensions. The transformed data were then symmetrized.

TOCSY 2-D NMR spectra were acquired on an AM-500 spectrometer in the phase-sensitive mode using the MLEV-17 pulse sequence for spin locking.[106] Time proportional phase incrementation (TPPI) was used to obtain the phase-sensitive data.[107,108] Spectra were obtained in 8 scans for each of the 256 FID's that contained 2K data points in the F2 dimension. The spectral width in F2 was 2.941 kHz. The 90° ^{1}H pulse width for the spin lock pulse in the 5 mm broadband inverse probe was adjusted to 25.3 μs. A 1.0 s relaxation delay was used. The length of the spin lock mixing time was 80 ms. A trim pulse of 2.5 ms was used just before and after the spin lock period. Zero-filling once in the F1 dimension resulted in a digital resolution of 2.872 Hz/point in both dimensions. During the real 2-D Fourier transformation a sine-bell squared window function shifted by $\pi/2$ was applied in both dimensions. The data were not symmetrized.

Deuterium NMR spectra obtained on the AM-500 spectrometer were recorded at 76.774 MHz using a 5 mm dual frequency ^{1}H - ^{13}C probe. The spectra were acquired in 360 scans over a spectral width of 2.000 Hz in 16K data points (4.096 s acquisition time) through the deuterium lock channel. The FID's were processed using exponential multiplication (line broadening 5.0 Hz).

Phosphorus-31 NMR spectra were obtained on an AC-300 spectrometer were recorded at 121.497 MHz using a 10 mm QNR probe. The spectra were acquired over a 19.200 kHz spectral width in 16K data points (0.426 s acquisition time). The ^{31}P pulse was 3.7 μs. The FID's were processed using exponential multiplication (line broadening 3.0 Hz).

Carbon-13 NMR spectra obtained on an AM-500 spectrometer were recorded at 125.759 MHz using a 5 mm ^{1}H-^{13}C broad band inverse probe. The

spectra were acquired over a 34.400 kHz spectral width in 16K data points (0.279 s acquisition time). The ^{13}C pulse width was 2.5 μs (35° flip angle). The FID's were processed using exponential multiplication (line broadening 3.0 Hz). The ^{13}C spectra acquired on a AC-200 spectrometer were obtained at 50.324 MHz using a 5 mm ^{1}H-^{13}C dual frequency probe. The spectra were recorded over 12.581 kHz spectral width in 16K data points (0.672 s acquisition time). The ^{13}C pulse width was 1.5 μs (45° flip angle). The FID's were processed using exponential multiplication (line broadening 3.0 Hz).

J-modulated spin sort spectra were acquired on an AM-500 spectrometer using the 5 mm broadband inverse probe and the standard pulse sequences. Spectra were obtained in 16K data points over a 31.250 kHz spectral width (0.262 s acquisition time). A relaxation-delay of 1.0 s was applied and the ^{13}C 90° pulse width was 10.5 μs. The FID's were processed using exponential multiplication (line broadening: 5.0 Hz).

Inverse detected ^{1}H-^{13}C 2-D chemical shift correlation spectra were recorded in the phase-sensitive detection mode using an AM-500 spectrometer and a 5 mm broadband inverse probe. The FID's in the F2 (^{1}H) dimension were recorded over a 2.941 kHz spectral width in 2K data points. The 128 FID's in the F1 (^{13}C) dimension were obtained over a 11.363 kHz spectral width. Each FID was acquired in 32 scans. The fixed delays during the pulse sequence were a 1.0 s relaxation delay, a 0.003571 s delay for the BIRD pulse, a 0.4 s delay between the BIRD pulse and the inverse pulse sequence , and a polarization transfer delay of 0.003571 s. The 90° ^{1} pulse was 9.2 μs while the ^{13}C 90° pulse was 10.1 μs. The data were processed using a sine-bell squared window function shifted by $\pi/2$ in

both dimensions.

The ^{13}C-^{1}H 2-D chemical shift correlation spectra were acquired on an AM-500 spectrometer and a 5 mm dual frequency^{1}H - ^{13}C probe, using the standard pulse sequence incorporating the BIRD pulse during the evolution period for ^{1}H-^{1}H decoupling in F1. The spectra in F2 were recorded in a spectral width of 2.173 kHz in 2K data points. The 256 FID's in F1 were obtained over a spectral width of 1.087 kHz. The fixed delays in the pulse sequence were a 1.0 s relaxation delay, BIRD pulse and polarization transfer delays (1/2 J_{CH}) of 0.003571 s, and a refocussing delay (1/4 J_{CH}) of 0.001786 s. The data were processed using exponential multiplication (line broadening: 4 Hz) in F2 and unshifted sine-bell in F1. Zero-filling in F1 resulted in a 1K x 1K data matrix.

8.3 Mass spectra

Fast Atom Bombardment (FAB) was performed on a VG analytical micromass ZAB-ZE spectrometer with an accelerating power of 8 kV and a resolving power of 10,000 and a VG11/250 data system. 3-Nitrobenzyl alcohol was used as the sample matrix and Helium as the bombarding gas.

8.4 IR spectra

All infrared spectra were obtained on a Bio Rad FTS-40 FT-IR spectrometer and a SPC 3200 work station using NaCℓ 0.1 mm solution cells. A Beckman polystyrene calibration sample was used as a standard.

8.5 Microanalyses were performed by Guelph Chemical Laboratories in Guelph, Ontario.

8.6 X-ray crystallography

Tables regarding crystal data, data collection, solution and refinement, atomic coordinates and equivalent isotropic displacement coefficients, bond length and bond angles are collected in the appendix. Additional information has been stored on a 5.25" disk (departmental thesis copy). The files A.SFT through G.SFT contain the tables of observed and calculated structure factors according to the numbering scheme shown below. The files can be loaded into WordPerfect. The following trivial names have been assigned:

cppH, **6**	A
$(\eta^6$-cppH)$Cr(CO)_3$, **8**	B
$(\eta^6$-H_2cppH)$Cr(CO)_3$, **11**	C
$(\eta^6$-H_8cppH)$Cr(CO)_3$, **12**	D
$(\eta^6$-cppH)$Fe(\eta^5$-$C_5H_5)$ PF_6, **14**	E
$(\eta^5$-cpp)$Mn(CO)_3$, **29**	F
$(\eta^1$-cpp)$Mn(CO)_3(P(Et)_3)_2$, **60**	G

Crystals of **6** (cppH) were grown by slow cooling of a concentrated solution of **6** in n-hexane to -20°C. Crystals of **8**, **11**, **12**, **14** and **29** were grown by vapour diffusion techniques[77] using 1,2-dichloroethane and n-heptane at -22 °C. Crystals of **60** were grown by slow evaporation of the solvent of **60** in dichloromethane, 1,2-dichloroethane, n-hexane and n-heptane at ambient temperature. All crystals

except **6** were mounted on fine glass fibres with epoxy cement. Crystals of **6** were mounted in 0.3 mm capillaries by wedging to avoid dissolution into the epoxy cement used for fine glass fibre mounting. The unit cells were determined by automatic indexing of 25 centered reflections. Intensity data for **8**, **11**, **12** and **60** were collected on a Siemens P4 diffractometer fitted with a rotating anode using graphite-monochromated Mo Kα X-radiation (λ = 0.71073 Å) at room temperature. Data collection for **14** and **29** was performed on a Siemens R3m/V diffractometer using graphite-monochromated Ag Kα (λ = 0.56086 Å). Data collection for **6** was performed on a Rigaku AFC6R diffractometer fitted with a rotating anode using graphite-monochromated Cu Kα (λ = 1.54178 Å). Three check reflections were measured every 97 reflections. The heavy atom positions were obtained using Patterson methods or direct methods, and phase extension and Fourier difference techniques revealed the remaining non-hydrogen atoms. Hydrogen positions for **12** and **29** were determined by Fourier analysis. Hydrogen atoms for **29** were refined isotropically using individual U's. Hydrogen atoms for **12** were refined using a riding model and common isotropic temperature factors. Hydrogen atoms for **14**, **8** and **11** were included in calculated positions (d(C-H) = 0.96 Å) and refined using a riding model and common isotropic temperature factors. Hydrogen atoms for **6** were included in fixed, calculated positions (d(C-H) = 0.96 Å) and refined using common isotropic temperature factors. Thermal motion of the ligand in **11** and the C_5H_5 ring in **14** were corrected employing librational rigid-body motion analysis.[78] The disorder in the PF_6^- ion in **14** was modeled using two sets of PF_6 with a common central atom. The occupancy was refined to 0.84 : 0.16 using a common temperature factor. Consequently, refinement of isotropic

temperature factors was achieved with fixed occupancies. The disorder in the ligand position in **12** was refined using two sets of atom positions for C5a, C5, C6, C7, C8, C8a and C9. The atoms were refined isotropically with a distribution factor of 0.77 : 0.23 in anology to the procedure for **14**. The carbon atoms for two molecules in **6** were found using direct methods. Phase extension and Fourier difference analysis revealed disorder in the atom positions. The disorder was modeled using fragmentation approach for two sets of molecules per site and rigid group refinement. The atoms were refined isotropically with a distribution factor of 0.61 : 0.53 : 0.47 : 0.39 in anology to the procedure for **14**. The fragment parameters were taken from the X-ray crystal structure of **29**. Data collection for **60** was not completed because of instrument failure.

Scattering factors were supplied by the software. Data reduction, structure solution, refinement, graphics and table generation programs are contained in the SHELXTL and SHELXL program library.[109]

8.7 Molecular orbital calculations were performed via the extended Hückel method using weighted H_{ij}'s; orbital drawings were obtained by use of the programm CACAO.[110] The geometry of the polycyclic ligand was an idealized, planar version taken from the X-ray crystal structure of $(\eta^5\text{-cpp})Mn(CO)_3$. The following distances were used: Fe-Cp = 1.66 Å, Fe-cpp = 1.59 Å, Mn-cpp = 1.82 Å and Mn-CO = 1.79 Å. The angle ∢ OC-Mn-CO was set to 125°. Orbital parameters were taken from reference 25.

8.8 Numbering scheme in complexes of 4H-Cyclopenta[def]phenanthrene

For NMR assignments, following numbering scheme was established:

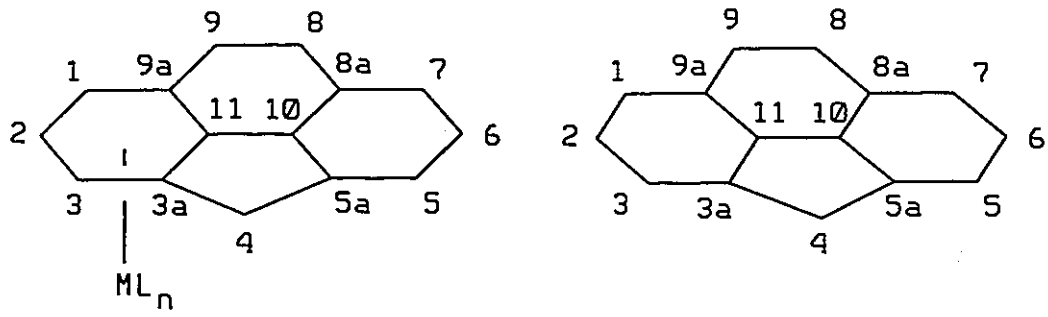

8.9 Synthesis and spectral data

4H-Cyclopenta[def]phenanthrene (cppH), 6, was obtained from Aldrich Chemical Company and was used without further purification. ^{1}H NMR (200 MHz, acetone-d_6) δ 7.87 (s, 2H, H-8,9), 7.85 (d, 7.9 Hz of d, 0.5 Hz, 2H, H-1,7), 7.72 (d, 7.1 Hz of d, 0.5 Hz, 2H, H-3,5), 7.65 (d, 7.9 Hz of d, 7.1 Hz, 2H, H-2,6, 4.35 (s, 2H, H-4). The H-3,5 attributions were made on the basis of their NOE interactions with the H-4 protons at 4.35 ppm. ^{13}C NMR (50 MHz, acetone-d_6) δ 142.7 (C-8a,9a), 139.0 (C-3a,5a), 128.9 (C-10,11), 128.0 (C-2,6), 125.9 (C-8,9), 121.9 (C-3,5), 123.4 (C-1,7), 37.8 (C-4). The C-3a,5a and C-8a,9a carbons were assigned on the basis of a ^{1}H-^{13}C coupled experiment with the delays adjusted for long-range couplings.

(η^6-4H-Cyclopenta[def]phenanthrene)$Cr(CO)_3$, 8. CppH, **6**, (1 g, 5.25 mmol) and $Cr(CO)_6$ (1.15 g, 5.25 mmol) were heated under reflux in 1,2-dimethoxyethane (70 mL) for 30h. After separation of unreacted $Cr(CO)_6$ by filtration, the solvent was removed on a rotary evaporator. Unreacted cppH was recovered by flash chromatography on silica using hexane as eluent; upon changing the solvent to 1:1 hexane/$CH_2C\ell_2$, **8** was eluted and yielded an orange-red solid (340 mg, 1.04 mmol, 20%), m.p. 193 °C (dec.). ^{1}H NMR (500 MHz, 9:1 acetone-d_6/benzene-d_6) δ 7.79 (d, 9.1 Hz, 1H, H-8), 7.76 (d, 7.2 Hz, 1H, H-7), 7.73 (d, 7.2 Hz, 1H, H-5), 7.67 (d, 7.2 Hz of d, 7.2 Hz, 1H, H-6), 7.62 (d, 9.1 Hz, 1H, H-9), 6.22 (d, 6.5 Hz, 1H, H-1), 6.14 (d, 6.0 Hz, 1H, H-3), 5.64 (d, 6.3 Hz of d, 6.3 Hz, 1H, H-2), 4.52 (s, 2H, H-4) (using benzene-d_6, the AB-system can be resolved: 3.98 (d, 20.0 Hz, 1H, H-4_{endo}), 3.56 (d, 20.0 Hz, 1H, H-4_{exo})). ^{13}C NMR (125 MHz, THF-d_8) δ 234.3 (Cr-CO), 130.4 (C-6), 130.0 (C-9), 125.6 (C-8), 124.6 (C-7), 124.5 (C-5), 94.1 (C-2), 90.9 (C-3), 88.5 (C-1) (aromatic C's); 142.0, 137.7, 129.0, 114.0, 111.1, ring junction C's); 38.5 (C-4). Mass spectrum (FAB+), m/z (%): 326 (86) $(M)^+$, 270 (100) $(M-2CO)^+$, 242 (57) $(M-3CO)^+$, 190 (58) $(C_{15}H_{10})^+$. Anal. Calcd for $C_{18}H_{10}CrO_3$: C, 66.12, H, 3.30. Found: C, 65.87, H, 3.21.

8,9-Dihydro-4H-cyclopenta[def]phenanthrene (H_2-cppH), 9. Ethylacetate (50 mL) and Pd/C 5% (30 mg) were stirred at room temperature. H_2 gas was admitted and the apparatus flushed with H_2 three times. After 1h for saturation of the catalyst, cppH, **6**, (190 mg, 1 mmol) was added and the reaction mixture stirred for 3d. The catalyst was filtered off using celite and the solvent evaporated under reduced pressure to yield a white powder (190 mg, 0.99 mmol, 99%). ^{1}H NMR (200 MHz, acetone-d_6) δ 7.31 (d, 7.2 Hz, 2H), 7.16 (t, 7.3 Hz, 2H), 7.07 (d,

7.2 Hz, 2H), 3.82 (s, 2H), 3.07 (s, 4H). ^{13}C NMR (50 MHz, acetone-d_6) δ 128.1 ,125.4, 123.5 (aromatic C's), 141.2, 139.9, 131.1 (ring junction C's); 37.7 (C-4); 26.7 (C-8,9).

(η^6-8,9-Dihydro-4H-cyclopenta[def]phenanthrene)Cr(CO)$_3$, 11. By analogy to the preparation of **8**, H_2-cppH, **9**, (310 mg, 1.6 mmol) and $Cr(CO)_6$ (540 mg, 2.45 mmol) were heated under reflux in $^nBu_2O$ (7 mL) and THF (3 mL) for 3.5d. Unreacted $Cr(CO)_6$ was filtered using Schlenk techniques and the solvent evaporated. The pure product was obtained via flash chromatography using $CH_2C\ell_2$:hexanes 2:1 to yield a yellow solid (246 mg, 0.75 mmol, 47%), m.p. 148 °C. ^{1}H NMR (200 MHz, acetone-d_6) δ 7.31 (d, 7.2 Hz, 1H), 7.23 (t, 7.2 Hz, 1H), 7.12 (d, 7.1 Hz, 1H), 5.99 (d, 6.1 Hz, 1H), 5.57 (t, 6.2 Hz, 1H), 5.49 (d, 6.2 Hz, 1H), 4.13 (d, 21.4 Hz, 1H), 3.92 (d, 21.4 Hz, 1H), 3.1 - 3.0 (m, 4H). Further assignment is possible on the basis of the asis effect: ^{1}H NMR (300 MHz, $CH_2H\ell_2$-d_2) δ 3.51 (d, 21.4 Hz, $H4_{endo}$), 3.28 (d, 21.4 Hz, $H4_{exo}$). ^{13}C NMR (50 MHz, acetone-d_6) δ 235.3 (Cr-CO); 130.1, 126.0, 123.7, 94.3, 90.7 (2C) (aromatic C's); 140.5, 136.7, 131.4, 114.6, 108.4, 107.2 (ring junction C's); 38.0 (C-4); 25.7, 25.6 (C-8,9). Mass spectrum (DEI+), m/z (%): 328 (25) $(M)^+$, 272 (27) $(M\text{-}2CO)^+$, 244 (100) $(M\text{-}3CO)^+$, 189 (8) $(C_{15}H_9)^+$.

Traces of a second product were identified as (η^6-5,5a,6,7,8,8a,9,10-octahydro-4H-cyclopenta[def]phenanthrene)Cr(CO)$_3$, **12**. Mass spectrum (DEI+), m/z (%): 334 (22) M^+, 278 (11) $M\text{-}2CO^+$, 250 (100) $M\text{-}3CO^+$, 158 (8) $C_{12}H_{14}^+$, 52 (52) Cr^+. ^{1}H NMR (500 MHz, $CD_2C\ell_2$) δ 5.45 (H1), 5.31 (H2), 5.05 (H1), 3.13 (H10), 3.07 (H4α), 2.69 (H9α), 2.63 (H9β), 2.54 (H5a), 2.34 (H4β), 2.03 (H8a), 1.88 (H8α), 1.88 (H8β), 1.57 (H6β), 1.56 (H5α), 1.43 (H7α), 1.19 (H6α), 0.96

(H7β), 0.71 (H5β). ^{13}C NMR (125 MHz, $CD_2C\ell_2$) δ 235.2 (CO), 93.5 (C2), 90.1 (C3), 89.6 (C1), 43.9 (C10), 42.1 (C5a), 38.1 (C4), 31.9 (C8a), 28.0 (C5), 27.5 (C8), 24.7 (C7), 24.3 (C6), 22.0 (C9); 119.9, 112.2, 111.0 (ring junction C's).

^2J couplings		$^3J_{a,a}$		$^3J_{a,e}$	
4α,4β	15.5	5a,5β	12.0	5α,6α	2.7
5α,5β	12.8	5β,6α	13.1	6α,7α	2.7
6α,6β	13.1	6α,7β	13.1	6β,7β	2.8
7α,7β	12.9	7β,8a	12.9	7α,8a	3.5
		8a,8β	10.6	8a,8α	3.5
		8β,9α	11.7	8α,9α	6.5
				8β,9β	6.5

$^3J_{e,e}$		others	
6β,7α	3.5	1,2	6.4
8α,9β	2.0	2,3	6.2
		4β,5a	5.8
		8a,10	5.8
		5a,10	5.8
		1,3	0.6

(η^6-4H-Cyclopenta[def]phenanthrene)Fe(η^5-C_5H_5)PF_6, 14. By analogy to the general procedure of Helling and Hendrickson[111], cppH, **6**, (0.95 g, 5 mmol) , Cp_2Fe (0.94 g, 5 mmol), aluminum powder (0.135 g, 5 mmol) and $A\ell C\ell_3$ (1.335

g, 10 mmol) were heated in decalin (10 mL) at 140 °C for 4h. The mixture was cooled to 0 °C, H_2O (25 mL) added and the inorganic solids removed on a sintered funnel. The aqueous layer was isolated and extracted with ether (2 x 25 mL), then treated with NH_4PF_6 (2g, 12.5 mmol) in H_2O (5 mL). The precipitate was collected on a sintered funnel and dried under high vacuum to yield a brown solid (0.52 g, 1.44 mmol, 23% based on cppH), m.p. 143 °C (dec). ^{1}H NMR (200 MHz, $CD_2C\ell_2$) δ 8.09 (d, 9.2 Hz, 1H), 7.92 (m, 2H), 7.88 (d, 6.2 Hz, 1H), 7.79 (d, 9.2 Hz, 1H), 6.93 (d, 5.7 Hz, 1H), 6.81 (d, 5.7 Hz, 1H), 6.19 (t, 5.7 Hz, 1H), 5.12 (d, 21.9 Hz, 1H), 4.69 (d, 21.9 Hz, 1H), 4.29 (s, 5H). ^{13}C NMR (50 MHz, acetone-d_6) δ 133.5, 131.8, 125.7, 93.3, 85.1, 84.1, 82.6, 77.8 (aromatic C's); 142.8, 137.8, 129.8, 126.1, 105.9, 100.4 (ring junction C's); 39.4 (C-4). Mass spectrum (FAB+) m/z (%): 311 (100) $((C_{15}H_{10})FeCp)^+$, 189 (14) $(C_{15}H_9)^+$. Anal. Calcd for $C_{20}H_{15}F_6FeP$: C, 52.66, H, 3.32. Found: C, 52.77, H, 3.16. Traces of a second product were identified as (*trans*-η^6,η^6-4H-Cyclopenta[def]phenanthrene)$(Fe(\eta^5\text{-}C_5H_5))_2(PF_6)_2$. ^{1}H NMR (200 MHz, acetone-d_6) δ 7.49 (d, 6.0 Hz, 2H), 6.89 (d, 6.0 Hz, 2H), 6.30 (t, 6.0 Hz, 2H), 5.62 (s, 2H), 4.84 (s, 10H)

[(η^6-4H-Cyclopenta[def]phenanthrene)Mn(CO)$_3$]$^+$ PF_6^-, 17. $BrMn(CO)_5$ (280 mg, 1 mmol), cppH, **6**, (190 mg, 1 mmol) and $A\ell C\ell_3$ (250 mg,1.9 mmol) were heated under reflux in n-hexane (50 mL, dried over NaH for 3d and freshly distilled prior to use) for 5h. Upon cooling, water (7.5 mL) and toluene (7.5 mL) were added and the precipitate removed on a sintered funnel. The aqueous layer was added dropwise to NH_4PF_6 (1.6 g, 9.8 mmol) in 5 ml water. The organic layer was extracted with water (2 x 5 mL) and the combined aqueous layers added to the NH_4PF_6 solution. The precipitate was filtered on a sintered funnel, washed with

water and dried in vacuo to yield the product **17** as a yellow powder (290 mg, 0.61 mmol, 61%), m.p. 137 °C. ^{1}H NMR (200 MHz, acetone-d_6) δ 8.48 (d, 9.1 Hz, 1H), 8.2 - 8.0 (m, 3H), 7.71 (d, 6.9 Hz, 1H), 7.51 (d, 6.9 Hz, 1H), 7.26 (d, 6.2 Hz, 1H), 6.86 (t, 6.5 Hz, 1H), 5.09 (d, 22.9 Hz, 1H), 4.96 (d, 22.9 Hz, 1H). ^{13}C NMR (50 MHz acetone-d_6) δ 137.0, 134.0, 126.7, 126.3, 97.0, 95.7, 95.2 (aromatic C's); 143.0, 139.2, 124.9, 127.1, 119.1, 118.0 (ring junction C's); 39.2 (C-4). Mass spectrum (FAB+), m/z (%): 329 (100) $((C_{15}H_{10})Mn(CO)_3)^+$, 245 (9) $((C_{15}H_{10})Mn)^+$, 190 (9.5) $(C_{15}H_{10})^+$.

[(η^6-8,9-Dihydro-4H-cyclopenta[def]phenanthrene)Mn(CO)$_3$]$^+$ PF_6^-, 18. By analogy to **17**, H_2-cppH, **9**, (190 mg, 1 mmol), $BrMn(CO)_5$ (275 mg, 1 mmol) and $A\ell C\ell_3$ (250 mg, 1.9 mmol) yielded a pale yellow powder (404 mg, 0.85 mmol, 85%), m.p. 168 °C (dec.). ^{1}H NMR (200 MHz, acetone-d_6) δ 7.59 (m, 2H), 7.40 (t, 1H), 7.20 (d, 6.4 Hz, 1H), 6.75 (d, 6.4 Hz, 1H), 6.66 (t, 6.4 Hz, 1H), 4.62 (d, 22.9 Hz, 1H), 4.43 (d, 22.9 Hz, 1H), 3.43 (m, 2H), 3.34 (m, 2H). ^{13}C NMR (50 MHz, acetone-d_6) δ 217.1 (Cr-CO); 134.2, 127.1, 124.9, 100.4, 98.7, 98.0 (aromatic C's); 143.1, 120.6, 115.6, 113.2, 97.1 (ring junction C's); 38.7 (C-4); 25.3, 25.0 (C-8,9). Mass spectrum (FAB+), m/z (%): 331 (100) $((C_{15}H_{12})Mn(CO)_3)^+$, 247 (14) $((C_{15}H_{12})Mn+H)^+$, 191 (8) $C_{15}H_{11}^+$. Anal. Calcd for $C_{18}H_{12}F_6MnO_3P$: C,45.40, H,2.54. Found: C,45.65, H,2.69.

4,4-d_2-4H-Cyclopenta[def]phenanthrene, 20. CppH, **6**, (400 mg, 2 mmol) and Na (1.8 g, 78 mmol) were heated to reflux in D_2O (99.9% d_2, 20 mL) for 3 days. The precipitate was collected on a sintered funnel, dried under HV and the product extracted using dry ether. Evaporating the solvent yielded a pale yellow solid (380 mg, 1.9 mmol, 95 %). ^{1}H NMR (200 MHz, acetone-d_6) δ 7.87 (s, 2H), 7.85 (d, 2H), 7.72 (d, 2H), 7.65 (d,d 2H).

Reaction of 4,4-d_2-4H-Cyclopenta[def]phenanthrene, 20, with $BrMn(CO)_5$. In analogy to the preparation of the non-deuterated complex, **17**, 4,4-d_2-4H-Cyclopenta[def]phenanthrene, **29**, (380 mg, 2 mmol), $BrMn(CO)_5$ (558 mg, 2 mmol) and $A\ell C\ell_3$ (500 mg, 3.8 mmol) were refluxed in n-hexane (40 mL) for 5h. After cooling to ambient temperature, H_2O (15 mL) and toluene (15 mL) were added. The aqueous layer was separated and added to NH_4PF_6 (3.3 g, 20 mmol) in H_2O (7.5 mL). The organic layer was extracted with H_2O (2 x 10 mL) and the combined aqueous phases added to the NH_4PF_6-solution. Immediate precipitation occurs and the product was collected on a sintered funnel, washed with H_2O and ether and finally dried under HV to yield a pale yellow powder (323 mg, 34%). ^{2}H-NMR (250 MHz, $CHC\ell_3$) δ 4.96 ppm. ^{1}H NMR (200 MHz, acetone-d_6) δ 8.48 (d, 9.1 Hz, 1H), 8.2 - 8.0 (m, 3H), 7.71 (d, 6.9 Hz, 1H), 7.51 (d, 6.9 Hz, 1H), 7.26 (d, 6.2 Hz, 1H), 6.86 (t, 6.5 Hz, 1H). Mass spectrum (FAB+), m/z (%): 333 (100) $(H_2cppH\text{-}d_2)Mn(CO)_3^+$, 249 (19) $(H_2cppH\text{-}d_2)Mn^+$, 192 (75) $cppH\text{-}d_2$.

(η^6-4H-Cyclopenta[def]phenanthrene)$Cr(CO)_3Na$, 21. In an NMR tube, an excess of solid NaH was treated with a solution of (η^6-cppH)$Cr(CO)_3$, **8**, and 15-crown-5 in THF-d_8 at -78°C. The solution turns dark red. ^{1}H NMR (500 MHz, THF-d_8, - 35°C) δ 7.79 (d, 8.9 Hz, 1H), 7.59 (d, 8.9 Hz, 1H), 7.54 (d, 7.4 Hz, 1H), 7.46 (d, 7.0 Hz of d, 7.4 Hz, 1H), 7.20 (d, 7.0 Hz, 1H), 5.81 (d, 6.9 Hz, 1H), 5.75 (s, 1H), 5.40 (d, 6.9 Hz of d, 5.7 Hz, 1H), 5.17 (d, 5.7 Hz, 1H). ^{13}C NMR (125 MHz, THF-d_8, -45 °C) δ 240.7 (Cr-CO); 130.5, 126.2, 125.2, 115.8, 111.0, 96.2, 81.2, 80.2, 79.1 (aromatic C's including C-4); 142.2, 127.5, 127.0, 125.5, 109.8, 97.0 (ring junction C's).

(η^5-4H-Cyclopenta[def]phenanthrene)$Cr(CO)_3Na$, 22. In an NMR tube, an excess of solid NaH was treated with a solution of (η^6-cppH)$Cr(CO)_3$, **8**, in THF-d_8 at room temperarure. The mixture was cooled to -30°C immediately after completion of the reaction. ^1H NMR (500 MHz, THF-d_8, -30°C) δ 7.68 (m, 2H), 7.53 (d, 6.7 Hz, 2H), 7.26 (m, 2H), 7.15 (m, 2H), 5.40 (s, 1H). ^{13}C NMR (125 MHz, THF-d_8, -30°C) δ 245.8 (Cr-CO); 126.1, 125.1, 122.5, 113.0 (aromatic C's); 134.1, 109.7, 101.4 (ring junction C's); 60.4 (C-4).

(η^6-4H-cyclopenta[def]phenanthrenyl)Fe(η^5-C_5H_5), 26. In an NMR tube, solid NaH was treated with a solution of (η^6-cppH)$FeCpPF_6$, **14**, in $CD_2C\ell_2$. The mixture changed colour from yellow to green immediately. ^1H NMR (500 MHz, $CD_2C\ell_2$) δ 8.27 (d, 8.9 Hz, 1H), 8.11 (d, 8.9 Hz, 1H), 8.09 (m, 1H), 8.03 (d, 7.0 Hz of d, 7.0 Hz, 1H), 7.70 (d, 7.0 Hz, 1H), 6.67 (d, 6.0 Hz, 1H), 6.18 (d, 6.0 Hz, 1H), 6.35 (s, H-4), 4.51 (m, 1H), 3.83 (s, 5H). ^{13}C NMR (125 MHz, $CD_2C\ell_2$) δ 131.9, 127.0, 126.5, 118.5, 113.9, 84.3, 72.5 (C_5H_5), 68.3, 67.9, 64.8.

Thermal treatment of (η^6-4H-cyclopenta[def]phenanthrenyl)Fe(η^5-C_5H_5), 26. (η^6-cpp)FeCp, **26**, was refluxed in $CD_2C\ell_2$ for 2h. According to ^1H and ^{13}C NMR, no rearrangement was observed. Refluxing (η^6-cpp)FeCp in 1,2-dichloroethane yielded decomposition products only.

(η^6-4H-Cyclopenta[def]phenanthrene)$Mn(CO)_3$, 28. In an NMR tube, an excess of solid 1,8-bis-(dimethylamino)naphthalene was treated with a solution of (η^6-cppH)$Mn(CO)_3PF_6$, **17**, in $CD_2C\ell_2$ at -40°C. The solution turns red immediately. ^1H NMR (500 MHz, $CD_2C\ell_2$, -25°C) δ 8.21 (d, 9.0 Hz, 1H), 7.01 (d, 7.5 Hz, 1H), 7.91 (t, 7.5 Hz, 1H), 7.84 (d, 9.0 Hz, 1H), 7.80 (d, 7.5 Hz), 6.22 (s, H-4), 6.06 (d,

7.1 Hz, 1H), 5.78 (d, 5.7 Hz, 1H), 5.64 (d, 7.1 Hz of d, 5.7 Hz, 1H). ^{13}C NMR (125 MHz, $CD_2C\ell_2$, -40°C) δ 222.1, 134.2, 128.7, 122.6, 120.5, 118.2, 95.4, 90.8, 77.1, 66.6.

(η^5-4H-Cyclopenta[def]phenanthrenyl)Mn(CO)$_3$, 29.

(a) *By deprotonation of* ***17***. (η^6-cppH)Mn(CO)$_3$PF$_6$, **17**, (0.35 g, 0.75 mmol) and 1,8-bis-(dimethylamino)naphthalene (0.16 g, 0.75 mmol) were dissolved in $CH_2C\ell_2$ (15 mL). The color of the reaction mixture changes from yellow to red immediately; stirring was continued for 3h. The solvent volume was reduced to 5 mL, n-hexane (15 mL) were added and the precipitate filtered using Schlenk techniques. The solvent was removed under high vacuum and the crude product purified via flash chromatography on silica using ether/hexanes 1:9 to yield a red solid, m.p. 77 °C. ^1H NMR (200 MHz, acetone-d_6) δ 7.87 (s, 2H, H-8,9), 7.77 (d, 8.0 Hz of d, 1.2 Hz, 2H, H-3,5), 7.68 (d, 7.9 Hz of d 8.0 Hz, 2H, H-2,6), 7.61 (d, 7.9 Hz of d, 1.2 Hz, 2H, H-1,7), 5.88 (s, 1H, H-4). H-1,7 attributions were made on the basis of their nOe interactions with H-8,9 at 7.87 ppm. ^{13}C NMR (125 MHz, acetone-d_6) δ 130.8 (C-2,6), 129.0 (C-8,9), 124.2 (C-3,5), 120.0 (C-1,7) (aromatic C's); 133.9, 104.9, 98.2 (ring junction C's); 58.2 (C-4). Mass spectrum (FAB+), m/z (%): 328 (27) $(M)^+$, 300 (21) $(M\text{-}CO)^+$, 272 (58) $(M\text{-}2CO)^+$, 244 (26) $(M\text{-}3CO)^+$, 189 (100) $(C_{15}H_9)^+$. Anal. Calcd. for $C_{18}H_9MnO_3$: C, 65.75, H, 2.95. Found: C, 65.26, H, 2.67.

(b) *From BrMn(CO)$_5$*. CppH, **6**, (190 mg, 1 mmol) and NaH (24 mg , 1 mmol) were heated to reflux in THF (5 mL) for 10h. The dark red mixture was filtered into a solution of $BrMn(CO)_5$ (274 mg, 1 mmol) in THF (10 mL) and the reaction mixture heated under reflux for 12h. The precipitate was filtered off and

the solvent removed under reduced pressure. The crude product was purified via flash chromatography on silica using hexanes/ether 9:1 and yielded a red solid (132 mg, 0.40 mmol, 40%). Spectral data were identical to those reported above.

Protonation of (η^5-4H-Cyclopenta[def]phenanthrenyl)Mn(CO)$_3$, 29. In analogy to the approach by Lokshin[60], (η^5-cpp)Mn(CO)$_3$, **29**, (395 mg, 1.2 mmol) in $CH_2C\ell_2$ (14 mL) was treated with CF_3COOH (4.2 mL). Within minutes, the solution changes color from red to yellow. After 0.5h, the solvent was evaporated and the product dried under HV to yield the very unstable (η^6-cppH)Mn(CO)$_3CF_3COO$. IR ($CH_2C\ell_2$): 2057, 2003 cm^{-1}. The solid was dissolved in acetone (8 mL) and treated with NH_4PF_6 (200 mg, 1.9 mmol) in H_2O (2 mL). No precipitation accured after addition of Ether (20 mL). The organic phase was dried over Na_2SO_4 and the solvent was evaporated. The crude product was dissolved in acetone (4 mL) and treated with NH_4PF_6 (200 mg, 1.9 mmol) in H_2O (8 mL). The light yellow precipitate was collected on a sintered funnel and dried under HV. This procedure was repeated five times. The product decomposed during the purification procedure and ^{1}H NMR showed signals for the free cppH-ligand, **6**, only.

(η^6-8,9-Dihydro-4H-cyclopenta[def]phenanthrene)Mn(CO)$_3$, 30. By analogy to the preparation of **28**, (H_2-cppH)Mn(CO)$_3PF_6$, **18**, (200 mg, 0.42 mmol) and 1,8-bis-(dimethylamino)naphthalene (90 mg, 0.42 mmol) afforded a dark red solid (71 mg, 0.21 mmol, 50%). ^{1}H NMR (200 MHz, acetone-d_6) δ 7.64 (d, 8.2 Hz of d, 7.1 Hz, 1H), 7.62 (d, 8.2 Hz, 1H), 7.10 (d, 7.0 Hz, 1H), 6.35 (t, 7.8 Hz, 1H), 5.99 (s, 1H), 5.88 (d, 5.8 Hz of d, 7.8 Hz, 1H), 5.55 (d, 5.8 Hz, 1H), 3.39 (m, 4H).

^{13}C NMR (50 MHz, acetone-d_6) δ 222.7 (Cr-CO); 129.2, 119.3, 117.8, 96.0, 93.3, 84.0 (aromatic C's); 144.8, 131.9, 130.2, 127.6, 116.3, 89.5 (ring junction C's); 71.1 (C-4); 27.7, 26.3 (CH_2 C's). Mass spectrum (FAB+), m/z (%): 660 (8) $(2M)^+$, 576 (10) $(2M-3CO)^+$, 331 (100) $(M+H)^+$, 274 (38) $(M-2CO)^+$, 247 (42) $(M-3CO)^+$, 191 (80) $(C_{15}H_{11})^+$.

(η^5-8,9-Dihydro-4H-Cyclopenta[def]phenanthrenyl)Mn(CO)$_3$, 31. Isomerization of **30** to **31** did not occur in solution (acetone) at ambient temperature within 72h. (η^6-H_2-cppH)Mn(CO)$_3$, **31**, was heated to reflux in n-hexane for 1h. The solvent was removed under reduced pressure and the orange solid dried under high vacuum, m.p. 79 °C. ^{1}H NMR (200 MHz, acetone-d_6) δ 7.38 (d, 8.6 Hz, 2H, H-3,5), 7.27 (d, 8.6 Hz of d, 6.7 Hz, 2H, H-2,6), 7.03 (d, 6.7 Hz, 2H, H-1,7), 5.66 (s, 1H, H-4), 3.6-3.4 (m, 2H), 3.4 - 3.2 (m, 2H). ^{13}C NMR (50 MHz, acetone-d_6) δ 130.8 (C-2,6), 122.6 (C-3,5), 121.3 (C-1,7) (aromatic C's); 137.1, 105.3, 97.2 (ring junctions); 58.3 (C-4), 26.7 (C-8,9). Mass spectrum (FAB+), m/z (%): 660 (2) $(2M)^+$, 576 (15) $(2M-3CO)^+$, 331 (80) $(M)^+$, 274 (34) $(M-2CO)^+$, 247 (75) $(M+H-3CO)^+$, 191 (100) $(C_{15}H_{11})^+$.

BrMn(CO)$_3$(dppm), 47. Following the procedure described by Singleton[94], $BrMn(CO)_5$ (0.4 g, 1.46 mmol) and dppm (1.34 g, 3.7 mmol) in benzene (60 mL) were radiated at 300 nm for 45 min. CO evolution occurs and the solution changes color from orange to orange-red. The solvent was evaporated and the product isolated using flash-chromatography ($CH_2C\ell_2$:Hexanes 2:1) to yield a yellow powder (0.75 g, 1.24 mmol, 85%). IR ($CH_2C\ell_2$): 3067 (m), 2025 (s), 1955 (s), 1919 (s), 1436 (m), 1099 (w) cm^{-1}. MS (FAB+), m/z (%): 520 (100) M-3CO$^+$ (^{81}Br), 518 (100) M-3CO (^{79}Br), 439 (60) M-Br-3CO$^+$, 385 (13) dppm+H$^+$, 199 (40)

$Ph_2PCH_2^+$, 121 (71) $PhP{=}CH^+$.

Radiation at 254 nm or using prolonged reaction times did not yield the expected product $BrMn(CO)(dppm)_2$, **44**. The same results were obtained using $BrMn(CO)_5$ and dppe.

$BrMn(CO)_2(dppm)_2$, 48. Employing the procedure by Riera[95], $BrMn(CO)_3(dppm)$ (440 mg, 0.73 mmol) and dppm (310 mg, 0.8 mmol) were heated to reflux in toluene (15 mL) for 5h. The yellow precipitate of impure cis-cis-$BrMn(CO)_2(dppm)_2$ was filtered off and the filtrate kept at -18°C for 2d. The precipitate was removed to yield a yellow powder (165 mg, 0.17 mmol, 24%). IR ($CH_2C\ell_2$): 3066 (m), 2988 (m), 1937 (s), 1867 (s), 1733 (m), 1604 (m) 1435 (s) cm^{-1}. MS (FAB+), m/z (%): 960 (3) M^+ (^{81}Br), 958 (3) M^+ (^{79}Br), 904 (20) $M\text{-}2CO^+$ (^{81}Br), 902 (20) $M\text{-}2CO^+$ (^{79}Br), 879 (11) $M\text{-}Br^+$, 855 (3) M-Br-CO+4H$^+$, 827 (5) M-B-2CO+4H$^+$, 520 (100) M-2CO-dppm (^{81}Br), 518 (100) M-2CO-dppm$^+$ (^{79}Br).

Radiation of $BrMn(CO)_2(dppm)_2$, 48. $BrMn(CO)_2(dppm)_2$ (165 mg) in benzene (15 mL) were radiated at 254nm and 300 nm for 4h. Separation using flash-chromatography ($CH_2C\ell_2$:Hexanes 2:1) afforded the starting material.

Reaction of (cpp)Na with $BrMn(CO)_2(dppm)_2$, 48. CppH, **6**, (190 mg, 1 mmol) and NaH (36 mg, 1.5 mmol) in THF (5 mL) were heated under reflux for 20h. Solid $BrMn(CO)_2(dppm)_2$, **48**, (340 mg, 0.35 mmol) was added and the mixture heated under reflux for 24h. The solvent was evaporated and the crude product purified using flash chromatography ($CH_2C\ell_2$: hexanes, 2:1) to yield a mixture of $(Mn(CO)_3(\mu\text{-}dppm))_2$[96], **52**, and 4,4-Di(4-4H-cyclopenta[def]-phenanthrenyl)-4H-cyclopenta[def]phenanthrene, **51**. Mass spectrum (FAB+), m/z

(%): 1130 (1) (cpp)$Mn(CO)_2(dppm)_2P_2^+$, 1014 (0.5) (cpp)$Mn(dppm)_2H_2^+$, 752 (5) $(C_{15}H_8)_4)^+$, 564 (9) $(C_{15}H_8)_3)^+$, 417 (14) $O{=}PPh_2CH_2PPh_2{=}O^+$, 401 (22) $PPh_2CH_2PPh_2OH^+$, 385 (40) $dppmH^+$, 377 (100) $(C_{15}H_8)_2^+$, 307 (15) (cpp)$MnP_2{+}H^+$, 189 (56) cpp^+, 154 (75) $PhPCH_2P{+}H^+$, 121 (60) $PhPCH^+$. IR ($CH_2C\ell_2$) : 3073 (w), 3046 (s), 2959 (s), 2928 (s), 2860 (m), 1935 (w), 1585 (m), 1443 (s), 1420 (s) cm^{-1}.

$(\eta^5\text{-}C_5H_5)Fe(CO)_2I$. Following the literature procedure[112], $[(\eta^5\text{-}C_5H_5)Fe(CO)_2]_2$ (50 g, 0.141 mol) and I_2 (50 g, 0.197 mol) were refluxed in $CHC\ell_3$ (250 mL) for 30 min. The mixture was extracted with an aqueous solution of $Na_2S_2O_3$ (4 x 25 g in 100 mL H_2O). The organic layer was filtered and the solvent evaporated. The solid was then tranferred to a sintered funnel and washed with pentane (4 x 35 mL) and air dried to yield a purple powder (67.75 g, 0.22 mol, 78%). ^1H NMR (200 MHz, acetone-d_6) δ 5.26. ^{13}C NMR (50 MHz, acetone-d_6) δ 214.7 (CO), 85.7 (C_5H_5). IR ($CH_2C\ell_2$): 2041 (s), 1997 (s) cm^{-1}.

$(\eta^1$-4H-Cyclopenta[def]phenanthrenyl)$Fe(CO)_2(\eta^5\text{-}C_5H_5)$, 54.

(a) *By direct addition.* CppH, **6**, (570 mg, 3 mmol) and NaH (72 mg, 3 mmol) were heated to reflux in THF (10 mL) for 20h. $(\eta^5\text{-}C_5H_5)Fe(CO)_2I$ (912 mg, 3mmol) were added and the reaction mixture stirred at room temperature for 4h. The solvent was removed under reduced pressure and the products separated via flash chromatography on silica using hexanes:$CH_2C\ell_2$ 2:1 to obtain pure **54** (222 mg, 0.61 mmol, 20%) as an orange solid. ^1H NMR (200 MHz, acetone-d_6) δ 7.79 (s, 2H), 7.70-7.57 (m, 6H), 4.78 (s, 1H), 4.09 (s, 5H). ^{13}C NMR (50 MHz, acetone-d_6) δ 218.1, 156.7 (q), 139.0 (q), 128.9 (q), 127.6, 126.2, 120.8, 120.7, 87.6 (C_5H_5), 23.2. IR ($CH_2C\ell_2$): 3054 (m), 2928 (m), 2856 (w), 2009 (vs), 1956 (s) cm^{-1}. Mass

spectrum (DEI+), m/z (%): 378 (19) (cpp-cpp)$^+$, 365 (0.5) (M)$^+$, 338 (0.5) (M-CO)$^+$, 310 (3) (M-2CO)$^+$, 253 (6) (cpp-cp-H)$^+$, 189 (100) $(C_{15}H_9)^+$, 121 (8) $(FeCp)^+$.

Several side products were obtained as well and identified as follows. *4H-cyclopenta[def]phenanthrene-4(4H-cyclopenta[def]phenanthren-4-ylidene),* **19**, (traces). ^{1}H NMR (200 MHz, acetone-d_6) δ 8.03 (d, 8.0 Hz of d, 0.7 Hz, 2H), 7.88 (s, 2H), 7.78 (d, 7.0 Hz of d, 0.7 Hz, 2H), 7.66 (d, 8.0 Hz of d, 7.0 Hz, 2H). Mass spectrum (DEI+), m/z (%): 376 (50) cpp-cpp ylidene $(C_{15}H_8)_2^+$, 189 (100) $C_{15}H_9^+$. *4H-cyclopenta[def]phenanthrene-(cyclopentadien-4-ylidene),* **57**, (traces). Mass spectrum (DEI+), m/z (%): 253 (50) cpp-Cp ylidene $(C_{15}H_8{=}C_5H_4\text{-}H)^+$, 189 (100) $C_{15}H_9^+$.

4,4-Di(4-4H-cyclopenta[def]phenanthrenyl)-4H-cyclopenta[def]phenanthrene, **51**, (traces) has been reported in the literature but characterized very poorly.[100] ^{1}H NMR (200 MHz, $CD_2C\ell_2$) δ 8.71 (d, 7.1 Hz of d, 0.65 Hz, 2H), 8.10 (d, 8.0 Hz of d, 0.65 Hz of d, 0.65 Hz, 2H), 7.95 (d, 8.0 Hz of d, 7.1 Hz, 2H), 7.86 (d, 8.9 Hz, 2H), 7.67 (d, 8.9 Hz, 2H), 7.59 (s, 2H), 7.53 (d, 8.0 Hz of d, 0.61 Hz, 2H), 7.34 (d, 8.0 Hz of d, 0.62 Hz of d, 0.62 Hz, 2H), 7.02 (d, 8.0 Hz of d, 7.2 Hz, 2H), 6.61 (d, 8.0 of d, 7.3 Hz, 2H), 6.45 (d, 7.2 Hz of d, 0.62 Hz, 2H), 6.36 (d, 0.8 Hz of d, 0.68 Hz, 2H), 5.18 (d, 7.3 Hz of d, 0.74 Hz, 2H). ^{13}C NMR (50 MHZ, $CD_2C\ell_2$) δ 145.8, 143.2, 142.8, 137.9, 137.8, 128.6 (ring junction C's); 127.8, 127.6, 127.0, 126.7, 125.8, 125.4, 125.3, 124.6, 124.5, 124.0, 123.1, 121.2, 120.5, 62.1 (C4), 56.1. Mass spectrum (DEI+), m/z (%): 567 (8) M+H$^+$, 504 (1) M-$C_5H_2^+$, 440 (1) M-2$(C_5H_3)^+$, 377 (100) $C_{15}H_8$-$C_{15}H_9^+$, 252 (20) 377-2(C_5H_3)-H$^+$, 189 (28) $C_{15}H_9^+$.

$IFe(CO)_2(\eta^5\text{-}C_5H_5)$, (62 mg, 0.2 mmol, 7% recovery). IR ($CH_2C\ell_2$): 2041 (s), 1997 (s) cm^{-1}.

[(η5-C_5H_5)Fe(CO)$_2$]$_2$, (200 mg, 0.56 mmol, 38 %). IR ($CH_2C\ell_2$): 1998 (s), 1956 (s), 1774 (s) cm^{-1}.

(b) *By dropwise addition of IFe(CO)$_2$(η^5-C_5H_5)*. CppH, **6**, (570 mg, 3 mmol) and NaH (72 mg, 3 mmol) were heated to reflux in THF (10 mL) for 20h. (η^5-C_5H_5)Fe(CO)$_2$I (912 mg, 3mmol) in THF (10 mL) were added dropwise over a period of 3h and the reaction mixture stirred at room temperature for an additional 2h. The solvent was removed under reduced pressure and the products separated via flash chromatography on silica using hexanes:$CH_2C\ell_2$ 2:1 to yield the following compounds:

4H-Cyclopenta[def]phenanthrene (cppH), **6**, (260 mg, 1.3 mmol, 44% recovery). Spectral data were identical to those reported above.

(η^1-4H-Cyclopenta[def]phenanthrenyl)Fe(CO)$_2$(η^5-C_5H_5), **54**, (110 mg, 0.3 mmol, 10 %). Spectral data were identical to those reported above.

4,4-Di(4-4H-cyclopenta[def]phenanthrenyl)-4H-cyclopenta[def]phenanthrene, **51**, (traces). Spectral data were identicai to those reported above.

IFe(CO)$_2$(η^5-C_5H_5) (150 mg, 0.5 mmol, 15% recovery). Spectral data were identical to those reported above.

[(η^5-C_5H_5)Fe(CO)$_2$]$_2$, **56**, (180 mg, 0.5 mmol, 30%). Spectral data were identical to those reported above.

(c) *By dropwise addition of Na(cpp)*. CppH, **6**, (570 mg, 3 mmol) and NaH (72 mg, 3 mmol) were heated to reflux in THF (10 mL) for 20h. The mixture was passed through a double jointed sintered funnel and added dropwise over a period of 3h to a solution of (η^5-C_5H_5)Fe(CO)$_2$I (912 mg, 3mmol) in THF (10 mL). The

reaction mixture stirred at room temperature for an additional 3h. The solvent was removed under reduced pressure and the products separated via flash chromatography on silica using hexanes:$CH_2C\ell_2$ 2:1 to yield the following compounds:

(η^1-4H-Cyclopenta[def]phenanthrenyl)Fe(CO)$_2$(η^5-C_5H_5), **54**, (132 mg, 0.27 mmol, 12%). Spectral data were identical to those reported above.

(η^1-C_5H_5)Fe(CO)$_2$(η^5-C_5H_5), **53**, (7 mg, 0.03 mmol, 1%). IR ($CH_2C\ell_2$): 2013 (s), 1962 (s) cm^{-1}.

4,4-Di(4-4H-cyclopenta[def]phenanthrenyl)-4H-cyclopenta[def]phenanthrene, **51**, (47 mg, 0.19 mmol, 6.5 %). Spectral data were identical to those reported above.

IFe(CO)$_2$(η^5-C_5H_5) (265 mg, 1.1 mmol, 30% recovery). Spectral data were identical to those reported above.

[(η^5-C_5H_5)Fe(CO)$_2$]$_2$, **56**, (55 mg, 0.2 mmol, 6%). Spectral data were identical to those reported above.

(η^1-4H-Cyclopenta[def]phenanthrene)Mn(CO)$_3$(P(Et)$_3$)$_2$, 60. (η^5-cpp)$Mn(CO)_3$ (45 mg, 0.13 mmol) in benzene (2 mL) was treated with $P(Et)_3$ (0.20 ml, 150 mg, 1.3 mmol). The color changes from red to yellow within minutes. The mixture was stirred for 5 min and the mixture concentrated to 0.5 mL. Hexane (5 mL) were added and the oily liquid chilled at -20°C overnight. The solvent was decanted and the yellow solid dried under HV. ^{1}H NMR (500 MHz, $CH_2C\ell_2$) δ 7.83 (s, 2H), 7.80 (d, 7.0 Hz, 2H), 7.65 (d, 7.5 Hz, 2H), 7.61 (d, 7.0 Hz of d, 7.5 Hz, 2H), 4.56 (d, 8.0 Hz of d, 8.2 Hz, 1H), 2.25 (d, 7.5 Hz of q, 7.5 Hz, 6H), 1.36 (t, 7.5 Hz of d, 14.2 Hz, 9H), 0.72 (d, 7.7 Hz of q, 7.7 Hz, 6H), 0.36 (t, 7.5 Hz of d, 14.8 Hz, 9H). ^{13}C NMR (benzene-d_6, 50 MHz) δ 223.2 (d, 18.8 Hz of d, 18.8 Hz,),

221.8 (d, 21.1 Hz of d, 18.8 Hz), 219.0 (d, 21.2 Hz of d, 18.8 Hz) (Mn-CO); 157.3, 136.1, 128.7 (ring junction C's); 126.1, 125.7, 119.0, 118.5 (aromatic C's); 27.0 (d, 7.5 Hz of d, 8.9 Hz) (C4); 19.9 (d, 21.4 Hz), 18.9 (d, 21.2 Hz) (methylene C's); 7.7, 6.9 (methyl C's). ^{31}P NMR (121.5 MHz, benzene-d_6) δ 47.1 (d, 14.5 Hz), 42.6 (d, 14.5 Hz). IR ($CH_2C\ell_2$): 3045 (w), 2974 (w), 2942 (w), 2885 (w), 1999 (w), 1913 (s), 1883 (m) cm^{-1}. Mass spectum (FAB+), m/z (%): 375 (29) $Mn(P(Et)_3)_2(CO)_3^+$, 319 (43) $Mn(P(Et)_3)_2(CO)^+$, 328 (62) $(cppH)Mn(CO)_3^+$, 291 (100) $Mn(P(Et)_3)_2^+$, 173 (50) $Mn(P(Et)_3)^+$, 119 (66) $P(Et)_3H^+$.

References

1. Miller, S.A.; Tebboth, J.A. and Tremaine, J.F. *J. Chem. Soc.*, **1952**, 632.
2. Pauson, P.L. and Kealy, T.J. *Nature*, **1951**, *168*, 1039.
3. Fischer, E.O. Pfab, W. *Z. Naturforschung* **1952**, *B7*, 377.
4. Wilkinson, G.; Rosenblum, M.; Whitting, M.C. and Woodward, R.B. *J. Am. Chem. Soc.* **1952**, *74*, 2125.
5. Dunitz, J.; Orgel, L.E. and Rich, A. *Acta Cryst.*, **1956**, *9*, 373.
6. Nesmeyanov, A.N.; Vol'kenau, N.A. and Bolesova, I.N. *Dokl. Akad. Nauk SSSR*, **1966**, *166*, 607.
7. Nesmeyanov, A.N.; Vol'kenau, N.A.; Sirotkina, E.I. and Debyabin, V.V. *Dokl. Akad. Nauk SSSR*, **1967**, *177*, 1110.
8. Krüerke, U. *Angew. Chem. Int. Ed. Engl.*, **1967**, *6*, 79.
9. Hein, F. *Berichte* **1919**, *52*, 195.
10. Fischer, E.O. and Hafner, W. *Z. Naturforschung* **1955**, *B10*, 665.
11. Timms, P.L. *J. Chem. Soc., Chem. Comm.* **1969**, 1033.
12. McGlinchey, M.J. in Hartley, F.R. and Patai, S.; "The chemistry of the metal-carbon bond", Volume 1, John Wiley & Sons, New York, 1983.
13. Zeiss, H.; Wheatley, P.J. and Winkler, H.J.S.; "Benzenoid-Metal Complexes", Ronald Press, New York, 1966.

14. Klabunde, K.J. *Ann. N.Y. Acad. Sci* **1977**, *295*, 83.

15. Weiss, E. and Fischer, E.O. *Z. Anorg. Allgem. Chem.* **1956**, *286*, 142.

16. Wheatley, P.J. *Perspect. Struct. Chem.* **1967**, *1*, 1.

17. Keulen, E. and Jellinek, E. *J. Organomet. Chem.* **1966**, *5*, 490.

18. Fischer, E.O. and Öefele, K. *Chem. Ber.* **1957**, *90*, 2532.

19. Nicholls, B. and Whiting, *Proc. Chem. Soc. (London)* **1958**, 152.

20. Fischer, E.O.; and Öefele, K. *Z. Naturforsch.* **1958**, *B13*, 458.

21 (a) Natta,G.; Ercoli, R. and Calderazzo, F. *Chim. Ind. (Milan)* **1958**, *40*, 287. (b) Natta, G.; Ercoli, R.; Calderazzo, F. and Santambrogio, E. *ibid.* **1958**, *40*, 1003.

22. Coffield, T.H.; Sandel, V. and Closson, R.D. *J. Am. Chem. Soc.* **1957**, *79*, 5826.

23. Elschenbroich, Ch.; Salzer A. *Organometallics - A Concise Introduction*; 2nd Edition, VCH Publishers, Weinheim, Germany, 1989, p. 345.

24. Fischer, E.O.; Kriebitzsch, N.; Fischer, R.D. *Chem. Ber.* **1959**, *92*, 3214.

25. Albright, T.A.; Hofmann, P.; Hoffmann, R.; Lillya, C.P.; Dobosh, P.A. *J. Am. Chem. Soc* **1983**, *105*, 3396.

26. O'Connor, J.M. and Casey, C.P. *Chem. Rev.* **1987**, 307 and references therein.

27. Dahl, L.F.; Wei, C.H. *Inorg. Chem.*, **1963**, *2*, 713.

28. Bennet, M.J.; Churchill, M.R.; Gerloch, M. and Mason, A. *Nature* (London), **1964**, *201*, 1318.

29. Huttner, G.; Brintzinger, H.H.; Bell, L.G.; Friedrich, P.; Bejenke, V. and Neugebauer, D.J. *J. Organomet. Chem.* **1978**, *145*, 329 and references therein.

30. Schonberg, P.R.; Paine, R.T.; Campana, C.F. and Duesler, E.N. *Organometallics* **1982**, *1*, 799.

31. Piper, T.S.; Wilkinson, G. *J. Inorg. Nucl. Chem.* **1956**, *2*, 38.

32. Wilkinson, G. and Cotton, F.A. *Prog. Inorg. Chem.* **1959**, *1*, 1.

33. Hames, B.W.; Legzdins, P. and Martin, D.T. *Inorg. Chem.* **1978**, *17*, 3644.

34. Rerek, E.M.; Ji, N.L. and Basolo, F. *J. Chem. Soc., Chem. Comm.* **1983**, 1208.

35. Müller, J.; Goser, P. and Elian, M. *Angew. Chem. Int. Ed. Engl.* **1969**, *8*, 374.

36. Dötz, K.H. and Diez, R. *Chem. Ber.* **1977**, *110*, 1555.

37. Scott, F.; Krüger, C. and Betz, P. *J. Organomet. Chem.* **1990**, *387*, 113.

38. Jonas, K. *J. Organomet. Chem.* **1974**, *73*, 273.

39. Stanger, A. and Vollhardt, K.P.C. *Organometallics* **1992**, *11*, 317.

40. Klein, H.F.; Ellrich; K., Lamac; S., Lull; G., Zsolnai, L. and Huttner, G. *Z. Naturforsch*, **1985**, *40b*, 1377.

41. Kirss, R.U. and Treichel, P.M. *J. Am. Chem. Soc* **1986**, *108*, 853

42. Oprunenko, Yu.K.; Malugina, S.G.; Ustynyuk, Yu.A.; Ustynyuk, N.A. and Krovtsov, D.N. *J. Organomet. Chem.* **1988**, *338*, 357.

43. Kündig, E.P.; Desobry, V.; Grivet, C.; Rudolph, B. and Spichiger, S. *Organometallics* **1987**, *6*, 1173.

44. Crabtree, R.H. and Parnell, C.H. *Organometallics* **1984**, *3*, 1727.

45. White, C.; Thompson, S.T.; and Maitiis, P.M. *J. Chem. Soc. Dalton* **1977**, 1654.

46. Stanger, A. and Boese, R. *J. Organomet. Chem.* **1992**, *430*, 235.

47. Treichel, P.M.; Johnson, J.W. *J. Organomet. Chem.* **1975**, *88*, 207.

48. Bang, H.; Lynch, T.J. and Basolo, F. *Organometallics* **1992**, *11*, 40.

49. Nesmeyanov, A.N.; Ustynyuk, N.A.; Makarova, L.G.; Andre, S.; Ustynyuk, Yu.A.; Novikova, L.N. and Luzikov, Yu.N. *J. Organomet. Chem.* **1978**, *154*, 45.

50. Novikova, L.N.; Ustynyuk, N.A.; Zvorykin, V.E.; Dneprovskaya, L.S. and Ustynyuk, Yu.A. *J. Organomet. Chem.* **1985**, *292*, 237.

51. Clark, D.T.; Mlekuz, M.; Sayer, B.G.; McCarry, B.E. and McGlinchey, M.J. *Organometallics* **1987**, *6*, 2201.

52. Fessenbeck, A.; Stephan, M.; Grimes, R.N.; Pritzkow, H.; Zenneck, U. and Siebert W. *J. Am. Chem. Soc.* **1991**, *113*, 3061.

53. (a) Ceccon, A. Gambarotto, A. *J. Organomet. Chem.* **1981**, *217*, 79. (b) Nesmeyanov, A.N.; Oprunenko, Yu.F.; Lokshin, B.V. and Ustynyuk, Yu.N. *Izv. Akad. Nauk SSSR, Ser. Khim.* **1979**, *9*, 1942.

54. Nicholas, K.M.; Kerber, R.C. and Stiefel, E.I. *Inorg. Chem.* **1971**, *10*, 1519.

55. Johnson, J.W. and Treichel, P.M. *Chem.Comm.* **1976**, 688.

56. (a) Treichel, P.M.; Johnson, J.W. *Inorg. Chem.* **1977**, *16*, 749. (b) Johnson, J.W.; Treichel, P.M. *J. Am. Chem. Soc.* **1977**, *99*, 1427.

57. Treichel, P.M.; Fivizzanai, K.P.; Haller, K.J. *Organometallics* **1982**, *1*, 931.

58. Hamon, J.R.; Astruc, D.; Román, E.; Batail, P. and Mayerle, J. *J. Am. Chem. Soc* **1981**, *103*, 2431.

59. Terrier, F.; Vichard, D.; Chatrousse, A.-P.; Top, S. and McGlinchey, M.J. submitted for publication.

60. Yezerintskaya, M.G.; Lokshin, B.V.; Zdanovich, V.I.; Lobanova, I.A. and Kolobova, N.E. *J. Organomet. Chem.* **1982**, *234*, 329.

61. Ustynyuk, N.A.; Pomazanova, N.A.; Novikova, L.N.; Kravtsov, D.N. and Ustynyuk, Yu.A. *Izv. Akad. Nauk. SSSR* **1986**, *7*, 1688.

62. Rerek, M.E. and Basolo, F. *Organometallics* **1984**, *3*, 647.

63. Ustynyuk, N.A.; Novikova, L.N.; Oprunenko, Yu.F.; Malyugina, S.G. and Ustynyuk, Yu.A. *J. Organomet. Chem.* **1984**, *277*, 75.

64. (a) Hawkins, J.M.; Meyer, A.; Lewis, T.A.; Loren, S. and Hollander, F.J. *Science*, **1991**, *252*, 312. (b) Hawkins, J.M.; Meyer, A.; Lewis, T.A.; Loren, S.; Heath, J.R.; Shibato, Y. and Saykally, R.R. *J. Org. Chem.* **1990**, *55*, 6250. (c) Hawkins, J.M.; Loren, S.; Meyer, A. and Nunlist, R.J. *J. Am. Chem. Soc.* **1991**, *113*, 9394. (d) Fagan, P.J.; Calabrese, J.C. and Malone, B. *Science*, **1991**, *252*, 1160. (e) Fagan, P.J.; Calabrese, J.C. and Malone, B. *J. Am. Chem. Soc.* **1991**, *113*, 9408. (f) Balch, A.L.; Catalano, V.J. and Lee, J.W. *Inorg. Chem.* **1991**, *30*, 3980. (g) Koefod, R.S.; Hudgens, M.F. and

Shapley, J.R. *J. Am. Chem. Soc.* **1991**, *113*, 8957. (h) Yoshida, T. Matsuda, T. and Otsuka, S. *Inorg. Synth.* **1990**, *28*, 122. (i) Rasinkangas, M.; Pakkanen, T.T.; Pakkanen, T.A.; Ahlgrén and Rouvinene, J. *J. Am. Chem. Soc.* **1993**, *115*, 4901. (j) for a more detailed discussion refer to Fagan, P.J.; Calabrese, F.C. and Malone, B. *Acc. Chem. Res.* **1992**, *25*, 134.

65. (a) Hanson, J.C.; Nordman, C.E. *Acta Cryst.* **1976**, *B32*, 1147. (b) Scott, L.T.; Hashemi, M.M.; Bratcher, M.S. *J. Am. Chem. Soc.* **1992**, *114*, 1920. (c) Borchardt, A.; Fuchicello, A.; Kilway, K.V.; Baldridge, K.K.; Siegel, J.S. *J. Am. Chem. Soc.* **1992**, *114*, 1921.

66. (a) Barth, W.E. and Lawton, R.G. *J. Am. Chem. Soc* **1971**, *93*, 1730. (b) Siegel, J.S. personal communication.

67. Ustynyuk, N.A.; Lokshin, B.V.; Oprunenko, Yu.F.; Roznyatovsky, V.A.; Luzikov, Yu.N. and Ustynyuk, Yu.A. *J. Organomet. Chem.* **1980**, *202*, 279.

68. Ustynyuk, N.A.; Uprenenko, Yu.F.; Malyugina, S.G.; Trifonova, O.I. and Ustynyuk, Yu.A. *J. Organomet. Chem.* **1984**, *270*, 185.

69. Ustynyuk, Yu.A.; Trifonova, O.I.; Oprunenko, Y.F.; Mstislavskiy, V.I. and Gloriozov, I.P. *Organometallics* **1990**, *9*, 1707.

70. Tisch, T.L.; Lynch, J. and Dominguez, R. *J. Organomet. Chem.* **1989**, *377*, 265.

71. (a) Muir, K.W.; Ferguson, G.; Sim, G.A. *J. Chem. Soc. B* **1968**, 467. (b) Hanic, F.; Mills, O.S. *J. Organomet. Chem.* **1968**, *11*, 151. (c) Rogers,

R.D.; Atwood, J.L.; Albright, T.A.; Lee, W.A.; Rausch, M.D. *Organometallics* **1984**, *3*, 263. (d) Sato, M.; Ishida, Y.; Nakamura, M.; Kajiwara, M. *Nippon Kagaku Zasshi* **1970**, *91*, 1188.

72. (a) Laszlo, P. *Progress in NMR Spectroscopy* **1967**, *3*, 231. (b) Ustynyuk, N.A.; Novikova, L.N.; Bel'skii, V.K.; Oprunenko, Yu.F.; Malyugina, S.G.; Trifonova, O.I.; Ustynyuk, Yu.A. *J. Organomet. Chem.* **1985**, *294*, 31.

73. Decken, A.; Hughes, D.W.; Britten, J.F. and McGlinchey, M.J., manuscript in preparation.

74. Whitton, A.J.; Kumberger, O.; Müller, G. and Schmidbaur, H. *Chem. Ber.* **1990**, *123*, 1931.

75. Muir, K.W.; Ferguson, G.; Sim, G.A. *J. Chem. Soc. B*, **1968**, 476.

76. Lee, C.C.; Demchuk, K.J.; Pannekoek, W.J.; Sutherland, R.G. *J. Organomet. Chem.* **1978**, *162*, 253.

77. Stout, G.H.; Jensen, L.H. "X-ray Structure Determination", Second Edition, John Wiley & Sons, Inc. New York (1989), p. 76.

78. Schomaker, V.; Trueblood, K.N. *Acta Cryst.* **1968**, *B24*, 63.

79. unpublished results from this laboratory.

80. Nesmeyanov, A.N.; Vol'kenau, N.A., Bolesova, I.N.; Polkovnikova, L.S. *Koord. Khim.* **1975**, *1*, 1252.

81. The isolated yields of 40% for (η^5-cpp)$Mn(CO)_3$ may be compared to those of (η^5-C_5H_5)$Mn(CO)_3$ (56%) and (η^5-$C_{13}H_9$)$Mn(CO)_3$ (11%): King, R.B.; Efraty, A. *J. Organomet. Chem.* **1970**, *23*, 527.

82. Mlekuz. M.; Bougeard, P.; Sayer, B. G.; McGlinchey, M. J.; Rodger, C. A.; Churchill, M. R.; Ziller, J. W.; Kang, S.-K.; Albright, T. A. *Organometallics* **1986**, *5*, 1656.

83. Westcott, S. A.; Kakkar, A. K.; Stringer, G.; Taylor, N. J.; Marder, T. B. *J. Organomet. Chem.* **1990**, *394*, 777.

84. Mösges, G.; Hampel, F.; Schleyer, P.v.R. *Organometallics* **1992**, *11*, 1769.

85. Atwood, J. L.; Shakir, R.; Mailto, J. T.; Herberhold, M.; Kremnitz, W.; Bernhagen, W. P.; Alt, H. G. *J. Organomet. Chem.* **1979**, *165*, 65.

86. Albright, T.A.; Hofmann, P.; Hoffmann, R.; Lillya, C.P.; Dobosh, P.A. *J. Am. Chem. Soc* **1983**, *105*, 3396 and references therein.

87. Nesmeyanov, A.N.; Ustynyuk, N.A.; Makarova, L.G.; Andrianov, V.G.; Struchkov, Y.T.; Andrae, S.; Ustynyuk, Y.A. and Malyugina, S.G.J. *J. Organomet. Chem.* **1979**, *159*, 189.

88. Nakasuji, K.; Jamaguchi, M.; Murata, I.; Tatsumi, K. and Nakamura, A. *Organometallics* **1984**, *3*, 1257.

89. Gal, A.W. and Van der Heijden, H. *Angew. Chem. Int. Ed. Engl.* **1981**, *20*, 978.

90. Merola, J.S.; Kacmarcik, R.T. and Van Engen, D.J. *J. Am. Chem. Soc.* **1986**, *108*, 329.

91. Ji, L.N.; Rerek, M.E. and Basolo, F. *Organometallics* **1984**, *3*, 740.

92. Young, K.M.; Miller, T.M. and Wrighton, M.S. *J. Am. Chem. Soc* **1990**, *112*, 1529.

93. Biagioni, R.N.; Lorkovic, I.; Scelton, J. and Hartung, J.B. *Organometallics* **1990**, *9*, 547.

94. Reimann, R.H. and Singleton, E. *J. Organomet. Chem.* **1972**, *38*, 113.

95. Carriero, G.A.; Riera, V. and Santamaria, J. *J. Organomet. Chem.* **1982**, *234*, 175.

96. The molecule was identified by comparison to the known infrared spectrum: King, R.B. and Raghuveer, K.S. *Inorg. Chem.* **1984**, *23*, 2482.

97. Piper, T.S.; Wilkinson, G. *J. Inorg. Nucl. Chem.* **1956**, *3*, 104.

98. Bennett, M.J.; Cotton, F.A.; Davison, A.; Faller, J.W.; Lippard, S.J. and Morehouse, S.M. *J. Am. Chem. Soc* **1966**, *88*, 4371.

99. The yields of 20 % for $(\eta^1\text{-cpp})Fe(CO)_2(\eta^5\text{-}C_5H_5)$ may be compared to those for $(\eta^1\text{-}C_5H_5)Fe(CO)_2(\eta^5\text{-}C_5H_5)$ (8%): see ref. 97

100. Black, D.St.C.; Deacon, G.B. and Thomas, N.C. *Inorg. Chim. Acta*, **1982**, *65*, L75.

101. Kimura, T.; Minabe, M. and Suzuki, K. *Bull. Chem. Soc. Jpn.* **1979**, *52*, 1447.

102. Decken, A. and McGlinchey, M.J.; unpublished results.

103. Perrin, D.D.; Perrin, D.R.; "Purification of Laboratory Chemicals", Pergamon Press, New-York(1980).

104. Jolly, W.L. *Inorg. Chem.* **1968**, *11*, 122.

105. Eisch, J.J. and King, R.B. *Organometallic Synth.* **1965**, *1*, 174.

106. Rutar, V. *J. Magn. Reson.* **1984**, *58*, 306.

107. Kalionowski, H.-O.; Berger, S. and Braun, S., *Carbon-13 NMR Spectroscopy*, J. Wiley and Sons, New York, 1988.

108. Stothers, J.B., *Carbon-13 NMR Spectroscopy*, Academic Press, New York, 1972.

109. Sheldrick, G.M. SHELXTL PC (1990) Release 4.1 Siemens Crystallographic Research Systems. Madison, WI 53719, U.S.A.

110. Mealli, C.; Proserpio, D. M. *J. Chem. Ed.* **1990**, *67*, 3399.

111. Helling, J.F.; Hendrickson, W.A. *J. Organomet. Chem.* **1977**, *141*, 99.

112. King, R.B. and Stone, F.G.A. *Inorg. Synth.*, **1963**, *7*, 110.

Appendix

Table A. Structure determination summary for cppH, **6**.

Crystal Data

Empirical Formula	$C_{15}\ H_{10}$
Color; Habit	colorless plate
Crystal size (mm)	0.3 x 0.1 x 0.03
Crystal System	Monoclinic
Space Group	Cc
Unit Cell Dimensions	$\underline{a}$ = 11.047(2) Å
	$\underline{b}$ = 11.126(2) Å
	$\underline{c}$ = 16.865(3) Å
	β = 101.18(3)°
Volume	2033.5(10) $Å^3$
Z	8
Formula weight	190.2
Density(calc.)	1.243 Mg/m^3
Absorption Coefficient	0.533 mm^{-1}
F(000)	800

Data Collection

Diffractometer Used	Rigaku AFC6R
Radiation	CuKα (λ = 1.54178 Å)
Temperature (K)	300 ± 10
Monochromator	graphite
2θ Range	5.35 to 120.0°
Scan Type	2θ-θ
Scan Speed	16°/min. in ω
Scan Range (ω)	1.4° plus Kα separation
Background Measurement	Stationary crystal and stationary counter at beginning and end of scan, each for 25% of total scan time
Standard Reflections	3 measured every 100 reflections
Index Ranges	$0 \leq h \leq 12$, $0 \leq k \leq 12$ $-18 \leq l \leq 18$ and $-12 \leq h \leq 0$, $-12 \leq k \leq 0$ $-18 \leq l \leq 18$
Reflections Collected	3220
Independent Reflections	3034 (R_{int} =3.39%)
Observed Reflections	1043 ($F \geq 4.0\sigma(F)$)
Absorption Correction	DIFABS correction
Min./Max. Absorption	0.644 / 1.107

Solution and Refinement

System Used	Siemens SHELXL and SHELXTL ?PLUS
Solution	Direct Methods
Refinement Method	Block
Quantity Minimized	$\Sigma w(\|F_o\|-\|F_c\|)^2$
Absolute Structure	N/A
Extinction Correction	χ = 0.0030(2), where $F^* = F\ [1+0.002\chi F^2/\sin(2\theta)\ ]^{-1/4}$
Hydrogen Atoms	calculated positions, riding model, common, isotropic U
Weighting Scheme	$w^{-1} = \sigma^2(F) + 0.0000F^2$
Number of Parameters Refined	89 (total), 46 (per block)
Final R Indices (obs. data)	R = 9.68 %, wR = 6.75 %
R Indices (all data)	R = 20.58 %, wR = 7.53 %
Goodness-of-Fit	2.65
Largest and Mean Δ/σ	0.271, 0.022
Data-to-Parameter Ratio	11.7:1
Largest Difference Peak	0.40 eÅ^{-3}
Largest Difference Hole	-0.36 eÅ^{-3}

Table A1. Atomic coordinates ($x10^4$) and equivalent isotropic displacement coefficients ($Å^2x10^3$) for cppH, **6**.

	x	y	z	U(eq)
Molecule A[a]				
C(4)	6956(11)	2816(6)	2448(6)	81(6)
C(1)	7423	1875	4926	105(7)
C(2)	7824	3028	4754	88(6)
C(3)	7742	3482	3989	118(8)
C(3A)	7222	2748	3324	65(5)
C(5A)	6314	1732	2148	79(6)
C(5)	5734	1246	1393	117(8)
C(6)	5178	147	1390	155(10)
C(7)	5159	-539	2082	97(7)
C(8)	5846	-650	3628	119(8)
C(8A)	5732	-141	2829	93(7)
C(9)	6390	-75	4305	102(7)
C(9A)	6913	1115	4305	84(6)
C(10)	6297	988	2822	88(6)
C(11)	6850	1591	3527	71(6)
Molecule B[a]				
C(4B)	2804(13)	1771(9)	2379(8)	230(19)
C(1B)	2578	1768	4891	128(11)
C(2B)	3645	2311	4690	72(7)
C(3B)	3870	2395	3909	111(10)
C(3AB)	2976	1904	3260	69(6)
C(5AB)	1590	1243	2096	109(11)
C(5B)	809	943	1339	170(15)
C(6B)	-345	470	1354	135(12)
C(7B)	-802	245	2067	58(6)
C(8B)	-321	347	3641	84(8)
C(8AB)	-85	480	2822	106(9)
C(9B)	488	707	4313	91(8)
C(9AB)	1676	1269	4287	96(9)
C(10B)	1096	966	2795	103(9)
C(11B)	1931	1352	3495	65(7)

a: occupation factors for molecules A-D

A : 0.61, B : 0.53, C : 0.47, D : 0.39

Molecule C[a]				
C(4C)	200(11)	593(8)	3889(7)	97(10)
C(1C)	790	1125	1543	89(10)
C(2C)	-337	639	1614	82(9)
C(3C)	-683	409	2325	199(19)
C(3AC)	144	676	3038	81(9)
C(5AC)	1322	1129	4279	72(8)
C(5C)	1911	1414	5065	77(8)
C(6C)	3007	1981	5167	74(8)
C(7C)	3595	2286	4546	279(26)
C(8C)	3492	2221	3033	135(13)
C(8AC)	3095	2008	3774	57(7)
C(9C)	2823	1940	2317	43(6)
C(9AC)	1636	1400	2215	89(11)
C(10C)	1971	1427	3681	34(5)
C(11C)	1271	1147	2936	61(7)

Molecule D[a]				
C(4D)	6069(20)	-53(12)	3969(12)	164(25)
C(1D)	8003	3264	4515	82(13)
C(2D)	7894	2525	5182	40(9)
C(3D)	7303	1423	5119	100(16)
C(3AD)	6762	994	4332	137(21)
C(5AD)	5893	74	3097	101(15)
C(5D)	5390	-613	2395	133(20)
C(6D)	5465	173	1650	88(14)
C(7D)	5970	993	1534	299(46)
C(8D)	7024	2900	2238	90(16)
C(8AD)	6442	1721	2183	149(24)
C(9D)	7505	3441	2950	89(14)
C(9AD)	7493	2899	3734	83(13)
C(10D)	6367	1218	2943	89(14)
C(11D)	6880	1776	3683	74(12)

a: occupation factors for molecules A-D

A : 0.61, B : 0.53, C : 0.47, D : 0.39

* Equivalent isotropic U defined as one third of the trace of the orthogonalized U_{ij} tensor

Table A2. Bond lengths (Å) for cppH, **6**.

Molecule A			
C(4)-C(3A)	1.451	C(4)-C(5A)	1.440
C(1)-C(2)	1.406	C(1)-C(9A)	1.378
C(2)-C(3)	1.373	C(3)-C(3A)	1.416
C(3A)-C(11)	1.413	C(5A)-C(5)	1.417
C(5A)-C(10)	1.408	C(5)-C(6)	1.368
C(6)-C(7)	1.398	C(7)-C(8A)	1.370
C(8)-C(8A)	1.445	C(8)-C(9)	1.345
C(8A)-C(10)	1.404	C(9)-C(9A)	1.444
C(9A)-C(11)	1.404	C(10)-C(11)	1.399
Molecule B			
C(4B)-C(3AB)	1.468	C(4B)-C(5AB)	1.458
C(1B)-C(2B)	1.423	C(1B)-C(9AB)	1.395
C(2B)-C(3B)	1.389	C(3B)-C(3AB)	1.433
C(3AB)-C(11B)	1.430	C(5AB)-C(5B)	1.434
C(5AB)-C(10B)	1.425	C(5B)-C(6B)	1.384
C(6B)-C(7B)	1.415	C(7B)-C(8AB)	1.387
C(8B)-C(8AB)	1.462	C(8B)-C(9B)	1.361
C(8AB)-C(10B)	1.421	C(9B)-C(9AB)	1.462
C(9AB)-C(11B)	1.421	C(10B)-C(11B)	1.416
Molecule C			
C(4C)-C(3AC)	1.428	C(4C)-C(5AC)	1.418
C(1C)-C(2C)	1.384	C(1C)-C(9AC)	1.357
C(2C)-C(3C)	1.351	C(3C)-C(3AC)	1.394
C(3AC)-C(11C)	1.391	C(5AC)-C(5C)	1.395
C(5AC)-C(10C)	1.386	C(5C)-C(6C)	1.346
C(6C)-C(7C)	1.376	C(7C)-C(8AC)	1.349
C(8C)-C(8AC)	1.422	C(8C)-C(9C)	1.324
C(8AC)-C(10C)	1.382	C(9C)-C(9AC)	1.422
C(9AC)-C(11C)	1.382	C(10C)-C(11C)	1.378
Molecule D			
C(4D)-C(3AD)	1.462	C(4D)-C(5AD)	1.451
C(1D)-C(2D)	1.417	C(1D)-C(9AD)	1.389
C(2D)-C(3D)	1.384	C(3D)-C(3AD)	1.427
C(3AD)-C(11D)	1.424	C(5AD)-C(5D)	1.428
C(5AD)-C(10D)	1.419	C(5D)-C(6D)	1.546
C(6D)-C(7D)	1.408	C(7D)-C(8AD)	1.381
C(8D)-C(8AD)	1.456	C(8D)-C(9D)	1.356
C(8AD)-C(10D)	1.415	C(9D)-C(9AD)	1.455
C(9AD)-C(11D)	1.416	C(10D)-C(11D)	1.410

Table A3. Bond angles (°) for cppH, **6**.

for all molecules

C(3A)-C(4)-C(5A)	107.6	C(2)-C(1)-C(9A)	120.1
C(1)-C(2)-C(3)	124.3	C(2)-C(3)-C(3A)	118.3
C(4)-C(3A)-C(3)	138.3	C(4)-C(3A)-C(11)	106.4
C(3)-C(3A)-C(11)	115.2	C(4)-C(5A)-C(5)	137.8
C(4)-C(5A)-C(10)	107.0	C(5)-C(5A)-C(10)	115.2
C(5A)-C(5)-C(6)	118.0	C(5)-C(6)-C(7)	124.3
C(6)-C(7)-C(8A)	120.9	C(8A)-C(8)-C(9)	123.3
C(7)-C(8A)-C(8)	132.3	C(7)-C(8A)-C(10)	114.1
C(8)-C(8A)-C(10)	113.7	C(8)-C(9)-C(9A)	123.3
C(1)-C(9A)-C(9)	131.8	C(1)-C(9A)-C(11)	114.7
C(9)-C(9A)-C(11)	113.5	C(5A)-C(10)-C(8A)	127.5
C(5A)-C(10)-C(11)	109.4	C(8A)-C(10)-C(11)	122.9
C(3A)-C(11)-C(9A)	127.3	C(3A)-C(11)-C(10)	109.3
C(9A)-C(11)-C(10)	123.2		

Table B. Structure determination summary for $(\eta^6\text{-cppH})Cr(CO)_3$, **8**.

Crystal Data

Empirical Formula	$C_{18}\ H_{10}\ Cr\ O_3$
Color; Habit	orange-red square biprism
Crystal size (mm)	0.65 x 0.5 x 0.4
Crystal System	Orthorhombic
Space Group	Pbca
Unit Cell Dimensions	$\underline{a}$ = 13.924(2) Å
	$\underline{b}$ = 12.639(2) Å
	$\underline{c}$ = 15.666(3) Å
Volume	2757(1) Å^3
Z	8
Formula weight	326.3
Density(calc.)	1.572 Mg/m^3
Absorption Coefficient	0.940 mm^{-1}
F(000)	1328

Data Collection

Diffractometer Used	Siemens P4
Radiation	MoKα (λ = 0.71073 Å)
Temperature (K)	300 ± 10
Monochromator	graphite
2θ Range	3.5 to 50.0°
Scan Type	2θ-θ
Scan Speed	Variable; 1.50 to 14.65°/min. in ω
Scan Range (ω)	1.20° plus Kα separation
Background Measurement	Stationary crystal and stationary counter at beginning and end of scan, each for 25% of total scan time
Standard Reflections	3 measured every 97 reflections
Index Ranges	$0 \leq h \leq 15$, $0 \leq k \leq 14$ $-17 \leq l \leq 0$
Reflections Collected	2493
Independent Reflections	2136
Observed Reflections	1642 ($F \geq 2.0\sigma(F)$)
Absorption Correction	psi-scan
Min./Max. Transmission	0.4332 / 0.4690

Solution and Refinement

System Used	Siemens SHELXTL PLUS (VMS)
Solution	Direct Methods
Refinement Method	Full-Matrix Least-Squares
Quantity Minimized	$\Sigma w(\|F_o\|-\|F_c\|)^2$
Absolute Structure	N/A
Extinction Correction	χ = 0.0019 (7), where $F^* = F\ (1+0.002\ \chi F^2/\sin(2\ \theta))^{-1/4}$
Hydrogen Atoms	Riding model; common, isotropic U
Weighting Scheme	$w^{-1} = \sigma^2(F) + 0.0009F^2$
Number of Parameters Refined	201
Final R Indices (obs. data)	R = 5.36 %, wR = 6.39 %
R indeces (all data)	R = 7.31 %, wR = 7.01%
Goodness-of-Fit	1.42
Largest and Mean Δ/σ	0.019, 0.003
Data-to-Parameter Ratio	8.2:1
Largest Difference Peak	0.23 eÅ^{-3}
Largest Difference Hole	-0.25 eÅ^{-3}

Table B1. Atomic coordinates ($x10^4$) and equivalent isotropic displacement coefficients ($Å^2x10^3$) (η^6-cppH)$Cr(CO)_3$, **8**.

	x	y	z	U(eq)
Cr	2059(1)	-26(1)	1335(1)	55(1)
O(1)	3168(2)	-1712(3)	2236(2)	90(1)
O(2)	1853(2)	970(3)	3058(2)	82(1)
O(3)	3911(3)	1144(3)	1076(2)	87(1)
C(1)	1827(3)	-323(4)	-45(3)	72(2)
C(2)	1504(3)	-1183(4)	412(3)	70(2)
C(3)	795(3)	-1093(3)	1082(3)	62(2)
C(3A)	444(3)	-90(3)	1259(2)	57(1)
C(4)	-315(3)	345(3)	1870(3)	63(1)
C(5)	-927(3)	2343(4)	1867(3)	78(2)
C(5A)	-377(3)	1508(3)	1622(3)	62(2)
C(6)	-794(4)	3320(4)	1464(3)	83(2)
C(7)	-154(4)	3498(4)	828(4)	82(2)
C(8)	1110(3)	2599(4)	-125(3)	77(2)
C(8A)	434(3)	2639(4)	536(3)	68(2)
C(9)	1599(3)	1701(4)	-346(3)	73(2)
C(9A)	1441(3)	708(3)	98(3)	60(2)
C(10)	289(3)	1696(3)	962(3)	57(1)
C(11)	761(3)	764(3)	747(2)	53(1)
C(21)	2743(3)	-1067(3)	1875(3)	61(2)
C(22)	1932(3)	618(3)	2376(3)	61(2)
C(23)	3193(3)	695(4)	1165(3)	65(2)

* Equivalent isotropic U defined as one third of the trace of the orthogonalized U_{ij} tensor

Table B2. Bond lengths (Å) (η^6-cppH)Cr(CO)$_3$, **8**.

Cr-C(1)	2.224 (4)	Cr-C(2)	2.197 (5)
Cr-C(3)	2.251 (4)	Cr-C(3A)	2.252 (4)
Cr-C(9A)	2.314 (4)	Cr-C(11)	2.261 (4)
Cr-C(21)	1.835 (4)	Cr-C(22)	1.832 (5)
Cr-C(23)	1.843 (5)	O(1)-C(21)	1.152 (5)
O(2)-C(22)	1.162 (6)	O(3)-C(23)	1.158 (6)
C(1)-C(2)	1.381 (7)	C(1)-C(9A)	1.428 (7)
C(2)-C(3)	1.446 (6)	C(3)-C(3A)	1.387 (6)
C(3A)-C(4)	1.528 (6)	C(3A)-C(11)	1.415 (5)
C(4)-C(5A)	1.523 (6)	C(5)-C(5A)	1.360 (7)
C(5)-C(6)	1.400 (7)	C(5A)-C(10)	1.408 (6)
C(6)-C(7)	1.356 (8)	C(7)-C(8A)	1.434 (7)
C(8)-C(8A)	1.405 (7)	C(8)-C(9)	1.366 (7)
C(8A)-C(10)	1.381 (6)	C(9)-C(9A)	1.451 (7)
C(9A)-C(11)	1.391 (5)	C(10)-C(11)	1.391 (6)

Table B3. Bond angles (°) (η^6-cppH)$Cr(CO)_3$, **8**.

C(1)-Cr-C(2)	36.4(2)
C(1)-Cr-C(3)	67.3(2)
C(2)-Cr-C(3)	37.9(2)
C(1)-Cr-C(3A)	78.3(2)
C(2)-Cr-C(3A)	65.9(2)
C(3)-Cr-C(3A)	35.9(1)
C(1)-Cr-C(9A)	36.6(2)
C(2)-Cr-C(9A)	65.5(2)
C(3)-Cr-C(9A)	78.6(2)
C(3A)-Cr-C(9A)	66.4(1)
C(1)-Cr-C(11)	64.0(2)
C(2)-Cr-C(11)	75.2(2)
C(3)-Cr-C(11)	64.4(1)
C(3A)-Cr-C(11)	36.5(1)
C(9A)-Cr-C(11)	35.4(1)
C(1)-Cr-C(21)	114.1(2)
C(2)-Cr-C(21)	90.6(2)
C(3)-Cr-C(21)	93.3(2)
C(3A)-Cr-C(21)	121.1(2)
C(9A)-Cr-C(21)	150.4(2)
C(11)-Cr-C(21)	157.1(2)
C(1)-Cr-C(22)	158.3(2)
C(2)-Cr-C(22)	148.0(2)
C(3)-Cr-C(22)	110.3(2)
C(3A)-Cr-C(22)	88.1(2)
C(9A)-Cr-C(22)	122.1(2)
C(11)-Cr-C(22)	95.1(2)
C(21)-Cr-C(22)	87.4(2)
C(1)-Cr-C(23)	93.8(2)
C(2)-Cr-C(23)	122.3(2)
C(3)-Cr-C(23)	160.1(2)
C(3A)-Cr-C(23)	149.9(2)
C(9A)-Cr-C(23)	90.0(2)
C(11)-Cr-C(23)	114.1(2)
C(21)-Cr-C(23)	88.7(2)
C(22)-Cr-C(23)	89.5(2)
Cr-C(1)-C(2)	70.7(3)
Cr-C(1)-C(9A)	75.1(2)
C(2)-C(1)-C(9A)	120.8(4)
Cr-C(2)-C(1)	72.9(3)
Cr-C(2)-C(3)	73.1(3)
C(1)-C(2)-C(3)	122.7(4)
Cr-C(3)-C(2)	69.0(2)
Cr-C(3)-C(3A)	72.1(3)
C(2)-C(3)-C(3A)	117.3(4)
Cr-C(3A)-C(3)	72.0(2)
Cr-C(3A)-C(4)	130.1(3)
C(3)-C(3A)-C(4)	134.3(4)
Cr-C(3A)-C(11)	72.0(2)
C(3)-C(3A)-C(11)	118.3(4)
C(4)-C(3A)-C(11)	107.2(3)
C(3A)-C(4)-C(5A)	103.1(3)
C(5A)-C(5)-C(6)	118.9(4)
C(4)-C(5A)-C(5)	135.1(4)

C(4)-C(5A)-C(10)	108.2(4)
C(5)-C(5A)-C(10)	116.6(4)
C(5)-C(6)-C(7)	124.4(5)
C(6)-C(7)-C(8A)	119.0(4)
C(8A)-C(8)-C(9)	123.3(5)
C(7)-C(8A)-C(8)	130.3(5)
C(7)-C(8A)-C(10)	114.5(4)
C(8)-C(8A)-C(10)	115.1(4)
C(8)-C(9)-C(9A)	121.5(4)
Cr-C(9A)-C(1)	68.2(2)
Cr-C(9A)-C(9)	133.7(3)
C(1)-C(9A)-C(9)	130.8(4)
Cr-C(9A)-C(11)	70.2(2)
C(1)-C(9A)-C(11)	114.8(4)
C(9)-C(9A)-C(11)	114.2(4)
C(5A)-C(10)-C(8A)	126.6(4)
C(5A)-C(10)-C(11)	110.2(4)
C(8A)-C(10)-C(11)	123.0(4)
Cr-C(11)-C(3A)	71.4(2)
Cr-C(11)-C(9A)	74.4(2)
C(3A)-C(11)-C(9A)	126.0(4)
Cr-C(11)-C(10)	130.8(3)
C(3A)-C(11)-C(10)	111.2(3)
C(9A)-C(11)-C(10)	122.8(4)
Cr-C(21)-O(1)	178.7(4)
Cr-C(22)-O(2)	176.1(4)
Cr-C(23)-O(3)	178.5(4)

Table C. Structure determination summary for $(\eta^6\text{-}H_2cppH)Cr(CO)_3$, **11.**

Crystal Data

Empirical Formula	$C_{18}\ H_{12}\ Cr\ O_3$
Color; Habit	yellow parallelepiped
Crystal size (mm)	0.7 x 0.4 x 0.4
Crystal System	Orthorhombic
Space Group	Pbca
Unit Cell Dimensions	a = 12.662(1) Å
	b = 14.594(2) Å
	c = 15.761(1) Å
Volume	2912.3(5) Å^3
Z	8
Formula weight	328.3
Density(calc.)	1.497 Mg/m^3
Absorption Coefficient	0.794 mm^{-1}
F(000)	1344

Data Collection

Diffractometer Used	Siemens P4
Radiation	MoKα (λ = 0.71073 Å)
Temperature (K)	300 ± 10
Monochromator	graphite
2θ Range	7.0 to 50.0°
Scan Type	2θ-θ
Scan Speed	Variable; 1.50 to 15.00°/min. in ω
Scan Range (ω)	0.78° plus Kα separation
Background Measurement	Stationary crystal and stationary counter at beginning and end of scan, each for 25% of total scan time
Standard Reflections	3 measured every 97 reflections
Index Ranges	$-1 \leq h \leq 15$, $-1 \leq k \leq 17$ $-1 \leq l \leq 18$
Reflections Collected	3240
Independent Reflections	2546 (R_{int} = 2.17%)
Observed Reflections	2012 ($F \geq 4.0\sigma(F)$)
Absorption Correction	psi-scan
Min./Max. Transm.	0.579/0.615

Solution and Refinement

System Used	Siemens SHELXTL PLUS (PC)
Solution	Direct Methods
Refinement Method	Full-Matrix Least-Squares
Quantity Minimized	$\Sigma w(\|F_o\|-\|F_c\|)^2$
Absolute Structure	N/A
Extinction Correction	N/A
Hydrogen Atoms	Riding model; fixed, isotropic U
Weighting Scheme	$w^{-1} = \sigma^2(F) + 0.0005F^2$
Number of Parameters Refined	201
Final R Indices (obs. data)	R = 5.94 %, wR = 6.46 %
Goodness-of-Fit	4.01
Largest and Mean Δ/σ	3.638, 0.224[e]
Data-to-Parameter Ratio	10.1:1
Largest Difference Peak	0.60 eÅ^{-3}
Largest Difference Hole	-0.47 eÅ^{-3}

e: non resolvable disorder in ligand position causes fluctuating temperature factors

Table C1. Atomic coordinates ($x10^4$) and equivalent isotropic displacement coefficients ($Å^2x10^3$) for (η^6-H_2cppH) $Cr(CO)_3$, **11**.

	x	y	z	U(eq)
Cr	553(1)	2034(1)	1290(1)	54(1)
C(1)	367(8)	2984(4)	2383(3)	99(3)
C(2)	-586(8)	2626(5)	2180(5)	109(3)
C(3)	-1041(5)	2699(4)	1378(5)	92(3)
C(3A)	-470(4)	3161(3)	751(3)	65(2)
C(4)	-696(7)	3420(5)	-156(5)	109(3)
C(5A)	332(8)	3897(4)	-428(4)	115(3)
C(5)	651(16)	4266(6)	-1178(5)	213(11)
C(6)	1624(18)	4609(10)	-1169(11)	204(14)
C(7)	2449(14)	4604(9)	-496(12)	232(12)
C(8)	2652(6)	4006(6)	1095(11)	207(8)
C(8A)	2047(7)	4221(4)	297(7)	133(4)
C(9)	1997(6)	3931(4)	1856(6)	122(3)
C(9A)	979(4)	3437(3)	1761(3)	70(2)
C(10)	1025(4)	3918(3)	262(3)	71(2)
C(11)	527(3)	3499(3)	965(3)	48(1)
C(21)	50(4)	873(4)	1489(4)	80(2)
C(22)	920(5)	1733(4)	201(4)	84(2)
C(23)	1840(4)	1607(3)	1636(3)	62(2)
O(1)	-253(3)	149(3)	1625(4)	119(2)
O(2)	1164(5)	1588(3)	-489(3)	133(2)
O(3)	2646(3)	1328(3)	1864(3)	89(2)

* Equivalent isotropic U defined as one third of the trace of the orthogonalized U_{ij} tensor

Table C2. Bond lengths (Å) for (η^6-H_2cppH)Cr(CO)$_3$, **11**.

Cr-C(1)	2.224	(6)	Cr-C(2)	2.190	(9)
Cr-C(3)	2.243	(6)	Cr-C(3A)	2.259	(5)
Cr-C(9A)	2.244	(5)	Cr-C(11)	2.199	(4)
Cr-C(21)	1.836	(5)	Cr-C(22)	1.832	(6)
Cr-C(23)	1.828	(5)	C(1)-C(2)	1.35	(1)
C(1)-C(9A)	1.414	(9)	C(2)-C(3)	1.39	(1)
C(3)-C(3A)	1.397	(9)	C(3A)-C(4)	1.507	(9)
C(3A)-C(11)	1.397	(6)	C(4)-C(5A)	1.54	(1)
C(5A)-C(5)	1.36	(1)	C(5A)-C(10)	1.40	(1)
C(5)-C(6)	1.33	(3)	C(6)-C(7)	1.49	(3)
C(7)-C(8A)	1.46	(2)	C(8)-C(8A)	1.51	(2)
C(8)-C(9)	1.46	(2)	C(8A)-C(10)	1.37	(1)
C(9)-C(9A)	1.484	(9)	C(9A)-C(11)	1.382	(7)
C(10)-C(11)	1.414	(7)	C(21)-O(1)	1.145	(7)
C(22)-O(2)	1.151	(7)	C(23)-O(3)	1.156	(6)

Table C3. Bond angles (°) for (η^6-H_2cppH)Cr(CO)$_3$, **11**.

C(1)-Cr-C(2)	35.7(3)	C(1)-Cr-C(3)	65.6(3)
C(2)-Cr-C(3)	36.6(3)	C(1)-Cr-C(3A)	77.1(2)
C(2)-Cr-C(3A)	64.9(3)	C(3)-Cr-C(3A)	36.2(2)
C(1)-Cr-C(9A)	36.9(2)	C(2)-Cr-C(9A)	65.6(3)
C(3)-Cr-C(9A)	78.6(2)	C(3A)-Cr-C(9A)	66.3(2)
C(1)-Cr-C(11)	64.7(2)	C(2)-Cr-C(11)	75.9(2)
C(3)-Cr-C(11)	65.2(2)	C(3A)-Cr-C(11)	36.5(2)
C(9A)-Cr-C(11)	36.2(2)	C(1)-Cr-C(21)	114.0(3)
C(2)-Cr-C(21)	91.5(3)	C(3)-Cr-C(21)	94.4(2)
C(3A)-Cr-C(21)	122.5(2)	C(9A)-Cr-C(21)	150.3(2)
C(11)-Cr-C(21)	158.7(2)	C(1)-Cr-C(22)	154.4(2)
C(2)-Cr-C(22)	149.6(3)	C(3)-Cr-C(22)	112.9(3)
C(3A)-Cr-C(22)	88.1(2)	C(9A)-Cr-C(22)	117.9(2)
C(11)-Cr-C(22)	91.1(2)	C(21)-Cr-C(22)	91.5(3)
C(1)-Cr-C(23)	94.4(3)	C(2)-Cr-C(23)	122.1(3)
C(3)-Cr-C(23)	158.7(3)	C(3A)-Cr-C(23)	150.6(2)
C(9A)-Cr-C(23)	89.9(2)	C(11)-Cr-C(23)	114.5(2)
C(21)-Cr-C(23)	86.8(2)	C(22)-Cr-C(23)	88.3(3)
Cr-C(1)-C(2)	70.8(4)	Cr-C(1)-C(9A)	72.3(3)
C(2)-C(1)-C(9A)	120.4(6)	Cr-C(2)-C(1)	73.5(5)
Cr-C(2)-C(3)	73.8(5)	C(1)-C(2)-C(3)	123.6(7)
Cr-C(3)-C(2)	69.6(4)	Cr-C(3)-C(3A)	72.5(3)
C(2)-C(3)-C(3A)	117.6(6)	Cr-C(3A)-C(3)	71.3(3)
Cr-C(3A)-C(4)	130.4(4)	C(3)-C(3A)-C(4)	133.9(6)
Cr-C(3A)-C(11)	69.4(3)	C(3)-C(3A)-C(11)	117.9(5)
C(4)-C(3A)-C(11)	108.2(5)	C(3A)-C(4)-C(5A)	102.5(6)
C(4)-C(5A)-C(5)	132(1)	C(4)-C(5A)-C(10)	108.9(5)
C(5)-C(5A)-C(10)	119(1)	C(5A)-C(5)-C(6)	115(1)
C(5)-C(6)-C(7)	131(2)	C(6)-C(7)-C(8A)	112(1)
C(8A)-C(8)-C(9)	114.4(7)	C(7)-C(8A)-C(8)	128(1)
C(7)-C(8A)-C(10)	115(1)	C(8)-C(8A)-C(10)	116.6(8)
C(8)-C(9)-C(9A)	116.5(7)	Cr-C(9A)-C(1)	70.8(3)
Cr-C(9A)-C(9)	133.3(4)	C(1)-C(9A)-C(9)	129.3(6)
Cr-C(9A)-C(11)	70.1(3)	C(1)-C(9A)-C(11)	115.6(5)
C(9)-C(9A)-C(11)	114.8(5)	C(5A)-C(10)-C(8A)	129.2(7)
C(5A)-C(10)-C(11)	108.7(5)	C(8A)-C(10)-C(11)	121.9(6)
Cr-C(11)-C(3A)	74.1(3)	Cr-C(11)-C(9A)	73.7(3)
C(3A)-C(11)-C(9A)	124.8(4)	Cr-C(11)-C(10)	126.6(3)
C(3A)-C(11)-C(10)	111.4(4)	C(9A)-C(11)-C(10)	123.8(4)
Cr-C(21)-O(1)	178.8(6)	Cr-C(22)-O(2)	176.7(5)
Cr-C(23)-O(3)	178.9(4)		

Table D. Structure determination summary for $(\eta^6\text{-}H_8cppH)Cr(CO)_3$, **12**.

Crystal Data

Empirical Formula	$C_{18}\ H_{18}\ Cr\ O_3$
Color; Habit	yellow plate
Crystal size (mm)	0.40 x 0.29 x 0.09
Crystal System	Monoclinic
Space Group	$P2_1/n$
Unit Cell Dimensions	$\underline{a}$ = 10.278(4) Å
	$\underline{b}$ = 11.413(3) Å
	$\underline{c}$ = 13.534(3) Å
	$\underline{\beta}$ = 105.30(2)°
Volume	1531.4(10) $Å^3$
Z	4
Formula weight	334.3
Density(calc.)	1.450 Mg/m^3
Absorption Coefficient	0.756 mm^{-1}
F(000)	696

Data Collection

Diffractometer Used	Siemens P4
Radiation	MoKα (λ = 0.71073 Å)
Temperature (K)	300 ± 10
Monochromator	graphite
2θ Range	7.0 to 45.0°
Scan Type	2θ-θ
Scan Speed	Variable; 1.50 to 60.00°/min. in ω
Scan Range (ω)	1.20° plus Kα separation
Background Measurement	Stationary crystal and stationary counter at beginning and end of scan, each for 25% of total scan time
Standard Reflections	3 measured every 97 reflections
Index Ranges	$-1 \leq h \leq 13$, $-1 \leq k \leq 15$, $-18 \leq l \leq 17$
Reflections Collected	4899
Independent Reflections	3851 (R_{int} =2.82%)
Observed Reflections	2862 ($F \geq 4.0\sigma(F)$)
Absorption Correction	psi-scan
Min./Max. Transmission	0.6850 / 0.7970

Solution and Refinement

System Used	Siemens SHELXTL PLUS (PC)
Solution	Patterson
Refinement Method	Full-Matrix Least-Squares
Quantity Minimized	$\Sigma w(\|F_o\|-\|F_c\|)^2$
Absolute Structure	N/A
Extinction Correction	N/A
Hydrogen Atoms	riding model; common, isotropic U
Weighting Scheme	$w^{-1} = \sigma^2(F) + 0.0000F^2$
Number of Parameters Refined	183
Final R Indices (obs. data)	R = 6.10 %, wR = 6.75 %
R Indices (all data)	R = 7.84 %, wR = 6.91 %
Goodness-of-Fit	2.72
Largest and Mean Δ/σ	0.028,0.001
Data-to-Parameter Ratio	15.6:1
Largest Difference Peak	0.56 eÅ^{-3}
Largest Difference Hole	-0.45 eÅ^{-3}

Table D1. Atomic coordinates ($x10^4$) and equivalent isotropic displacement coefficients ($Å^2x10^3$) for $(\eta^6\text{-}H_8cppH)Cr(CO)_3$, **12**.

	x	y	z	U(eq)
Cr	1377(1)	6931(1)	7192(1)	47(1)
C(1)	499(3)	8653(3)	7384(3)	50(1)
C(2)	77(3)	8329(3)	6342(3)	54(1)
C(3)	-577(3)	7270(3)	6045(3)	55(1)
C(3A)	-850(3)	6517(3)	6795(3)	50(1)
C(4)[b]	-1734(4)	5416(5)	6699(4)	49(1)
C(4B)[c]	603(19)	7927(16)	9413(14)	49(1)
C(5A)[b]	-2052(5)	5370(5)	7685(4)	57(1)
C(5AB)[c]	-561(18)	7194(15)	9631(13)	57(1)
C(5)[b]	-3302(5)	6069(5)	7607(4)	66(1)
C(5B)[c]	-1785(18)	7886(16)	9485(15)	66(1)
C(6)[b]	-3488(6)	6424(6)	8652(5)	71(2)
C(6B)[c]	-3035(20)	7069(19)	9265(15)	71(2)
C(7)[b]	-2338(5)	7163(5)	9240(4)	60(1)
C(7B)[c]	-3248(20)	6188(18)	8407(16)	60(1)
C(8)[b]	224(5)	7236(4)	9901(4)	57(1)
C(8B)[c]	-1767(18)	4789(17)	7657(12)	57(1)
C(8A)[b]	-1008(4)	6482(5)	9435(3)	53(1)
C(8AB)[c]	-1848(15)	5521(14)	8592(12)	53(1)
C(9)[b]	486(5)	8270(4)	9232(3)	49(1)
C(9B)[c]	-1326(19)	5299(16)	6630(13)	49(1)
C(9A)	242(3)	7917(3)	8137(2)	45(1)
C(10)	-396(3)	6848(3)	7826(2)	44(1)
C(11)[b]	-805(4)	5934(4)	8459(3)	46(1)
C(11B)[c]	-617(15)	6235(14)	8877(12)	46(1)
C(21)	2916(4)	7668(4)	7085(3)	66(1)
C(22)	1643(4)	5722(4)	6385(3)	74(2)
C(23)	2394(3)	6157(3)	8315(2)	53(1)
O(1)	3899(3)	8138(3)	7037(3)	96(2)
O(2)	1773(4)	4952(4)	5872(2)	117(2)
O(3)	3025(3)	5678(3)	9031(2)	77(1)

a: occupation factor : 0.77

b: occupation factor : 0.23

* Equivalent isotropic U defined as one third of the trace of the orthogonalized U_{ij} tensor

Table D2. Bond lengths (Å) for (η^6-H_8cppH)Cr(CO)$_3$, **12**.

Cr-C(1)	2.207	(4)	Cr-C(2)	2.200	(4)
Cr-C(3)	2.224	(3)	Cr-C(3A)	2.259	(4)
Cr-C(9A)	2.247	(4)	Cr-C(10)	2.212	(4)
Cr-C(21)	1.831	(4)	Cr-C(22)	1.825	(5)
Cr-C(23)	1.829	(3)	C(1)-C(2)	1.411	(5)
C(1)-C(9A)	1.398	(5)	C(2)-C(3)	1.390	(5)
C(3)-C(3A)	1.413	(5)	C(3A)-C(4)	1.536	(6)
C(3A)-C(9B)	1.47	(2)	C(3A)-C(10)	1.402	(4)
C(4)-C(5A)	1.455	(8)	C(4)-C(8B)	1.49	(2)
C(4)-C(9B)	0.47	(2)	C(4B)-C(5AB)	1.55	(3)
C(4B)-C(8)	1.16	(2)	C(4B)-C(9)	0.46	(2)
C(4B)-C(9A)	1.67	(2)	C(5A)-C(5)	1.492	(8)
C(5A)-C(7B)	1.99	(2)	C(5A)-C(8B)	0.73	(2)
C(5A)-C(8AB)	1.20	(2)	C(5A)-C(9B)	1.78	(2)
C(5A)-C(11)	1.564	(6)	C(5AB)-C(5B)	1.45	(3)
C(5AB)-C(7)	1.76	(2)	C(5AB)-C(8)	0.79	(2)
C(5AB)-C(8A)	0.94	(2)	C(5AB)-C(9)	1.81	(2)
C(5AB)-C(11B)	1.49	(2)	C(5)-C(6)	1.530	(9)
C(5)-C(7B)	1.08	(2)	C(5)-C(8AB)	1.83	(1)
C(5B)-C(6B)	1.55	(2)	C(5B)-C(7)	1.01	(2)
C(5B)-C(8A)	1.80	(2)	C(6)-C(6B)	1.12	(2)
C(6)-C(7)	1.499	(8)	C(6)-C(7B)	0.54	(2)
C(6)-C(8AB)	2.00	(2)	C(6B)-C(7)	0.73	(2)
C(6B)-C(7B)	1.51	(3)	C(7)-C(7B)	1.68	(2)
C(7)-C(8A)	1.534	(7)	C(7B)-C(8AB)	1.59	(3)
C(8)-C(8A)	1.524	(7)	C(8)-C(9)	1.552	(7)
C(8)-C(11B)	1.83	(2)	C(8B)-C(8AB)	1.54	(3)
C(8B)-C(9B)	1.68	(3)	C(8B)-C(11)	1.82	(2)
C(8A)-C(8AB)	1.65	(2)	C(8A)-C(11)	1.526	(7)
C(8A)-C(11B)	0.99	(2)	C(8AB)-C(11)	1.23	(2)
C(8AB)-C(11B)	1.47	(2)	C(9)-C(9A)	1.493	(6)
C(9A)-C(10)	1.396	(4)	C(10)-C(11)	1.479	(6)
C(10)-C(11B)	1.65	(2)	C(11)-C(11B)	0.65	(2)
C(21)-O(1)	1.161	(5)	C(22)-O(2)	1.149	(6)
C(23)-O(3)	1.151	(4)			

Table D3. Bond angles (°) for (η^6-H_8cppH)Cr(CO)$_3$, **12**.

C(1)-Cr-C(2)	37.3(1)	C(1)-Cr-C(3)	66.8(1)
C(2)-Cr-C(3)	36.6(1)	C(1)-Cr-C(3A)	78.1(1)
C(2)-Cr-C(3A)	65.8(1)	C(3)-Cr-C(3A)	36.7(1)
C(1)-Cr-C(9A)	36.6(1)	C(2)-Cr-C(9A)	66.4(1)
C(3)-Cr-C(9A)	78.5(1)	C(3A)-Cr-C(9A)	66.1(1)
C(1)-Cr-C(10)	65.7(1)	C(2)-Cr-C(10)	77.6(1)
C(3)-Cr-C(10)	66.0(1)	C(3A)-Cr-C(10)	36.5(1)
C(9A)-Cr-C(10)	36.5(1)	C(1)-Cr-C(21)	89.4(2)
C(2)-Cr-C(21)	92.5(2)	C(3)-Cr-C(21)	120.4(2)
C(3A)-Cr-C(21)	156.9(2)	C(9A)-Cr-C(21)	113.9(2)
C(10)-Cr-C(21)	150.2(2)	C(1)-Cr-C(22)	151.0(1)
C(2)-Cr-C(22)	113.7(2)	C(3)-Cr-C(22)	87.9(2)
C(3A)-Cr-C(22)	90.1(2)	C(9A)-Cr-C(22)	154.4(2)
C(10)-Cr-C(22)	117.9(2)	C(21)-Cr-C(22)	91.8(2)
C(1)-Cr-C(23)	119.6(1)	C(2)-Cr-C(23)	156.9(2)
C(3)-Cr-C(23)	151.2(2)	C(3A)-Cr-C(23)	114.7(1)
C(9A)-Cr-C(23)	92.1(1)	C(10)-Cr-C(23)	90.3(1)
C(21)-Cr-C(23)	88.4(2)	C(22)-Cr-C(23)	89.4(2)
Cr-C(1)-C(2)	71.1(2)	Cr-C(1)-C(9A)	73.3(2)
C(2)-C(1)-C(9A)	120.2(3)	Cr-C(2)-C(1)	71.6(2)
Cr-C(2)-C(3)	72.6(2)	C(1)-C(2)-C(3)	121.0(3)
Cr-C(3)-C(2)	70.8(2)	Cr-C(3)-C(3A)	73.0(2)
C(2)-C(3)-C(3A)	119.6(3)	Cr-C(3A)-C(3)	70.3(2)
Cr-C(3A)-C(4)	137.0(3)	C(3)-C(3A)-C(4)	131.5(3)
Cr-C(3A)-C(9B)	120.6(8)	C(3)-C(3A)-C(9B)	125.9(8)
C(4)-C(3A)-C(9B)	17.9(8)	Cr-C(3A)-C(10)	69.9(2)
C(3)-C(3A)-C(10)	118.3(3)	C(4)-C(3A)-C(10)	109.8(3)
C(9B)-C(3A)-C(10)	114.6(7)	C(3A)-C(4)-C(5A)	102.9(4)
C(3A)-C(4)-C(8B)	118.0(7)	C(5A)-C(4)-C(8B)	29(1)
C(3A)-C(4)-C(9B)	73(2)	C(5A)-C(4)-C(9B)	127(2)
C(8B)-C(4)-C(9B)	105(2)	C(5AB)-C(4B)-C(8)	29.9(8)
C(5AB)-C(4B)-C(9)	117(3)	C(8)-C(4B)-C(9)	143(4)
C(5AB)-C(4B)-C(9A)	103(1)	C(8)-C(4B)-C(9A)	124(1)
C(9)-C(4B)-C(9A)	60(2)	C(4)-C(5A)-C(5)	108.3(4)
C(4)-C(5A)-C(7B)	138.5(7)	C(5)-C(5A)-C(7B)	32.1(6)
C(4)-C(5A)-C(8B)	78(2)	C(5)-C(5A)-C(8B)	146(1)
C(7B)-C(5A)-C(8B)	139(2)	C(4)-C(5A)-C(8AB)	155.5(9)
C(5)-C(5A)-C(8AB)	84.8(8)	C(7B)-C(5A)-C(8AB)	52.8(9)
C(8B)-C(5A)-C(8AB)	103(2)	C(4)-C(5A)-C(9B)	12.3(6)
C(5)-C(5A)-C(9B)	120.2(7)	C(7B)-C(5A)-C(9B)	149.2(9)
C(8B)-C(5A)-C(9B)	70(2)	C(8AB)-C(5A)-C(9B)	146(1)
C(4)-C(5A)-C(11)	104.9(4)	C(5)-C(5A)-C(11)	111.4(4)
C(7B)-C(5A)-C(11)	88.9(6)	C(8B)-C(5A)-C(11)	98(1)
C(8AB)-C(5A)-C(11)	50.6(8)	C(9B)-C(5A)-C(11)	97(1)
C(4B)-C(5AB)-C(5B)	111(2)	C(4B)-C(5AB)-C(7)	138(1)
C(5B)-C(5AB)-C(7)	34.8(8)	C(4B)-C(5AB)-C(8)	47(1)
C(5B)-C(5AB)-C(8)	140(2)	C(7)-C(5AB)-C(8)	170(2)
C(4B)-C(5AB)-C(8A)	139(2)	C(5B)-C(5AB)-C(8A)	95(2)
C(7)-C(5AB)-C(8A)	60(1)	C(8)-C(5AB)-C(8A)	123(2)
C(4B)-C(5AB)-C(9)	13.1(7)	C(5B)-C(5AB)-C(9)	99(1)
C(7)-C(5AB)-C(9)	125(1)	C(8)-C(5AB)-C(9)	59(1)
C(8A)-C(5AB)-C(9)	142(2)	C(4B)-C(5AB)-C(11B)	99(2)

C(5B)-C(5AB)-C(11B)	116(1)	C(7)-C(5AB)-C(11B)	86(1)
C(8)-C(5AB)-C(11B)	102(2)	C(8A)-C(5AB)-C(11B)	41(1)
C(9)-C(5AB)-C(11B)	102(1)	C(5A)-C(5)-C(6)	113.1(4)
C(5A)-C(5)-C(7B)	101(1)	C(6)-C(5)-C(7B)	12(1)
C(5A)-C(5)-C(8AB)	40.9(6)	C(6)-C(5)-C(8AB)	72.2(6)
C(7B)-C(5)-C(8AB)	60(1)	C(5AB)-C(5B)-C(6B)	110(2)
C(5AB)-C(5B)-C(7)	90(1)	C(6B)-C(5B)-C(7)	23(1)
C(5AB)-C(5B)-C(8A)	31.2(8)	C(6B)-C(5B)-C(8A)	79(1)
C(7)-C(5B)-C(8A)	58(1)	C(5)-C(6)-C(6B)	137(1)
C(5)-C(6)-C(7)	111.5(5)	C(6B)-C(6)-C(7)	28(1)
C(5)-C(6)-C(7B)	26(2)	C(6B)-C(6)-C(7B)	129(3)
C(7)-C(6)-C(7B)	101(2)	C(5)-C(6)-C(8AB)	60.9(5)
C(6B)-C(6)-C(8AB)	100(1)	C(7)-C(6)-C(8AB)	75.9(6)
C(7B)-C(6)-C(8AB)	35(2)	C(5B)-C(6B)-C(6)	135(2)
C(5B)-C(6B)-C(7)	32(1)	C(6)-C(6B)-C(7)	107(2)
C(5B)-C(6B)-C(7B)	120(2)	C(6)-C(6B)-C(7B)	16(1)
C(7)-C(6B)-C(7B)	91(2)	C(5AB)-C(7)-C(5B)	56(1)
C(5AB)-C(7)-C(6)	141.2(8)	C(5B)-C(7)-C(6)	159(1)
C(5AB)-C(7)-C(6B)	159(2)	C(5B)-C(7)-C(6B)	125(2)
C(6)-C(7)-C(6B)	46(2)	C(5AB)-C(7)-C(7B)	124(1)
C(5B)-C(7)-C(7B)	158(2)	C(6)-C(7)-C(7B)	18.2(8)
C(6B)-C(7)-C(7B)	64(2)	C(5AB)-C(7)-C(8A)	32.1(6)
C(5B)-C(7)-C(8A)	88(1)	C(6)-C(7)-C(8A)	110.4(5)
C(6B)-C(7)-C(8A)	139(2)	C(7B)-C(7)-C(8A)	95.3(8)
C(5A)-C(7B)-C(5)	47.4(9)	C(5A)-C(7B)-C(6)	170(3)
C(5)-C(7B)-C(6)	141(3)	C(5A)-C(7B)-C(6B)	135(2)
C(5)-C(7B)-C(6B)	145(2)	C(6)-C(7B)-C(6B)	35(2)
C(5A)-C(7B)-C(7)	109(1)	C(5)-C(7B)-C(7)	129(2)
C(6)-C(7B)-C(7)	61(2)	C(6B)-C(7B)-C(7)	25.9(9)
C(5A)-C(7B)-C(8AB)	37.1(8)	C(5)-C(7B)-C(8AB)	84(1)
C(6)-C(7B)-C(8AB)	134(3)	C(6B)-C(7B)-C(8AB)	105(1)
C(7)-C(7B)-C(8AB)	84(1)	C(4B)-C(8)-C(5AB)	104(1)
C(4B)-C(8)-C(8A)	121.1(9)	C(5AB)-C(8)-C(8A)	31(1)
C(4B)-C(8)-C(9)	10(1)	C(5AB)-C(8)-C(9)	95(1)
C(8A)-C(8)-C(9)	116.2(4)	C(4B)-C(8)-C(11B)	99(1)
C(5AB)-C(8)-C(11B)	53(2)	C(8A)-C(8)-C(11B)	32.6(6)
C(9)-C(8)-C(11B)	98.9(6)	C(4)-C(8B)-C(5A)	73(1)
C(4)-C(8B)-C(8AB)	118(1)	C(5A)-C(8B)-C(8AB)	50(1)
C(4)-C(8B)-C(9B)	16(1)	C(5A)-C(8B)-C(9B)	86(2)
C(8AB)-C(8B)-C(9B)	125(2)	C(4)-C(8B)-C(11)	92(1)
C(5A)-C(8B)-C(11)	59(1)	C(8AB)-C(8B)-C(11)	41.9(8)
C(9B)-C(8B)-C(11)	91(1)	C(5AB)-C(8A)-C(5B)	54(1)
C(5AB)-C(8A)-C(7)	88(1)	C(5B)-C(8A)-C(7)	34.0(6)
C(5AB)-C(8A)-C(8)	26(1)	C(5B)-C(8A)-C(8)	79.0(6)
C(7)-C(8A)-C(8)	113.0(4)	C(5AB)-C(8A)-C(8AB)	154(1)
C(5B)-C(8A)-C(8AB)	117.4(8)	C(7)-C(8A)-C(8AB)	86.5(6)
C(8)-C(8A)-C(8AB)	152.4(7)	C(5AB)-C(8A)-C(11)	116(1)
C(5B)-C(8A)-C(11)	124.1(7)	C(7)-C(8A)-C(11)	112.2(4)
C(8)-C(8A)-C(11)	107.5(4)	C(8AB)-C(8A)-C(11)	45.2(6)
C(5AB)-C(8A)-C(11B)	101(2)	C(5B)-C(8A)-C(11B)	124(1)
C(7)-C(8A)-C(11B)	122.5(9)	C(8)-C(8A)-C(11B)	91(1)
C(8AB)-C(8A)-C(11B)	62(1)	C(11)-C(8A)-C(11B)	16.7(9)
C(5A)-C(8AB)-C(5)	54.3(6)	C(5A)-C(8AB)-C(6)	101.2(9)
C(5)-C(8AB)-C(6)	46.9(4)	C(5A)-C(8AB)-C(7B)	90(1)
C(5)-C(8AB)-C(7B)	35.9(8)	C(6)-C(8AB)-C(7B)	11.2(8)
C(5A)-C(8AB)-C(8B)	27.6(8)	C(5)-C(8AB)-C(8B)	78.3(9)

C(6)-C(8AB)-C(8B)	123(1)	C(7B)-C(8AB)-C(8B)	112(1)
C(5A)-C(8AB)-C(8A)	136(1)	C(5)-C(8AB)-C(8A)	117.0(9)
C(6)-C(8AB)-C(8A)	85.6(8)	C(7B)-C(8AB)-C(8A)	94(1)
C(8B)-C(8AB)-C(8A)	143(1)	C(5A)-C(8AB)-C(11)	80(1)
C(5)-C(8AB)-C(11)	110(1)	C(6)-C(8AB)-C(11)	126(1)
C(7B)-C(8AB)-C(11)	126(1)	C(8B)-C(8AB)-C(11)	81(1)
C(8A)-C(8AB)-C(11)	61.9(7)	C(5A)-C(8AB)-C(11B)	105(1)
C(5)-C(8AB)-C(11B)	119(1)	C(6)-C(8AB)-C(11B)	112(1)
C(7B)-C(8AB)-C(11B)	117(1)	C(8B)-C(8AB)-C(11B)	107(1)
C(8A)-C(8AB)-C(11B)	36.2(8)	C(11)-C(8AB)-C(11B)	25.9(8)
C(4B)-C(9)-C(5AB)	50(3)	C(4B)-C(9)-C(8)	27(3)
C(5AB)-C(9)-C(8)	26.0(5)	C(4B)-C(9)-C(9A)	105(2)
C(5AB)-C(9)-C(9A)	99.0(6)	C(8)-C(9)-C(9A)	111.3(4)
C(3A)-C(9B)-C(4)	89(2)	C(3A)-C(9B)-C(5A)	92(1)
C(4)-C(9B)-C(5A)	41(2)	C(3A)-C(9B)-C(8B)	111(1)
C(4)-C(9B)-C(8B)	59(2)	C(5A)-C(9B)-C(8B)	24.1(7)
Cr-C(9A)-C(1)	70.2(2)	Cr-C(9A)-C(4B)	125.9(7)
C(1)-C(9A)-C(4B)	135.8(7)	Cr-C(9A)-C(9)	136.4(3)
C(1)-C(9A)-C(9)	123.1(3)	C(4B)-C(9A)-C(9)	15.5(7)
Cr-C(9A)-C(10)	70.4(2)	C(1)-C(9A)-C(10)	118.1(3)
C(4B)-C(9A)-C(10)	106.0(7)	C(9)-C(9A)-C(10)	118.5(3)
Cr-C(10)-C(3A)	73.6(2)	Cr-C(10)-C(9A)	73.1(2)
C(3A)-C(10)-C(9A)	122.8(3)	Cr-C(10)-C(11)	130.1(3)
C(3A)-C(10)-C(11)	108.4(3)	C(9A)-C(10)-C(11)	128.7(3)
Cr-C(10)-C(11B)	131.8(6)	C(3A)-C(10)-C(11B)	131.1(6)
C(9A)-C(10)-C(11B)	105.7(6)	C(11)-C(10)-C(11B)	23.0(5)
C(5A)-C(11)-C(8B)	23.4(6)	C(5A)-C(11)-C(8A)	118.3(4)
C(8B)-C(11)-C(8A)	129.4(7)	C(5A)-C(11)-C(8AB)	49.3(8)
C(8B)-C(11)-C(8AB)	57(1)	C(8A)-C(11)-C(8AB)	72.8(8)
C(5A)-C(11)-C(10)	102.2(3)	C(8B)-C(11)-C(10)	110.8(6)
C(8A)-C(11)-C(10)	109.7(4)	C(8AB)-C(11)-C(10)	138.5(8)
C(5A)-C(11)-C(11B)	144(2)	C(8B)-C(11)-C(11B)	154(2)
C(8A)-C(11)-C(11B)	26(2)	C(8AB)-C(11)-C(11B)	98(2)
C(10)-C(11)-C(11B)	94(2)	C(5AB)-C(11B)-C(8)	25.1(7)
C(5AB)-C(11B)-C(8A)	38(1)	C(8)-C(11B)-C(8A)	56.5(8)
C(5AB)-C(11B)-C(8AB)	118(2)	C(8)-C(11B)-C(8AB)	139(1)
C(8A)-C(11B)-C(8AB)	82(1)	C(5AB)-C(11B)-C(10)	107(1)
C(8)-C(11B)-C(10)	104.0(9)	C(8A)-C(11B)-C(10)	136(1)
C(8AB)-C(11B)-C(10)	108(1)	C(5AB)-C(11B)-C(11)	160(2)
C(8)-C(11B)-C(11)	165(2)	C(8A)-C(11B)-C(11)	137(2)
C(8AB)-C(11B)-C(11)	56(1)	C(10)-C(11B)-C(11)	63(1)
Cr-C(21)-O(1)	178.7(4)	Cr-C(22)-O(2)	178.1(4)
Cr-C(23)-O(3)	179.0(3)		

Table E. Structure determination summary for

$(\eta^6\text{-cppH})Fe(\eta^5\text{-}C_5H_5)PF_6$, **14**.

Crystal Data

Empirical Formula	$C_{20}\ H_{15}\ F_6\ Fe\ P$
Color; Habit	yellow plate
Crystal size (mm)	0.25 x 0.40 x 0.70
Crystal System	Monoclinic
Space Group	$P2_1/c$
Unit Cell Dimensions	$\underline{a}$ = 7.619(2) Å
	$\underline{b}$ = 16.558(2) Å
	$\underline{c}$ = 14.346(2) Å
	$\underline{\beta}$ = 102.00(2)°
Volume	1770.3(6) $Å^3$
Z	4
Formula weight	456.1
Density(calc.)	1.711 Mg/m^3
Absorption Coefficient	1.005 mm^{-1}
F(000)	920

Data Collection

Diffractometer Used	Siemens R3m/V
Radiation	AgKα (λ = 0.56086 Å)
Temperature (K)	300 ± 10
Monochromator	graphite
2θ Range	5.0 to 42.0°
Scan Type	2θ-θ
Scan Speed	16°/min. in ω
Scan Range (ω)	1.00° plus Kα-separation
Background Measurement	Stationary crystal and stationary counter at beginning and end of scan, each for 25% of total scan time
Standard Reflections	3 measured every 97 reflections
Index Ranges	$0 \leq h \leq 9$, $0 \leq k \leq 21$ $-18 \leq l \leq 18$
Reflections Collected	4557
Independent Reflections	4089 (R_{int} = 1.87%)
Observed Reflections	3053 ($F \geq 4.0\sigma(F)$)
Absorption Correction	psi-scan
Min./Max. Transmission	0.520 / 0.583

Solution and Refinement

System Used	Siemens SHELXTL PLUS (VMS)
Solution	Direct Methods
Refinement Method	Full-Matrix Least-Squares
Quantity Minimized	$\Sigma w(\lvert F_o \rvert - \lvert F_c \rvert)^2$
Absolute Structure	N/A
Extinction Correction	N/A
Hydrogen Atoms	Riding model; common, isotropic U
Weighting Scheme	$w^{-1} = \sigma^2(F) + 0.0015F^2$
Number of Parameters Refined	281
Final R Indices (obs. data)	R = 5.90 %, wR = 7.65 %
R Indices (all data)	R = 7.41 %, wR = 7.92 %
Goodness-of-Fit	1.43
Largest and Mean Δ/σ	0.490[a], 0.045
Data-to-Parameter Ratio	10.9:1
Largest Difference Peak	0.66 eÅ^{-3}
Largest Difference Hole	-0.39 eÅ^{-3}

a: disorder in the PF_6 anion causes positional and thermal parameters of the fluorine atoms to fluctuate

Table E1. Atomic coordinates ($x10^4$) and equivalent isotropic displacement coefficients ($Å^2x10^3$) for $(\eta^6\text{-cppH})Fe(\eta^5\text{-}C_5H_5)PF_6$, **14**.

	x	y	z	U(eq)
Fe	4588(1)	4190(1)	8043(1)	50(1)
P	-428(1)	3176(1)	997(1)	63(1)
F(1)[d]	-1109(8)	2858(3)	-42(3)	174(3)
F(2)	-750(6)	2332(2)	1395(4)	148(3)
F(3)	1537(5)	2963(3)	986(5)	165(4)
F(4)	153(7)	3534(3)	2010(2)	153(3)
F(5)	-148(5)	4027(2)	566(3)	100(2)
F(6)	-2424(4)	3422(3)	997(4)	132(3)
F(1A)[e]	-2300(11)	3154(9)	328(9)	87(6)
F(2A)	-113(21)	2276(4)	760(13)	117(9)
F(3A)	439(18)	3449(11)	159(8)	38(10)
F(4A)	1470(11)	3188(8)	1675(9)	67(5)
F(5A)	-703(22)	4072(5)	1251(13)	172(14)
F(6A)	-1258(18)	2901(11)	1851(8)	131(10)
C(1)	6524(6)	5109(3)	8218(3)	71(2)
C(2)	7324(6)	4352(4)	8358(3)	79(2)
C(3)	6898(6)	3705(3)	7696(3)	72(2)
C(3A)	5635(5)	3847(3)	6847(3)	52(1)
C(4)	4777(6)	3348(3)	5958(3)	63(2)
C(5)	2444(6)	3946(4)	4462(3)	74(2)
C(5A)	3556(5)	3964(3)	5343(3)	54(1)
C(6)	1563(6)	4646(4)	4112(3)	79(2)
C(7)	1689(6)	5361(4)	4604(3)	74(2)
C(8)	3072(7)	6065(3)	6188(4)	76(2)
C(8A)	2784(5)	5408(3)	5524(3)	61(2)
C(9)	4229(7)	6014(3)	7053(4)	74(2)
C(9A)	5273(6)	5276(3)	7367(3)	58(1)
C(10)	3686(5)	4703(2)	5840(3)	46(1)
C(11)	4922(5)	4632(2)	6716(3)	44(1)
C(12)	3987(7)	3771(5)	9265(4)	102(3)
C(13)	3075(7)	4459(3)	9041(4)	78(2)
C(14)	2031(7)	4403(5)	8206(5)	94(3)
C(15)	2129(10)	3694(6)	7837(5)	116(3)
C(16)	3382(14)	3207(3)	8466(9)	152(5)

d: occupation factors for atoms F(1)-F(6) : 0.84

e: occupation factors for atoms F(1B)-F(6B) : 0.16

* Equivalent isotropic U defined as one third of the trace of the orthogonalized U_{ij} tensor

Table E2. Bond lengths (Å) for (η^6-cppH)Fe(η^5-C_5H_5)PF_6, **14**.

Fe-C(1)	2.098	(5)	Fe-C(2)	2.057	(4)
Fe-C(3)	2.087	(5)	Fe-C(3A)	2.115	(4)
Fe-C(9A)	2.158	(4)	Fe-C(11)	2.105	(4)
Fe-C(12)	2.023	(7)	Fe-C(13)	2.064	(6)
Fe-C(14)	2.040	(6)	Fe-C(15)	2.010	(8)
Fe-C(16)	2.023	(9)	P-F(1)	1.563	(4)
P-F(2)	1.547	(4)	P-F(3)	1.541	(4)
P-F(4)	1.548	(4)	P-F(5)	1.572	(4)
P-F(6)	1.574	(4)	P-F(1A)	1.545	(9)
P-F(2A)	1.558	(9)	P-F(3A)	1.56	(1)
P-F(4A)	1.567	(8)	P-F(5A)	1.553	(9)
P-F(6A)	1.56	(1)	C(1)-C(2)	1.389	(8)
C(1)-C(9A)	1.411	(6)	C(2)-C(3)	1.424	(8)
C(3)-C(3A)	1.407	(6)	C(3A)-C(4)	1.545	(6)
C(3A)-C(11)	1.407	(6)	C(4)-C(5A)	1.531	(6)
C(5)-C(5A)	1.368	(6)	C(5)-C(6)	1.379	(8)
C(5A)-C(10)	1.409	(6)	C(6)-C(7)	1.372	(9)
C(7)-C(8A)	1.410	(6)	C(8)-C(8A)	1.432	(7)
C(8)-C(9)	1.367	(7)	C(8A)-C(10)	1.383	(6)
C(9)-C(9A)	1.477	(6)	C(9A)-C(11)	1.405	(5)
C(10)-C(11)	1.410	(4)	C(12)-C(13)	1.34	(1)
C(12)-C(16)	1.48	(1)	C(13)-C(14)	1.297	(8)
C(14)-C(15)	1.30	(1)	C(15)-C(16)	1.42	(1)

Table E3. Bond angles (°) for (η^6-cppH)Fe(η^5-C_5H_5)PF_6, **14**.

C(1)-Fe-C(2)	39.0(2)	C(1)-Fe-C(3)	72.5(2)
C(2)-Fe-C(3)	40.2(2)	C(1)-Fe-C(3A)	85.2(2)
C(2)-Fe-C(3A)	71-2(2)	C(3)-Fe-C(3A)	39.1(2)
C(1)-Fe-C(9A)	38.7(2)	C(2)-Fe-C(9A)	70.2(2)
C(3)-Fe-C(9A)	85.3(2)	C(3A)-Fe-C(9A)	72.0(2)
C(1)-Fe-C(11)	69.0(2)	C(2)-Fe-C(11)	81.1(2)
C(3)-Fe-C(11)	69.6(2)	C(3A)-Fe-C(11)	38.9(2)
C(9A)-Fe-C(11)	38.5(1)	C(1)-Fe-C(12)	115.2(2)
C(2)-Fe-C(12)	104.8(2)	C(3)-Fe-C(12)	115.4(2)
C(3A)-Fe-C(12)	143.4(3)	C(9A)-Fe-C(12)	142.6(3)
C(11)-Fe-C(12)	174.0(2)	C(1)-Fe-C(13)	103.9(2)
C(2)-Fe-C(13)	120.4(2)	C(3)-Fe-C(13)	150.3(2)
C(3A)-Fe-C(13)	168.4(2)	C(9A)-Fe-C(13)	110.7(2)
C(11)-Fe-C(13)	137.9(2)	C(12)-Fe-C(13)	38.2(3)
C(1)-Fe-C(14)	121.7(3)	C(2)-Fe-C(14)	154.2(2)
C(3)-Fe-C(14)	165.2(2)	C(3A)-Fe-C(14)	132.0(2)
C(9A)-Fe-C(14)	103.5(2)	C(11)-Fe-C(14)	109.9(2)
C(12)-Fe-C(14)	64.4(2)	C(13)-Fe-C(14)	36.8(2)
C(1)-Fe-C(15)	157.6(3)	C(2)-Fe-C(15)	163.1(3)
C(3)-Fe-C(15)	127.9(3)	C(3A)-Fe-C(15)	105.6(2)
C(9A)-Fe-C(15)	125.4(3)	C(11)-Fe-C(15)	107.1(2)
C(12)-Fe-C(15)	67.4(2)	C(13)-Fe-C(15)	63.4(3)
C(14)-Fe-C(15)	37.3(3)	C(1)-Fe-C(16)	154.1(3)
C(2)-Fe-C(16)	122.8(3)	C(3)-Fe-C(16)	102.7(3)
C(3A)-Fe-C(16)	107.4(4)	C(9A)-Fe-C(16)	166.5(3)
C(11)-Fe-C(16)	134.4(4)	C(12)-Fe-C(16)	42.8(4)
C(13)-Fe-C(16)	67.2(4)	C(14)-Fe-C(16)	66.5(3)
C(15)-Fe-C(16)	41.2(4)	F(1)-P-F(2)	90-1(3)
F(1)-P-F(3)	92.6(3)	F(2)-P-F(3)	91-5(3)
F(1)-P-F(4)	176.3(3)	F(2)-P-F(4)	92.1(3)
F(3)-P-F(4)	90.4(3)	F(1)-P-F(5)	88.4(2)
F(2)-P-F(5)	178.3(2)	F(3)-P-F(5)	89.4(2)
F(4)-P-F(5)	89.4(2)	F(1)-P-F(6)	87.6(3)
F(2)-P-F(6)	90.4(3)	F(3)-P-F(6)	178.1(3)
F(4)-P-F(6)	89-3(3)	F(5)-P-F(6)	88.7(2)
F(1A)-P-F(2A)	90.4(8)	F(1A)-P-F(3A)	90.7(7)
F(2A)-P-F(3A)	90(1)	F(1A)-P-F(4A)	179.4(8)
F(2A)-P-F(4A)	89.0(7)	F(3A)-P-F(4A)	89.5(6)
F(1A)-P-F(5A)	90.9(8)	F(2A)-P-F(5A)	178.7(6)
F(3A)-P-F(5A)	90(1)	F(4A)-P-F(5A)	89.7(8)
F(1A)-P-F(6A)	90.5(7)	F(2A)-P-F(6A)	90(1)
F(3A)-P-F(6A)	178.8(7)	F(4A)-P-F(6A)	89.3(6)
F(5A)-P-F(6A)	90(1)	Fe-C(1)-C(2)	68.9(3)
Fe-C(1)-C(9A)	73.0(3)	C(2)-C(1)-C(9A)	119-9(4)
Fe-C(2)-C(1)	72.1(3)	Fe-C(2)-C(3)	71-0(3)
C(1)-C(2)-C(3)	123.3(4)	Fe-C(3)-C(2)	68.8(3)
Fe-C(3)-C(3A)	71.5(3)	C(2)-C(3)-C(3A)	118.2(5)
Fe-C(3A)-C(3)	69.3(3)	Fe-C(3A)-C(4)	130.3(3)
C(3)-C(3A)-C(4)	136.2(4)	Fe-C(3A)-C(11)	70.1(2)
C(3)-C(3A)-C(11)	116.4(4)	C(4)-C(3A)-C(11)	107.4(3)
C(3A)-C(4)-C(5A)	102.9(3)	C(5A)-C(5)-C(6)	118-6(5)
C(4)-C(5A)-C(5)	134.8(4)	C(4)-C(5A)-C(10)	108.4(3)
C(5)-C(5A)-C(10)	116.8(4)	C(5)-C(6)-C(7)	124-2(4)
C(6)-C(7)-C(8A)	119.6(5)	C(8A)-C(8)-C(9)	122-6(4)

C(7)-C(8A)-C(8)	130.1(5)	C(7)-C(8A)-C(10)	114-7(4)
C(8)-C(8A)-C(10)	115.2(4)	C(8)-C(9)-C(9A)	122.1(4)

Table F. Structure determination summary for (η^5-cpp)Mn(CO)$_3$, **29**.

Crystal Data

Empirical Formula	C_{18} H_9 Mn O_3
Color; Habit	red square prism
Crystal size (mm)	0.35 x 0.40 x 0.45
Crystal System	Monoclinic
Space Group	$P2_1/c$
Unit Cell Dimensions	$\underline{a}$ = 11.274(2) Å
	$\underline{b}$ = 8.752(2) Å
	$\underline{c}$ = 14.404(3) Å
	$\underline{\beta}$ = 98.64(3)°
Volume	1405.1(7) Å^3
Z	4
Formula weight	328.2
Density(calc.)	1.551 Mg/m^3
Absorption Coefficient	0.948 mm^{-1}
F(000)	664

Data Collection

Diffractometer Used	Siemens R3m/V
Radiation	AgKα (λ = 0.56086 Å)
Temperature (K)	300 ± 10
Monochromator	graphite
2θ Range	7.0 to 45.0°
Scan Type	2θ-θ
Scan Speed	Variable; 2.00 to 29.30°/min. in ω
Scan Range (ω)	1.00° plus Kα separation
Background Measurement	Stationary crystal and stationary counter at beginning and end of scan, each for 25% of total scan time
Standard Reflections	3 measured every 100 reflections
Index Ranges	$0 \leq h \leq 15$, $0 \leq k \leq 11$ $-19 \leq l \leq 19$
Reflections Collected	3938
Independent Reflections	3764 (R_{int} = 1.24%)
Observed Reflections	2609 ($F \geq 4.0\sigma(F)$)
Absorption Correction	psi-scan
Min./Max. Transm.	0.724/0.786

Solution and Refinement

System Used	Siemens SHELXTL PLUS (PC)
Solution	Patterson
Refinement Method	Full-Matrix Least-Squares
Quantity Minimized	$\Sigma w(\|F_o\|-\|F_c\|)^2$
Absolute Structure	N/A
Extinction Correction	N/A
Hydrogen Atoms	refined; individual, isotropic U
Weighting Scheme	$w^{-1} = \sigma^2(F) + 0.0015F^2$
Number of Parameters Refined	235
Final R Indices (obs. data)	R = 3.71 %, wR = 4.68 %
R Indices (all data)	R = 5.34 %, wR = 5.14 %
Goodness-of-Fit	0.92
Largest and Mean Δ/σ	0.021, 0.002
Data-to-Parameter Ratio	11.1:1
Largest Difference Peak	0.45 eÅ^{-3}
Largest Difference Hole	-0.25 eÅ^{-3}

Table F1. Atomic coordinates ($x10^4$) and equivalent isotropic displacement coefficients ($Å^2x10^3$) for $(\eta^5$-cpp)$Mn(CO)_3$, **29**.

	x	y	z	U(eq)
Mn	2408(1)	2175(1)	391(1)	40(1)
C(1)	3767(3)	6063(3)	-474(2)	63(1)
C(2)	3383(2)	5315(4)	-1330(2)	62(1)
C(3)	2470(2)	4259(3)	-1466(2)	54(1)
C(3A)	1860(2)	3914(3)	-694(1)	43(1)
C(4)	870(2)	2968(3)	-510(2)	45(1)
C(5)	-163(2)	2860(3)	1057(2)	51(1)
C(5A)	664(2)	3283(3)	447(1)	43(1)
C(6)	-4(3)	3457(3)	1953(2)	59(1)
C(7)	930(3)	4467(3)	2311(2)	58(1)
C(8)	2770(3)	5971(3)	1922(2)	61(1)
C(8A)	1766(2)	4920(3)	1754(2)	50(1)
C(9)	3447(3)	6357(3)	1259(2)	62(1)
C(9A)	3240(2)	5755(3)	308(2)	51(1)
C(10)	1597(2)	4284(3)	843(1)	41(1)
C(11)	2306(2)	4670(3)	155(2)	42(1)
C(21)	3278(3)	1178(3)	-358(2)	62(1)
C(22)	1844(2)	422(3)	771(2)	56(1)
C(23)	3637(2)	2212(3)	1347(2)	48(1)
O(21)	3836(2)	554(3)	-838(2)	105(1)
O(22)	1454(2)	-695(3)	1016(2)	91(1)
O(23)	4402(2)	2248(3)	1962(1)	78(1)

* Equivalent isotropic U defined as one third of the trace of the orthogonalized U_{ij} tensor

Table F2. Bond lengths (Å) for (η^5-cpp)Mn(CO)$_3$, **29**.

Mn-C(3A)	2.203(2)	Mn-C(4)	2.121(2)
Mn-C(5A)	2.205(2)	Mn-C(10)	2.202(2)
Mn-C(11)	2.210(2)	Mn-C(21)	2.790(3)
Mn-C(22)	1.778(3)	Mn-C(23)	1.801(2)
C(1)-C(2)	1.405(4)	C(1)-C(5A)	1.377(4)
C(1)-H(1)	0.85(3)	C(2)-C(3)	1.375(4)
C(2)-H(2)	0.94(3)	C(3)-C(3A)	1.424(3)
C(3)-H(3)	1.00(3)	C(3A)-C(4)	1.446(3)
C(3A)-C(11)	1.415(3)	C(4)-C(5A)	1.457(3)
C(4)-H(4)	0.85(2)	C(5)-C(5A)	1.423(3)
C(5)-C(6)	1.380(4)	C(5)-H(5)	0.87(3)
C(5A)-C(10)	1.421(3)	C(6)-C(7)	1.412(4)
C(6)-H(6)	0.98(3)	C(7)-C(8A)	1.385(4)
C(7)-H(7)	1.00(3)	C(8)-C(8A)	1.450(4)
C(8)-C(9)	1.352(4)	C(8)-H(8)	0.93(3)
C(8A)-C(10)	1.411(3)	C(9)-C(9A)	1.453(4)
C(9)-H(9)	1.02(3)	C(9A)-C(11)	1.411(3)
C(10)-C(11)	1.405(3)	C(21)-O(21)	1.141(4)
C(22)-O(22)	1.149(4)	C(23)-O(23)	1.140(3)

Table F3. Bond angles (°) for (η^5-cpp)Mn(CO)$_3$, **29**.

C(3A)-Mn-C(4)	39.0(1)
C(3A)-Mn-C(5A)	64.2(1)
C(4)-Mn-C(5A)	39.3(1)
C(3A)-Mn-C(10)	63.0(1)
C(4)-Mn-C(10)	64.4(1)
C(5A)-Mn-C(10)	37.6(1)
C(3A)-Mn-C(11)	37.4(1)
C(5)-Mn-C(11)	64.1(1)
C(5A)-Mn-C(11)	62.9(1)
C(10)-Mn-C(11)	37.1(1)
C(3A)-Mn-C(21)	91.7(1)
C(4)-Mn-C(21)	105.2(1)
C(5A)-Mn-C(21)	143.9(1)
C(10)-Mn-C(21)	151.2(1)
C(11)-Mn-C(21)	114.2(1)
C(3A)-Mn-C(22)	137.7(1)
C(4)-Mn-C(22)	100.0(1)
C(5A)-Mn-C(22)	90.4(1)
C(10)-Mn-C(22)	116.6(1)
C(11)-Mn-C(22)	152.5(1)
C(21)-Mn-C(22)	91.1(1)
C(3A)-Mn-C(23)	129.2(1)
C(4)-Mn-C(23)	157.9(1)
C(5A)-Mn-C(23)	123.5(1)
C(10)-Mn-C(23)	93.7(1)
C(11)-Mn-C(23)	96.7(1)
C(21)-Mn-C(23)	92.4(1)
C(22)-Mn-C(23)	92.8(1)
C(2)-C(1)-C(9A)	120.9(3)
C(2)-C(1)-H(1)	116(2)
C(9A)-C(1)-H(1)	123(2)
C(1)-C(2)-C(3)	124.3(3)
C(1)-C(2)-H(2)	116(2)
C(3)-C(2)-H(2)	120(2)
C(2)-C(3)-C(3A)	118.0(2)
C(2)-C(3)-H(3)	123(2)
C(3A)-C(3)-H(3)	120(2)
Mn-C(3A)-C(3)	125.7(2)
Mn-C(3A)-C(4)	67.4(1)
C(3)-C(3A)-C(4)	137.9(2)
Mn-C(3A)-C(11)	71.6(1)
C(3)-C(3A)-C(11)	115.7(7)
C(4)-C(3A)-C(11)	107.0(7)
Mn-C(4)-C(3A)	73.6(1)
Mn-C(4)-C(5A)	73.5(1)
C(3A)-C(4)-C(5A)	107.6(7)
Mn-C(4)-H(4)	124(2)
C(3A)-C(4)-H(4)	126(2)
C(5A)-C(4)-H(4)	126(2)
C(5A)-C(5)-C(6)	118.3(5)
C(5A)-C(5)-H(5)	123(2)
C(6)-C(5)-H(5)	119(2)
Mn-C(5A)-C(4)	67.2(1)
Mn-C(5A)-C(5)	125.4(2)

C(4)-C(5A)-C(5)	138.3(2)
Mn-C(5A)-C(10)	71.1(1)
C(4)-C(5A)-C(10)	106.5(2)
C(5)-C(5A)-C(10)	115.2(2)
C(5)-C(6)-C(7)	124.3(3)
C(5)-C(6)-H(6)	116(2)
C(7)-C(6)-H(6)	120(2)
C(6)-C(7)-C(8A)	120.2(2)
C(6)-C(7)-H(7)	119(2)
C(8A)-C(7)-H(7)	121(2)
C(8A)-C(8)-C(9)	123.3(2)
C(8A)-C(8)-H(8)	119(2)
C(9)-C(8)-H(8)	118(2)
C(7)-C(8A)-C(8)	131.8(2)
C(7)-C(8A)-C(10)	114.7(2)
C(8)-C(8A)-C(10)	113.5(2)
C(8)-C(9)-C(9A)	123.2(2)
C(8)-C(9)-H(9)	120(2)
C(9A)-C(9)-H(9)	117(2)
C(1)-C(9A)-C(9)	132.2(2)
C(1)-C(9A)-C(11)	114.1(2)
C(5)-C(5A)-C(11)	113.7(2)
Mn-C(10)-C(5A)	71.3(1)
Mn-C(10)-C(8A)	127.0(2)
C(5A)-C(10)-C(8A)	127.3(2)
Mn-C(10)-C(11)	71.7(1)
C(5A)-C(10)-C(11)	109.2(2)
C(8A)-C(10)-C(11)	123.3(2)
Mn-C(11)-C(3A)	71.0(1)
Mn-C(11)-C(9A)	128.4(2)
C(3A)-C(11)-C(9A)	127.5(2)
Mn-C(11)-C(10)	71.1(1)
C(3A)-C(11)-C(10)	109.4(2)
C(9)-C(11)-C(10)	122.8(2)
Mn-C(21)-O(21)	179.4(3)
Mn-C(22)-O(22)	178.4(2)
Mn-C(23)-O(23)	178.8(2)

Table F4. H-Atom coordinates ($x10^4$) and isotropic displacement coefficients ($Å^2x10^3$) for $(\eta^5$-cpp)$Mn(CO)_3$, **29**.

	X	Y	Z	U
H(1)	4341(30)	6697(40)	-474(25)	84(10)
H(2)	3775(23)	5593(32)	-1835(20)	62(8)
H(3)	2257(25)	3732(35)	-2079(21)	61(8)
H(4)	435(21)	2413(27)	-906(18)	35(6)
H(5)	-740(28)	2205(34)	896(21)	63(9)
H(6)	-596(28)	3140(35)	2348(21)	75(9)
H(7)	965(25)	4876(39)	2960(23)	79(9)
H(8)	2952(26)	6414(38)	5510(23)	75(9)
H(9)	4121(30)	7134(35)	1414(53)	71(9)

Table G. Structure determination summary for $(\eta^1\text{-cpp})Mn(CO)_3(P(Et)_3)_2$, **60**.

Crystal Data

Empirical Formula	$C_{30}\ H_{39}\ Mn\ O_3\ P_2$
Color; Habit	yellow plate
Crystal size (mm)	0.4 x 0.3 x 0.15
Crystal System	Monoclinic
Space Group	$P2_1/c$
Unit Cell Dimensions	$\underline{a}$ = 16.277(3) Å
	$\underline{b}$ = 14.448(3) Å
	$\underline{c}$ = 13.216(3) Å
	β = 109.57(3)°
Volume	2928.5(11) $Å^3$
Z	4
Formula weight	564.5
Density(calc.)	1.280 Mg/m^3
Absorption Coefficient	0.588 mm^{-1}
F(000)	1192

Data Collection

Diffractometer Used	Siemens P4
Radiation	MoKα (λ = 0.71073 Å)
Temperature (K)	300 ± 10
Monochromator	graphite
2θ Range	4.0 to 40.0°
Scan Type	2θ-θ
Scan Speed	Variable; 5.00 to 50.00°/min. in ω
Scan Range (ω)	1.00° plus Kα-separation
Background Measurement	Stationary crystal and stationary counter at beginning and end of scan, each for 25% of total scan time
Standard Reflections	3 measured every 97 reflections
Index Ranges	$-19 \leq h \leq 18$, $-17 \leq k \leq 1$ $-1 \leq l \leq 7$
Reflections Collected	4302
Independent Reflections	3293 (R_{int} = 1.94%)
Observed Reflections	1903 ($F \geq 4.0\sigma(F)$)
Absorption Correction	N/A

Solution and Refinement

System Used	Siemens SHELXTL PLUS (PC)
Solution	Direct Methods
Refinement Method	Full-Matrix Least-Squares
Quantity Minimized	$\Sigma w(\|F_o\|-\|F_c\|)^2$
Absolute Structure	N/A
Extinction Correction	N/A
Hydrogen Atoms	Riding model; fixed, isotropic U
Weighting Scheme	N/A
Number of Parameters Refined	145
Final R Indices (obs. data)	R = 6.78 %, wR = 6.93 %
R Indices (all data)	R = 11.79 %, wR = 10.42 %
Goodness-of-Fit	2.90
Largest and Mean Δ/σ	0.047,0.007
Data-to-Parameter Ratio	13.1:1
Largest Difference Peak	0.55 $eÅ^{-3}$
Largest Difference Hole	-0.46 $eÅ^{-3}$

Table G1. Atomic coordinates ($x10^4$) and equivalent isotropic displacement coefficients ($Å^2x10^3$) for $(\eta^1$-cpp)$Mn(CO)_3(P(Et)_3)_2$, **60**.

	x	y	z	U(eq)
Mn	2286(1)	126(1)	4478(1)	34(1)
P(1)	2220(2)	-1038(2)	5653(3)	40(1)
P(2)	2426(2)	1456(2)	3545(3)	39(1)
C(4)	2277(6)	-948(6)	3214(9)	44(3)
O(41)	4226(4)	48(5)	5354(6)	57(2)
O(40)	377(5)	16(5)	3402(7)	67(2)
C(3A)	1998(6)	-602(6)	2080(9)	39(2)
O(42)	2145(5)	1377(6)	6149(8)	78(3)
C(8A)	4162(6)	-1423(7)	2260(10)	51(3)
C(24)	3237(6)	-1290(7)	6730(9)	54(3)
C(10)	3387(6)	-1173(6)	2441(10)	38(2)
C(5A)	3164(5)	-1392(6)	3354(9)	37(2)
C(30)	1409(6)	2075(7)	2833(9)	52(3)
C(34)	3058(6)	2335(7)	4483(9)	51(3)
C(22)	1858(6)	-2210(6)	5153(9)	48(3)
C(42)	2203(7)	879(8)	5458(11)	59(3)
C(41)	3483(6)	79(6)	5006(9)	42(2)
C(40)	1120(6)	75(7)	3826(9)	48(3)
C(7)	4738(6)	-1938(6)	3086(10)	49(3)
C(20)	1478(7)	-770(7)	6402(9)	56(3)
C(32)	2955(6)	1461(7)	2523(9)	51(3)
C(3)	1240(7)	-206(7)	1383(11)	57(3)
C(11)	2701(6)	-712(6)	1691(10)	41(3)
C(9A)	2722(7)	-454(7)	659(12)	59(3)
C(5)	3753(6)	-1929(6)	4123(9)	45(3)
C(25)	3625(7)	-492(8)	7497(10)	71(4)
C(35)	3265(7)	3237(7)	4035(10)	63(3)
C(6)	4526(6)	-2195(7)	3959(10)	51(3)
C(33)	3905(6)	1161(7)	2904(10)	63(3)
C(31)	939(7)	2463(8)	3555(10)	72(4)
C(21)	1445(8)	-1467(8)	7253(10)	75(4)
C(23)	901(7)	-2323(8)	4502(10)	73(4)
C(1)	1959(7)	-56(8)	7(11)	69(3)
C(2)	1254(7)	50(8)	336(12)	70(3)
C(8)	4182(7)	-1126(8)	1235(11)	67(3)
C(9)	3525(7)	-690(8)	501(11)	71(4)

* Equivalent isotropic U defined as one third of the trace of the orthogonalized U_{ij} tensor

Table G2. Bond lengths (Å) for (η^1-cpp)Mn(CO)$_3$(P(Et)$_3$)$_2$, **60**.

Mn-P(1)	2.315 (3)	Mn-P(2)	2.335 (3)
Mn-C(4)	2.28 (1)	Mn-C(42)	1.73 (1)
Mn-C(41)	1.838 (9)	Mn-C(40)	1.804 (9)
P(1)-C(24)	1.823 (9)	P(1)-C(22)	1.842 (9)
P(1)-C(20)	1.84 (1)	P(2)-C(30)	1.84 (1)
P(2)-C(34)	1.83 (1)	P(2)-C(32)	1.83 (1)
C(4)-C(3A)	1.50 (2)	C(4)-C(5A)	1.53 (1)
O(41)-C(41)	1.14 (1)	O(40)-C(40)	1.15 (1)
C(3A)-C(3)	1.39 (1)	C(3A)-C(11)	1.41 (2)
O(42)-C(42)	1.19 (2)	C(8A)-C(10)	1.41 (2)
C(8A)-C(7)	1.39 (1)	C(8A)-C(8)	1.43 (2)
C(24)-C(25)	1.53 (2)	C(10)-C(5A)	1.41 (2)
C(10)-C(11)	1.39 (1)	C(5A)-C(5)	1.38 (1)
C(30)-C(31)	1.51 (2)	C(34)-C(35)	1.52 (2)
C(22)-C(23)	1.52 (1)	C(7)-C(6)	1.36 (2)
C(20)-C(21)	1.52 (2)	C(32)-C(33)	1.52 (1)
C(3)-C(2)	1.44 (2)	C(11)-C(9A)	1.43 (2)
C(9A)-C(1)	1.38 (2)	C(9A)-C(9)	1.43 (2)
C(5)-C(6)	1.40 (2)	C(1)-C(2)	1.37 (2)
C(8)-C(9)	1.34 (2)		

Table G3. Bond angles (°) for (η^1-cpp)Mn(CO)$_3$(P(Et)$_3$)$_2$, **60**.

P(1)-Mn-P(2)	170.5(1)	P(1)-Mn-C(4)	90.4(3)
P(2)-Mn-C(4)	98.7(3)	P(1)-Mn-C(42)	85.5(4)
P(2)-Mn-C(42)	85.6(4)	C(4)-Mn-C(42)	174.0(5)
P(1)-Mn-C(41)	90.1(3)	P(2)-Mn-C(41)	87.2(3)
C(4)-Mn-C(41)	89.9(4)	C(42)-Mn-C(41)	94.5(5)
P(1)-Mn-C(40)	90.8(4)	P(2)-Mn-C(40)	93.1(3)
C(4)-Mn-C(40)	82.8(4)	C(42)-Mn-C(40)	92.8(5)
C(41)-Mn-C(40)	172.7(5)	Mn-P(1)-C(24)	115.8(4)
Mn-P(1)-C(22)	120.6(4)	C(24)-P(1)-C(22)	101.2(4)
Mn-P(1)-C(20)	113.2(3)	C(24)-P(1)-C(20)	102.1(5)
C(22)-P(1)-C(20)	101.4(5)	Mn-P(2)-C(30)	116.1(4)
Mn-P(2)-C(34)	110.2(4)	C(30)-P(2)-C(34)	102.4(4)
Mn-P(2)-C(32)	123.1(3)	C(30)-P(2)-C(32)	100.7(5)
C(34)-P(2)-C(32)	101.5(5)	Mn-C(4)-C(3A)	115.6(6)
Mn-C(4)-C(5A)	115.0(6)	C(3A)-C(4)-C(5A)	103(1)
C(4)-C(3A)-C(3)	135(1)	C(4)-C(3A)-C(11)	108.4(8)
C(3)-C(3A)-C(11)	117(1)	C(10)-C(8A)-C(7)	114(1)
C(10)-C(8A)-C(8)	112.9(9)	C(7)-C(8A)-C(8)	133(1)
P(1)-C(24)-C(25)	115.7(7)	C(8A)-C(10)-C(5A)	126.2(9)
C(8A)-C(10)-C(11)	124(1)	C(5A)-C(10)-C(11)	110(1)
C(4)-C(5A)-C(10)	107.7(8)	C(4)-C(5A)-C(5)	136(1)
C(10)-C(5A)-C(5)	116.3(9)	P(2)-C(30)-C(31)	114.5(8)
P(2)-C(34)-C(35)	118.7(8)	P(1)-C(22)-C(23)	116.5(7)
Mn-C(42)-O(42)	178(1)	Mn-C(41)-O(41)	179(1)
Mn-C(40)-O(40)	178.0(8)	C(8A)-C(7)-C(6)	121(1)
P(1)-C(20)-C(21)	116.8(8)	P(2)-C(32)-C(33)	115.6(8)
C(3A)-C(3)-C(2)	117(1)	C(3A)-C(11)-C(10)	110(1)
C(3A)-C(11)-C(9A)	127.0(9)	C(10)-C(11)-C(9A)	123(1)
C(11)-C(9A)-C(1)	114(1)	C(11)-C(9A)-C(9)	113(1)
C(1)-C(9A)-C(9)	133(2)	C(5A)-C(5)-C(6)	119(1)
C(7)-C(6)-C(5)	123.5(9)	C(9A)-C(1)-C(2)	122(1)
C(3)-C(2)-C(1)	124(1)	C(8A)-C(8)-C(9)	124(1)
C(9A)-C(9)-C(8)	124(1)		